

**MECHANISMS THAT REGULATE ANDROGEN RECEPTOR
TRANSCRIPTIONAL ACTIVITY**

Emily Blair Askew

A dissertation submitted to the faculty of the University of North Carolina at Chapel Hill in
partial fulfillment of the requirement for the degree of Doctor of Philosophy in the
Curriculum in Toxicology.

Chapel Hill
2010

Approved by:

Elizabeth M Wilson, Ph.D.

Frank S. French, M.D.

Matthew R. Redinbo, Ph.D.

David J. Holbrook, Ph.D.

Richard B. Mailman, Ph.D.

©2010
Emily Blair Askew
ALL RIGHTS RESERVED

ABSTRACT

EMILY B. ASKEW: Mechanisms that Regulate Androgen Receptor Transcriptional Activity
(Under the direction of Elizabeth M. Wilson, Ph.D.)

Testosterone (T) and dihydrotestosterone (DHT) are natural ligands for the androgen receptor (AR), an intracellular transcription factor and nuclear receptor. DHT is a more potent androgen than T *in vivo*. In this study, the mechanistic basis for the differential effects of T and DHT on AR activity was investigated. Dissociation kinetics, motif binding affinity and activation function 2 (AF2) transactivation measurements reveal that the slow dissociation of DHT relative to T from AR results from weaker T-induced AR FXXLF motif binding to the AF2 site. T acquires DHT-like activity when the AR ligand binding domain (LBD) contains the H874Y somatic prostate cancer mutation that results in the formation of direct hydrogen bonds between external and core helices 4 and 5, improving AF2 motif binding. The studies reveal that DHT better stabilizes the AR LBD core from the ligand binding pocket to the AF2 surface for maximal AR transactivation.

To further define the mechanisms whereby the AR specific coregulator melanoma antigen gene protein-A11 (MAGE-11) modulates AR activity, we pursued observations that MAGE-11 increases AR transcriptional activity independent of AF2. We sought to characterize the effects of MAGE-11 and the coactivators transcription intermediary factor 2 (TIF2) and p300 on AR transcriptional activity. The site of interaction in MAGE-11 that binds the AR FXXLF motif is an F-box within the MAGE homology domain. MAGE-11 Ser-

174 is phosphorylated by MAP kinase which influences the interaction of the MAGE-11 F-box with AR. MAGE-11 forms a complex with TIF2 and p300 to modulate AR transactivation independent of AF2. This research provides evidence for a novel function for an F-box protein in which F-box/FXXLF like motif interactions modulate AR transcriptional activity in the absence and presence of ligand.

ACKNOWLEDGEMENTS

I would like to thank my thesis advisor and mentor, Dr. Elizabeth M. Wilson for her continued support and guidance throughout my years as an undergraduate and graduate student in The Laboratories for Reproductive Biology. Dr. Wilson is an excellent example of how hard work within the laboratory can dramatically impact scientific theory and the community at large. I am also grateful for my committee members, Dr. Frank S. French, Dr. Matthew R. Redinbo, Dr. David J. Holbrook and Dr. Richard B. Mailman, whom provided helpful guidance and advice during my time as a doctoral student. I am also appreciative of the support received by my current and former coworkers within The Laboratories for Reproductive Biology. In particular I would like to thank Dr. Suxia Bai for educating me in the technical aspects of molecular biology and for her continued patience during our time together in the laboratory. Finally, this work would have not been possible without the enduring love and support of my family and friends. I would especially like to thank my parents, Lynn and Phil Askew, who were willing to sacrifice their own dreams during my pursuit of higher education. To my husband, Scott Lovett, I am eternally indebted to you for your unconditional love and patience throughout our time together. To my unborn son, Samuel Winston Lovett, may this work be an example to you of how your dreams can come true, no matter the obstacles that stand in your way. I would like to dedicate this work to my late paternal grandparents, Sam and Ruth Askew, whom will always be with me in spirit.

TABLE OF CONTENTS

LIST OF TABLES	viii
LIST OF FIGURES	ix
LIST OF ABBREVIATIONS.....	xi
Chapter 1: INTRODUCTION.....	1
A. The Androgen Receptor.....	1
B. The Androgen Receptor Coregulator MAGE-11	9
C. Dissertation Research Objectives	13
D. References	14
E. Figures.....	20
Chapter 2: MODULATION OF ANDROGEN RECEPTOR ACTIVATION FUNCTION BY TESTOSTERONE AND DIHYDROTESTOSTERONE... ..	22
A. Abstract.....	22
B. Introduction	23
C. Materials and Methods.....	25
D. Results	33
E. Discussion.....	42
F. References.....	52
G. Figures.....	57
H. Tables.....	71
Chapter 3: MELANOMA ANTIGEN GENE PROTEIN-A11 (MAGE-11) F-BOX LINKS THE ANDROGEN RECEPTOR NH ₂ -TERMINAL TRANSACTIVATION DOMAIN TO p160 COACTIVATORS	76
A. Abstract.....	76
B. Introduction	76
C. Materials and Methods.....	79
D. Results.....	87
E. Discussion.....	96
F. References.....	102
G. Figures.....	108
Chapter 4: TRANSCRIPTIONAL SYNERGY BETWEEN MAGE-11 AND p300 IN ANDROGEN RECEPTOR SIGNALING.....	125
A. Abstract.....	125
B. Introduction	126
C. Materials and Methods.....	127
D. Results.....	132
E. Discussion.....	141
F. References.....	149
G. Figures.....	153

Chapter 5: SUMMARY AND FUTURE PERSPECTIVES.....	166
A. Molecular Determinants of Testosterone (T) and Dihydrotestosterone (DHT)	
Binding to the Androgen Receptor	166
B. Mechanisms of the Melanoma Antigen Gene Protein-A11 (MAGE-11)	
Dependent Increase in Androgen Receptor Gene Mediated Transcription	167
C. MAGE-11 as a Prostate Cancer Therapeutic Target.....	168
D. Role of MAGE-11 in Infertility	169
E. References	171

LIST OF TABLES

Table

2-1.	Androgen Dependent AR LBD and AR-H874Y LBD Binding Affinities for AR FXXLF and TIF2 LXXLL Peptides.....	71
2-2.	Dissociation Half-times of [³ H]T and [³ H]DHT.....	71
2-3.	Crystallographic Data and Refinement Statistics	72
2-4.	Hydrogen Bond Distances and Angles for WT AR LBD Bound With T and AR FXXLF Peptide or DHT and LXXLL Peptide	73

LIST OF FIGURES

Figure

1-1. Schematic of AR Functional Domains	20
1-2. Chemical Structure of Testosterone (T) and Dihydrotestosterone (DHT) ...	20
1-3. MAGE-11 Gene Structure and Protein.....	21
2-1. AF2 Activity in the AR LBD	57
2-2. Increased AR-H874Y LBD AF2 Activity Response to T	59
2-3. Increased Transcriptional Activity of AR-H874Y Response by T and Adrenal Androgens	60
2-4. MAGE-11 Increases AR-H874Y Activity Response to T and DHT.....	61
2-5. Fluorescence Binding Isotherms	62
2-6. Kinetics of T and DHT Dissociation from AR and AR-H874Y	63
2-7. Crystal Structures of WT and H874Y AR LBD Bound with T and AR FXXLF or TIF2 LXXLL Peptide	64
2-8. Potential A-ring and Water-Mediated H-bonding Schemes For T and DHT.....	66
2-9. Comparison of WT AR LBD-T-AR FXXLF and WT AR LBD-DHT LXXLL.....	67
2-10. Detailed Crystal Structure Comparison of WT and H874Y AR LBD Bound to T and AR FXXLF Peptide.....	68
2-11. Structural Differences Between the Steroid and Non-Steroid Ligand Binding Pockets.....	70
3-1. Dependence of AR Transactivation on MAGE-11 and TIF2.....	108
3-2. Requirement for a MAGE-11 F-box in AR Transactivation.....	110
3-3. Requirement for MAGE-11 F-box in AR Transactivation by TIF2.....	111
3-4. Interaction Between MAGE-11 F-box and AR FXXLF Motif.....	113
3-5. Serum Stimulation of MAPK Kinase Phosphorylation of MAGE-11 Ser-174.....	115

3-6. MAGE-11 and TIF2-Dependent Increase in AR AF1 Activity	116
3-7. Interaction Between MAGE-11 and TIF2	117
3-8. MAGE-11 and TIF2 Interaction Domains.....	118
3-9. MAGE-11 Increases TIF2 AD1 Activity	120
3-10. FXXLF and F-box Related Sequences in AR, MAGE-11, TIF2 Skp1, and Skp2	121
3-11. MAGE-11 FXXIF Motif-Dependent Interactions with TIF2.....	122
3-12. Interactions Between AR, MAGE-11, and TIF2.....	124
4-1. MAGE-11 and p300 Increase AR Transcriptional Activity.....	153
4-2. MAGE-11 Interacts with the p300 NH ₂ -terminal Region	154
4-3. MAGE-11 Domains Interact with p300	155
4-4. Identification of MAGE-11 ¹⁸⁵ MDAIF ¹⁸⁹ and ⁹⁴ ITQIF ⁹⁸ Interaction Sites for p300	156
4-5. Functional Effects of AR and p300 NH ₂ -terminal FXXLF motifs	158
4-6. Dependence of GAL-p300-(2–300) Transcriptional Activity on MAGE-11 and TIF2.....	159
4-7. MAGE-11 Links p300 to AR N/C Interaction-Mediated Transactivation.	160
4-8. Dependence of AR Transcription Activity on p300 Acetyltransferase Activity	161
4-9. MAGE-11 Influences p300 Acetylation of TIF2	162
4-10. Transient Increase in Endogenous MAGE-11	164
4-11. Functional Interactions Between AR, MAGE-11, p300 and TIF2.....	165

ABBREVIATIONS

AD1	activation domain 1
AF1	activation function 1
AF2	activation function 2
AR	androgen receptor
Androstanediol	5 α -androstane-3 α ,17 β -diol
Androstenedione	4-androstene-3,17-dione
AR	androgen receptor
CBP	CREB binding protein
DHT	dihydrotestosterone
DBD	DNA binding domain
E1A	adenovirus early region protein 1A
EGF	epidermal growth factor
ERK1	extracellular signal-regulated kinase 1
GAL	<i>Saccharomyces cerevisiae</i> GAL-4 DNA binding domain, amino acid residues 1 to 147
GST	glutathione S-transferase
HAT	histone acetyltransferase
H-bond	hydrogen-bond
IB	immunoblot
IP	immunoprecipitation
LBD	ligand binding domain
MAGE-11	melanoma antigen gene protein-A11

MAP kinase	mitogen-activated protein kinase
MMTV-Luc	mouse mammary tumor virus luciferase reporter vector
N/C interaction	NH ₂ -terminal/carboxyl terminal interaction
PBS	phosphate buffered saline
PCR	polymerase chain reaction
PSA-Enh-Luc	prostate-specific antigen enhancer luciferase reporter vector
R1881	17 α -methyltrienolone
RMSD	root mean squared difference
RT-PCR	reverse transcription polymerase chain reaction
SCF	Skp1-cullin-F-box
siRNA	small inhibitory RNA
SRC	steroid receptor coactivator
T	testosterone
TIF2	transcription intermediary factor 2
WT	wild-type

CHAPTER 1

INTRODUCTION

The Androgen Receptor

Molecular Structure and Androgen Receptor (AR) N/C Interaction-The AR is a ligand activated transcription factor and member of the steroid and nuclear receptor superfamily (1). The AR gene is located at Xq11-12 (2), is more than 90 kb (3) and codes for a 919 amino acid protein. As with other nuclear receptor family members, the AR has a multi-domain structure composed of an NH₂-terminal transactivation domain, central DNA binding domain (DBD), linker hinge region and carboxyl-terminal ligand binding domain (LBD) (4) (Fig.1-1). AR is expressed in androgen target tissues including the prostate, skeletal muscle, central nervous system and liver, with highest levels in prostate, adrenal gland and epididymis (5).

Androgen-induced transcriptional activity depends on activation function 1 (AF1) within the unstructured NH₂-terminal region (4), and the activation function 2 (AF2) hydrophobic interface in the LBD that is stabilized by androgen binding (6). AR is unique among other family members based on the presence of a strong androgen-dependent AR NH₂-and carboxyl-terminal AR (N/C) interaction between the AR²³FQNLF²⁷ FXXLF motif within the AR NH₂-terminal domain and AF2 in the LBD (6-10). The AR N/C interaction is required for AR transactivation of certain androgen-regulated genes, including prostate-specific antigen (PSA) and probasin (11-14).

Agonist potency at low physiological androgen concentrations is facilitated by the AR N/C interaction, which was previously shown through transcription, dimerization and DNA binding assays (15). The androgen-dependent AR N/C interaction slows dissociation of bound androgen (16) and stabilizes AR binding of androgen response element DNA (9). The functional significance of the AR N/C interaction is demonstrated by patients with the androgen insensitivity syndrome, in which defects in AR residues that modulate the AR N/C interaction result in incomplete masculinization despite normal androgen binding kinetics (8,10,17-19).

Androgen Receptor Activation by Testosterone (T) and Dihydrotestosterone (DHT)-T is synthesized from cholesterol in the Leydig cells of the testis in response to luteinizing hormone secretion from the anterior pituitary gland. T is the major male circulating hormone and, unlike DHT, has a double bond in ring A between carbons four and five. On average, adult men produce 3-10 mg of T daily and have circulating levels ranging from 300-700 ng/dL (5). In the prostate, approximately 90% of free T within cells is irreversibly converted to DHT by the 5 α -reductase type 2 enzyme (Fig. 1-2) (20).

Male organ development is modulated by T and DHT binding to AR. During embryogenesis, T mediates the development and differentiation of the Wolffian ducts into seminal vesicles, epididymis and vas deferens (21), while DHT is required for the differentiation of the urogenital sinus into the prostate, urethra, penis and scrotum (22). Post-natally, T is the major androgen in muscle (23) while DHT is primarily responsible for androgen-mediated events of male sexual maturation at puberty, including growth of facial and body hair and maturation of the external genitalia (24). The physiological importance of DHT is evident in patients with steroid 5 α -reductase deficiency in which affected males

present with external female genitalia at birth due to the decreased ability to convert T to DHT (21,22,24).

In contrast to other steroid hormone receptors, AR binds both T and DHT with similar equilibrium binding affinity (25). High affinity binding of T and DHT to AR depends on hydrophobic and electrostatic interactions as well as hydrogen bonds to critical residues in the AR ligand binding pocket (6,26), and results in approximately a 6-fold increase in AR stability (27). T dissociates three times faster from AR than DHT (25). Furthermore, there is no evidence that T and DHT activate different gene targets. In support of this, previously published studies report that T is as effective as DHT in regulating AR gene mediated transcription when present at high concentrations. In particular, Grino et al. showed that a 10 fold higher concentration of T than DHT results in AR mediated transactivation in fibroblasts derived from a patient with 5 α -reductase deficiency (28). Additionally, Deslypere et al. found that both T and DHT increased AR induced mouse mammary tumor virus chloramphenicol acetyltransferase (MMTV-CAT) activity in Chinese hamster ovary cells unable to convert T to DHT. DHT was 10 fold more potent than T (23).

Androgen Action in Castration-Recurrent Prostate Cancer-Androgens are required for growth of the prostate and have a role in the pathogenesis of prostate cancer (29), the second most common form of cancer in American men. The mainstay treatment for prostate cancer is androgen deprivation therapy that removes testicular androgens through physical or chemical castration, leading to the regression of the prostate cancer tumor (20). Prostate cancer recurs within 18-20 months despite aggressive treatment in a majority of cases (30).

AR signaling remains a growth-promoting pathway in castration-recurrent prostate cancer, and data indicate the presence of residual androgens in castration-recurrent prostate

cancer specimens. Belanger et al. reported that intraprostatic DHT levels remain at 40% after the removal of testicular androgen (31), while another report found that DHT levels in prostate of cancer patients that had previously undergone androgen deprivation therapy remained at 25% of their original concentration before treatment (32). The level of DHT required for growth stimulation of recurrent prostate cancer is four orders of magnitude lower than required by androgen-dependent prostate carcinoma cells (33,34), suggesting that DHT-mediated stimulation of the AR contributes to the progression and growth of castration-recurrent prostate cancer.

T levels persist in castration-recurrent prostate cancer tissue at concentrations similar to benign prostatic hyperplasia (35), potentially contributing to the growth of recurrent prostate cancer cells that undergo recurrent growth after androgen withdrawal therapy. AR prostate cancer somatic mutations that slow the dissociation rate of T may also facilitate growth of castration-recurrent prostate cancer through AR-associated mechanisms including increased AR stability, increased retention time of bound androgen and increased FXXLF and LXXLL motif binding to AR AF2 (36).

It is of clinical importance to elucidate the molecular determinants for the differential effects of T and DHT in normal prostate and prostate carcinoma in order to develop more targeted drug therapies to combat prostate cancer development and post castration-recurrence.

Regulation of AR AF2 Activity-AR AF2 is a hydrophobic cleft in the LBD formed by helices 3, 3', 4, and 12 (1) that was first recognized as a coactivator binding site in the thyroid hormone receptor using scanning surface mutagenesis by Feng et al. (37). This study was later supported by observations of AF2 in crystal structures of the glucocorticoid

receptor LBD bound to dexamethasone and LXXLL coactivator motif peptide, as well as the peroxisome proliferator-activated receptor- γ LBD bound to rosiglitazone and LXXLL motif peptide (38,39). In the AR, androgen binding stabilizes helix 12 to complete the AF2 hydrophobic cleft that interacts with LXXLL-related motifs (1,36,40).

AR FXXLF and SRC/p160 coactivator LXXLL motifs bind the same AR AF2 site (6). AR FXXLF motif binding to AF2 in the AR N/C interaction competitively inhibits the interaction of AF2 with the LXXLL motifs of SRC/p160 coactivators (27). The interaction of the AR FXXLF motif with AF2 involves the binding of a conserved α -amphipathic helix with the hydrophobic surface of AF2 in a similar fashion to the interaction of the LXXLL motifs of SRC/p160 coactivators with the AR AF2 docking surface. Charge patches bordering AF2 align with oppositely charged residues flanking the FXXLF or LXXLL motif sequences (1). AR FXXLF motif hydrogen bonds to AR charge clamp residues Glu-897 and Lys-720 while the LXXLL motifs of SRC/p160 coactivators lack the charge clamp bond to AR residue Glu-897 but retain the hydrogen bond to AR charge clamp residue Lys-720 (1).

Transcriptional activity from AR AF2 is influenced not only by androgen binding and the AR N/C interaction, but also by cofactors that are often expressed at high levels in cancer. For example, the amplified in breast cancer-1 coactivator (AIB1) is overexpressed and interacts with the estrogen receptor, leading to increased estrogen regulated gene transcription in breast cancer (41). A majority of recurrent prostate cancer tissue specimens express high levels of TIF2 and steroid receptor coactivator-1 (SRC1) (42) while the AR coactivator ARA-70 enhances transcription of androgen-responsive genes in the DU145 metastatic prostate cancer cell line (43). In agreement with these findings, Linja et al. reported that the SRC1 gene is amplified in the LuCaP70 prostate cancer xenograft

established from a hormone-refractory prostate carcinoma (44). Furthermore, the AR specific coregulator, melanoma antigen gene protein-A11 (MAGE-11) of the MAGEA gene subfamily, increases ligand mediated AF2 activity and is expressed in AR positive prostate cancer cell lines (45). LXXLL motif interactions are enhanced at the AF2 interaction surface upon androgen binding when MAGE-11 binds the AR FXXLF motif and inhibits the formation of the AR N/C interaction (45,46).

Somatic AR Prostate Cancer Mutations- Prostate cancer accounts for approximately 10% of cancer-related deaths in men (47). The American Cancer Society estimates that there were approximately 192,280 new cases of prostate cancer in the United States in 2009 and 27,360 deaths. In initial and intermediate stages, androgen-dependent prostatic tumors are treated with androgen ablation therapy, which ceases to be effective over time, leading to castration-recurrent prostate cancer.

Evidence suggests that the AR plays a role in mediating castration-recurrent growth of prostate cancer. AR protein levels are similar in androgen-dependent and castration-recurrent prostate cancer, in association with the expression of AR-regulated genes in castration-recurrent prostate cancer (48). AR mutation or overexpression (49,50), altered expression or activity of coregulators (42) and growth factor signaling leading to AR phosphorylation (34) can also influence AR activity in castration-recurrent prostate cancer cells.

AR AF2 motif interactions are altered by somatic AR prostate cancer mutations which affect communication with the ligand binding pocket (36). Somatic AR mutations in prostate cancer are most often functional, suggesting positive selection for prostate tumor cell survival. AR is more sensitive to low levels of physiologic ligand and/or activated by an

increased number of ligands that bind to the AR ligand binding pocket (20,51-54). For example, the prostate cancer somatic mutant AR-V730M increases AF2 binding of SRC1 (6,36), while the castration-recurrent prostate cancer mutation V715M increases AR transactivation in the presence of TIF2 without modifying androgen equilibrium binding affinity (36).

Another prostate cancer somatic mutation is the AR histidine to tyrosine mutation at amino acid 874. His-874 is located in AR helix 10 above rings C and D of the bound androgen, proximal to the ligand binding pocket and AF2. The AR-H874Y recurrent prostate cancer mutation was identified in the human prostate cancer CWR22 xenograft isolated from a patient with a bone marrow metastases who was treated with flutamide and a luteinizing hormone releasing hormone agonist (55). This CWR22 mutant AR is responsive to the antiandrogen hydroxyflutamide, dehydroepiandrosterone, estradiol and progesterone (55), while retaining similar binding affinities for T and DHT (36,54-56). The synthetic androgen R1881 has a two-fold slower dissociation rate from AR-H874Y than from wild-type AR (36). AR-H874Y increases AR functional activity which likely favors prostate cancer cell survival and expansion through mechanisms including increased retention time of bound androgen, SRC/p160 coactivator recruitment, AR stability and AR AF2 activity.

It is critical to determine the mechanism whereby residues proximal to the ligand binding pocket and AF2 regulate hormone binding, AR activity and AF2 motif binding in both normal prostate and castration-recurrent prostate cancer in order to develop new drug therapies that disrupt AR-mediated gene signaling in cancer development and progression.

Effect of Endocrine-Disrupting Chemicals on AR Transcriptional Activity-Since evidence from epidemiological studies, animal studies and *in vitro* analysis indicates that

endocrine-disrupting compounds can influence AR activity (57), it is critical to understand the molecular basis for AR regulated gene expression. In fact, risk assessment for endocrine disrupting chemicals includes several key areas, such as biological half-life and exposure levels in addition to the activity and binding kinetics for AR (58). Thus, an in depth characterization into the mechanisms underlying AR transcriptional activity which focus on hormone binding and coregulator interactions is critical for the complete understanding of the molecular effects of xenobiotics on AR. Therefore, the studies presented here in this dissertation may provide a framework for exploring how endocrine active substances in the environment affect health in humans and animals by altering AR structure and function in normal physiology and disease.

Vinclozolin is a fungicide whose two metabolites, M1 and M2, have antiandrogenic properties and compete with T and DHT for binding of the AR and block AR mediated gene activation in males, resulting in physical abnormalities (59-62). Gray et al. showed that perinatal exposure of rodents to vinclozolin caused impaired ejaculation, hypospadias and ectopic scrotum (63). While the pesticide 1,1,1-trichloro-2,2-bis (*p*-chlorophenyl) ethane (DDT) is known to be an environmental estrogen that binds to estrogen receptor α and β (64), its major metabolite, 1,1-dichloro-2,2-bis(*p*-chlorophenyl) ethylene (DDE) (65), has antiandrogen properties (59,64). DDE inhibits AR binding of androgen as indicated by competitive binding assays, and androgen-induced AR transactivation is blocked by DDE (64).

One source of an endocrine active substance in the environment is the synthetic androgen trenbolone acetate excreted from cattle given anabolic steroids to improve beef production (66,67). Trenbolone acetate was found to have a potency similar to DHT and the

synthetic androgen R1881 (66). Whole-water samples obtained from feedlot runoff, which contain the trenbolone acetate metabolites 17 α - and 17 β -trenbolone, elicited an androgenic response (67). In the environment, exposure of female mosquitofish to 17 β -trenbolone resulted in masculinization (68), while masculinization of female mosquitofish downstream of paper mill effluent correlated with the presence of the androgen precursor progesterone, which is naturally present in the loblolly pine (69).

Diadzein is another potential environmental contaminant with androgenic properties. Diadzein is an isoflavone, and was previously found to have activity for the rat estrogen receptor α and β (70). Chen et al. found that even though it is a known phytoestrogen, diadzein can also elicit androgen effects in PC-3 and LNCaP prostate cancer cells transfected AR and/or the AR coactivators ARA55 and ARA70 (71).

Overall, research directed at understanding the basic mechanisms underlying the fundamental key processes and target molecules in AR gene mediated reproduction and development is vital since the reproductive system is affected by androgenic and antiandrogenic factors present in the environment.

The Androgen Receptor Coregulator MAGE-11

MAGE Gene Superfamily-van der Bruggen et al. first reported the discovery of MAGE-A1 based on its ability to induce the expression of the tumor antigen MZ2-E in the human melanoma cell line, MZ2-MEL3.0 (72-74). Since this original report, MAGE-A1 has been detected in specimens of small cell lung cancer, bronchial squamous cell cancer, colon carcinoma and chronic and acute myeloid leukemia, yet undetectable in normal tissues of the liver, muscle, skin, lung, brain and kidney (72). MAGE-A1 was later discovered to be 1 of 12 members of the human MAGE-A gene subfamily, from which the other 11 members were

identified by using MAGE-A1 sequence to probe cosmid libraries (75,76). The MAGE-A gene family is encoded by a 3.5-Mb segment of DNA located at position Xq28 on the X chromosome, is found in human and primates (76), and is expressed in tumors, testis and placenta (75,77). Additional MAGE gene subfamilies, including MAGE-B, and MAGE-C, are also located on the X chromosome at positions Xp21 and Xq26-27, respectively (73,74,78). Similar to the MAGE-A subfamily, expression of MAGE-B and MAGE-C is absent in normal tissues except for male germ cells and placenta (73,74,78). The remaining MAGE gene family members are positioned on chromosomes 3 and 15 in addition to the X chromosome, and are part of the MAGE gene subfamilies (73,74).

To date, a total of 52 known members of the MAGE gene superfamily have been identified (73). Analysis of the protein sequence of the MAGE family of proteins highlights a region of high homology within the carboxyl-terminus, referred to as the MAGE homology domain. Since MAGE genes share sequence similarity within this region, it has been suggested that the gene family has undergone rapid evolution, and are products of retropositioning and gene duplication (73).

MAGE-11-AR transcriptional activity at androgen-regulated gene promoters requiring the AR N/C interaction is enhanced by the increased expression of the SRC/p160 coactivator TIF2 (11). Studies to understand what factors modulate the AR N/C interaction and the accessibility of AF2 led to the identification of MAGE-11 as an AR cofactor. MAGE-11 is a member of the MAGE-A gene subfamily encoded on the human X chromosome (45).

MAGE-11 was originally described by De Plaen et al. in cosmid libraries (75), and later isolated from human epithelial cervical carcinoma (HeLa) cells by Jurk et al. (79). Even though Junk and coworkers reported that MAGE-11 was a 319 residue, 48 kDa protein

localized primarily to the nucleus, MAGE-11 is in fact 60-65 kDa (45). MAGE-11 contains 3 additional upstream exons that code for an additional 110 NH₂-terminal residues and has a nuclear localization signal that is located within this extended NH₂-terminal region, between residues 14 and 23 (Fig. 1-3) (45,46,80). The MAGE-11 gene is located on the X chromosome at position Xq28 downstream of the AR (45,73-75). The full-length MAGE-11 gene includes 5 exons, 4 of which are coding exons for a 429 amino acid protein (45). MAGE-11 contains the MAGE homology domain between residues 222 and 421 (Fig. 1-3).

MAGE-11 is an AR specific coregulator expressed in tissues of the human male and female reproductive tracts, including testis, ovary, prostate, breast and adrenal gland (45). MAGE-11 is expressed in glandular epithelial cell nuclei of the endometrium during the window of implantation (81). MAGE-11 mRNA was observed in several cell lines, including HeLa, ovarian cancer cells, and prostate cancer cell lines (45).

The MAGE-11 – AR Interaction and Effect on AR Transcriptional Activity-MAGE-11 binds the AR NH₂-terminal FXXLF motif and relieves repression of AF2 caused by the agonist-induced AR N/C interaction, leading to increased accessibility of AF2 to coactivator binding (45). Mutational analysis and two-hybrid assays have revealed that the interaction of MAGE-11 with the AR²³FONLF²⁷ FXXLF motif requires AR residues 16-36; however, AF2 binding of the AR FXXLF motif is dependent on AR residues 20-30 (45). This finding suggests this extended region is required for MAGE-11 to effectively compete with AR AF2 for binding of the AR FXXLF motif in the presence of androgen (45).

Immunohistochemical evidence reveals that MAGE-11 interacts and stabilizes AR in the cytoplasm in the absence of androgen. In the presence of androgen, both proteins colocalize to the nucleus (45). Post-translational modification of MAGE-11 induced by

epidermal growth factor (EGF) results in the cell cycle checkpoint kinase 1 (Chk1)-dependent phosphorylation of MAGE-11 Thr-360. Phosphorylation of MAGE-11 at Thr-360 stimulates the monoubiquitinylation of MAGE-11 residues Lys-240 and 245 that is required for the interaction of MAGE-11 with the AR FXXLF motif (46).

The EGF-induced stabilization of the MAGE-11 – AR – DHT requires 7-10 hours exposure of cultured cells to EGF (46). This results in the inhibition of the AR N/C interaction, increased recruitment of SRC/p160 coactivators to the AF2 surface and enhanced AF2 activity (45,46). MAGE-11 phosphorylation and ubiquitinylation sites are conserved throughout the MAGE gene family, allowing one to postulate that the observed regulatory mechanism modulating the MAGE-11 – AR FXXLF motif interaction may apply to other members of the MAGE superfamily.

MAGE-11 in Castration-Recurrent Prostate Cancer-AR AF2 function in prostate cancer is selectively regulated through several mechanisms, including coactivator binding. Castration-recurrent prostate cancer tissue specimens express high levels of TIF2 and SRC1 which bind to the AF2 site (42). MAGE-11 increases ligand mediated AF2 activity, and evidence reveals that MAGE-11 mRNA is found in prostate cancer cell lines that express AR (45,46).

MAGE-11 levels increase during prostate cancer progression in the CWR22 human prostate cancer xenograft after androgen deprivation therapy and in approximately 30% of castration-recurrent prostate cancer patients, suggesting that MAGE-11 increases AR signaling and drives prostate cancer growth (82). AR mRNA levels also increase in the CWR22 tumor after castration, albeit to a lesser extent than MAGE-11 (82). MAGE-11 is upregulated in prostate cancer xenografts, clinical specimens, and prostate cancer cell lines

by hypomethylation of CpG islands near the MAGE-11 transcription start site (82). Overall, the MAGE-11 interaction with AR and its coregulators provides a mechanism for increased AR action in castration-recurrent prostate cancer. Thus, it is important to further elucidate the MAGE-11 dependent increases in AR transcriptional activity.

Dissertation Research Objectives

The first objective of my dissertation was to elucidate the basis for the differences in the ability of T and DHT to increase AR activity through biochemical and crystal structure analysis of wild-type AR and a prostate cancer somatic mutant AR-H874Y LBD bound to T. An additional research objective was to define the mechanisms whereby MAGE-11 contributes to ligand-dependent and independent AR transcriptional activity, pursuing observations that MAGE-11 increases the constitutive activity of an AR NH₂-terminal fragment. The effects of MAGE-11 and TIF2 on AR transcriptional activity were characterized and the AR FXXLF motif binding site in the MAGE-11 carboxyl-terminal region defined.

Sequence homology exists between MAGE-11 and the adenovirus early region protein 1A (E1A), which binds to the nuclear receptor coactivator and histone acetyltransferase p300. Thus, a further goal was to elucidate the mechanisms of increased AR transcriptional activation by MAGE-11 and p300, define and characterize the interaction regions within MAGE-11 and p300, and to understand the post-translational modifications by p300 which influence AR transcriptional activity.

REFERENCES

1. He, B., and Wilson, E. M. (2003) *Mol. Cell Biol.* **23**, 2135-2150
2. Brown, C. J., Goss, S. J., Lubahn, D. B., Joseph, D. R., Wilson, E. M., French, F. S., and Willard, H. F. (1989) *Am. J. Hum. Genet.* **44**, 264-269
3. Lubahn, D. B., Joseph, D. R., Sar, M., Tan, J., Higgs, H. N., Larson, R. E., French, F. S., and Wilson, E. M. (1988) *Mol. Endocrinol.* **2**, 1265-1275
4. Simental, J. A., Sar, M., Lane, M. V., French, F. S., and Wilson, E. M. (1991) *J. Biol. Chem.* **266**, 510-518
5. Gao, W., Bohl, C. E., and Dalton, J. T. (2005) *Chem. Rev.* **105**, 3352-3370
6. He, B., Gampe, R. T., Jr., Kole, A. J., Hnat, A. T., Stanley, T. B., An, G., Stewart, E. L., Kalman, R. I., Minges, J. T., and Wilson, E. M. (2004) *Mol. Cell* **16**, 425-438
7. Langley, E., Zhou, Z. X., and Wilson, E. M. (1995) *J. Biol. Chem.* **270**, 29983-29990
8. Langley, E., Kemppainen, J. A., and Wilson, E. M. (1998) *J. Biol. Chem.* **273**, 92-101
9. Wong, C. I., Zhou, Z. X., Sar, M., and Wilson, E. M. (1993) *J. Biol. Chem.* **268**, 19004-19012
10. He, B., Kemppainen, J. A., Voegel, J. J., Gronemeyer, H., and Wilson, E. M. (1999) *J. Biol. Chem.* **274**, 37219-37225
11. He, B., Lee, L. W., Minges, J. T., and Wilson, E. M. (2002) *J. Biol. Chem.* **277**, 25631-25639
12. Callewaert, L., Verrijdt, G., Christiaens, V., Haelens, A., and Claessens, F. (2003) *J. Biol. Chem.* **278**, 8212-8218
13. Li, J., Fu, J., Toumazou, C., Yoon, H. G., and Wong, J. (2006) *Mol. Endocrinol.* **20**, 776-785
14. Hsu, C. L., Chen, Y. L., Ting, H. J., Lin, W. J., Yang, Z., Zhang, Y., Wang, L., Wu, C. T., Chang, H. C., Yeh, S., Pimplikar, S. W., and Chang, C. (2005) *Mol. Endocrinol.* **19**, 350-361
15. Kemppainen, J. A., Lane, M. V., Sar, M., and Wilson, E. M. (1992) *J. Biol. Chem.* **267**, 968-974
16. Zhou, Z. X., Lane, M. V., Kemppainen, J. A., French, F. S., and Wilson, E. M. (1995) *Mol. Endocrinol.* **9**, 208-218

17. Quigley, C. A., Tan, J. A., He, B., Zhou, Z. X., Mebarki, F., Morel, Y., Forest, M. G., Chatelain, P., Ritzen, E. M., French, F. S., and Wilson, E. M. (2004) *Mech. Ageing Dev.* **125**, 683-695
18. Ghali, S. A., Gottlieb, B., Lumbroso, R., Beitel, L. K., Elhaji, Y., Wu, J., Pinsky, L., and Trifiro, M. A. (2003) *J. Clin. Endocrinol. Metab.* **88**, 2185-2193
19. Quigley, C. A., De Bellis, A., Marschke, K. B., el-Awady, M. K., Wilson, E. M., and French, F. S. (1995) *Endocr. Rev.* **16**, 271-321
20. Feldman, B. J., and Feldman, D. (2001) *Nat. Rev. Cancer* **1**, 34-45
21. Maes, M., Sultan, C., Zerhouni, N., Rothwell, S. W., and Migeon, C. J. (1979) *J. Steroid Biochem.* **11**, 1385-1392
22. Mahendroo, M. S., Cala, K. M., Hess, D. L., and Russell, D. W. (2001) *Endocrinology* **142**, 4652-4662
23. Deslypere, J. P., Young, M., Wilson, J. D., and McPhaul, M. J. (1992) *Mol. Cell Endocrinol.* **88**, 15-22
24. Wilson, J. D., Griffin, J. E., and Russell, D. W. (1993) *Endocr. Rev.* **14**, 577-593
25. Wilson, E. M., and French, F. S. (1976) *J. Biol. Chem.* **251**, 5620-5629
26. Sack, J. S., Kish, K. F., Wang, C., Attar, R. M., Kiefer, S. E., An, Y., Wu, G. Y., Scheffler, J. E., Salvati, M. E., Krystek, S. R., Jr., Weinmann, R., and Einspahr, H. M. (2001) *Proc. Natl. Acad. Sci. U S A* **98**, 4904-4909
27. He, B., Bowen, N. T., Minges, J. T., and Wilson, E. M. (2001) *J. Biol. Chem.* **276**, 42293-42301
28. Grino, P. B., Griffin, J. E., and Wilson, J. D. (1990) *Endocrinology* **126**, 1165-1172
29. Shaneyfelt, T., Husein, R., Bubley, G., and Mantzoros, C. S. (2000) *J. Clin. Oncol.* **18**, 847-853
30. Mostaghel, E. A., Montgomery, R. B., and Lin, D. W. (2007) *Curr. Urol. Rep.* **8**, 224-232
31. Belanger, B., Belanger, A., Labrie, F., Dupont, A., Cusan, L., and Monfette, G. (1989) *J. Steroid Biochem.* **32**, 695-698
32. Nishiyama, T., Hashimoto, Y., and Takahashi, K. (2004) *Clin. Cancer Res.* **10**, 7121-7126

33. So, A., Gleave, M., Hurtado-Col, A., and Nelson, C. (2005) *World J. Urol.* **23**, 1-9
34. Gregory, C. W., Johnson, R. T., Jr., Mohler, J. L., French, F. S., and Wilson, E. M. (2001) *Cancer Res.* **61**, 2892-2898
35. Mohler, J. L., Gregory, C. W., Ford, O. H., 3rd, Kim, D., Weaver, C. M., Petrusz, P., Wilson, E. M., and French, F. S. (2004) *Clin. Cancer Res.* **10**, 440-448
36. He, B., Gampe, R. T., Jr., Hnat, A. T., Faggart, J. L., Minges, J. T., French, F. S., and Wilson, E. M. (2006) *J. Biol. Chem.* **281**, 6648-6663
37. Feng, W., Ribeiro, R. C., Wagner, R. L., Nguyen, H., Apriletti, J. W., Fletterick, R. J., Baxter, J. D., Kushner, P. J., and West, B. L. (1998) *Science* **280**, 1747-1749
38. Bledsoe, R. K., Montana, V. G., Stanley, T. B., Delves, C. J., Apolito, C. J., McKee, D. D., Consler, T. G., Parks, D. J., Stewart, E. L., Willson, T. M., Lambert, M. H., Moore, J. T., Pearce, K. H., and Xu, H. E. (2002) *Cell* **110**, 93-105
39. Nolte, R. T., Wisely, G. B., Westin, S., Cobb, J. E., Lambert, M. H., Kurokawa, R., Rosenfeld, M. G., Willson, T. M., Glass, C. K., and Milburn, M. V. (1998) *Nature* **395**, 137-143
40. Hur, E., Pfaff, S. J., Payne, E. S., Gron, H., Buehrer, B. M., and Fletterick, R. J. (2004) *PLoS Biol.* **2**, E274
41. Anzick, S. L., Kononen, J., Walker, R. L., Azorsa, D. O., Tanner, M. M., Guan, X. Y., Sauter, G., Kallioniemi, O. P., Trent, J. M., and Meltzer, P. S. (1997) *Science* **277**, 965-968
42. Gregory, C. W., He, B., Johnson, R. T., Ford, O. H., Mohler, J. L., French, F. S., and Wilson, E. M. (2001) *Cancer Res.* **61**, 4315-4319
43. Miyamoto, H., Yeh, S., Wilding, G., and Chang, C. (1998) *Proc. Natl. Acad. Sci. USA* **95**, 7379-7384
44. Linja, M. J., Porkka, K. P., Kang, Z., Savinainen, K. J., Janne, O. A., Tammela, T. L., Vessella, R. L., Palvimo, J. J., and Visakorpi, T. (2004) *Clin. Cancer Res.* **10**, 1032-1040
45. Bai, S., He, B., and Wilson, E. M. (2005) *Mol. Cell Biol.* **25**, 1238-1257
46. Bai, S., and Wilson, E. M. (2008) *Mol. Cell Biol.* **28**, 1947-1963
47. Jemal, A., Siegel, R., Ward, E., Hao, Y., Xu, J., and Thun, M. J. (2009) *CA Cancer J. Clin.* **59**, 225-249

48. Gregory, C. W., Hamil, K. G., Kim, D., Hall, S. H., Pretlow, T. G., Mohler, J. L., and French, F. S. (1998) *Cancer Res.* **58**, 5718-5724
49. Koivisto, P., Hyytinen, E., Palmberg, C., Tammela, T., Visakorpi, T., Isola, J., and Kallioniemi, O. P. (1995) *Am. J. Pathol.* **147**, 1608-1614
50. Tilley, W. D., Buchanan, G., Hickey, T. E., and Bentel, J. M. (1996) *Clin. Cancer Res.* **2**, 277-285
51. Culig, Z., Hobisch, A., Cronauer, M. V., Cato, A. C., Hittmair, A., Radmayr, C., Eberle, J., Bartsch, G., and Klocker, H. (1993) *Mol. Endocrinol.* **7**, 1541-1550
52. Gregory, C. W., Fei, X., Ponguta, L. A., He, B., Bill, H. M., French, F. S., and Wilson, E. M. (2004) *J. Biol. Chem.* **279**, 7119-7130
53. Grossmann, M. E., Huang, H., and Tindall, D. J. (2001) *J. Natl. Cancer Inst.* **93**, 1687-1697
54. Taplin, M. E., Bubley, G. J., Shuster, T. D., Frantz, M. E., Spooner, A. E., Ogata, G. K., Keer, H. N., and Balk, S. P. (1995) *N. Engl. J. Med.* **332**, 1393-1398
55. Tan, J., Sharief, Y., Hamil, K. G., Gregory, C. W., Zang, D. Y., Sar, M., Gumerlock, P. H., deVere White, R. W., Pretlow, T. G., Harris, S. E., Wilson, E. M., Mohler, J. L., and French, F. S. (1997) *Mol. Endocrinol.* **11**, 450-459
56. Steketee, K., Timmerman, L., Ziel-van der Made, A. C., Doesburg, P., Brinkmann, A. O., and Trapman, J. (2002) *Int. J. Cancer* **100**, 309-317
57. Prins, G. S. (2008) *Endocr. Relat. Cancer* **15**, 649-656
58. Wilson, E. M. (2003) *Pure Appl. Chem.* **75**, 1685-1697
59. Kelce, W. R., and Wilson, E. M. (1997) *J. Mol. Med.* **75**, 198-207
60. Monosson, E., Kelce, W. R., Lambright, C., Ostby, J., and Gray, L. E., Jr. (1999) *Toxicol. Ind. Health* **15**, 65-79
61. Wong, C., Kelce, W. R., Sar, M., and Wilson, E. M. (1995) *J. Biol Chem* **270**, 19998-20003
62. Kelce, W. R., Monosson, E., Gamcsik, M. P., Laws, S. C., and Gray, L. E., Jr. (1994) *Toxicol. Appl. Pharmacol.* **126**, 276-285
63. Gray, L. E., Jr., Ostby, J. S., and Kelce, W. R. (1994) *Toxicol. Appl. Pharmacol.* **129**, 46-5264.

64. Kelce, W. R., Stone, C. R., Laws, S. C., Gray, L. E., Kemppainen, J. A., and Wilson, E. M. (1995) *Nature* **375**, 581-585
65. Schwartz, C., Beck, K., Mink, S., Schmolke, M., Budde, B., Wenning, D., and Klemmner, K. H. (2003) *EMBO J.* **22**, 882-892
66. Wilson, V. S., Lambright, C., Ostby, J., and Gray, L. E., Jr. (2002) *Toxicol. Sci.* **70**, 202-211
67. Durhan, E. J., Lambright, C. S., Makynen, E. A., Lazorchak, J., Hartig, P. C., Wilson, V. S., Gray, L. E., and Ankley, G. T. (2006) *Environ. Health Perspect.* **114 Suppl 1**, 65-68
68. Sone, K., Hinago, M., Itamoto, M., Katsu, Y., Watanabe, H., Urushitani, H., Tooi, O., Guillette, L. J., Jr., and Iguchi, T. (2005) *Gen. Comp. Endocrinol.* **143**, 151-160
69. Carson, J. D., Jenkins, R. L., Wilson, E. M., Howell, W. M., and Moore, R. (2008) *Environ. Toxicol. Chem.* **27**, 1273-1278
70. Casanova, M., You, L., Gaido, K. W., Archibeque-Engle, S., Janszen, D. B., and Heck, H. A. (1999) *Toxicol. Sci.* **51**, 236-244
71. Chen, J. J., and Chang, H. C. (2007) *Prostate* **67**, 457-462
72. van der Bruggen, P., Traversari, C., Chomez, P., Lurquin, C., De Plaen, E., Van den Eynde, B., Knuth, A., and Boon, T. (1991) *Science* **254**, 1643-1647
73. Chomez, P., De Backer, O., Bertrand, M., De Plaen, E., Boon, T., and Lucas, S. (2001) *Cancer Res.* **61**, 5544-5551
74. Barker, P. A., and Salehi, A. (2002) *J. Neurosci. Res.* **67**, 705-712
75. De Plaen, E., Arden, K., Traversari, C., Gaforio, J. J., Szikora, J. P., De Smet, C., Brasseur, F., van der Bruggen, P., Lethe, B., Lurquin, C., Chomez, P., De Backer, O., Boon, T., Arden, K., Cavenee, W., Brasseur, R. (1994) *Immunogenetics* **40**, 360-369
76. Rogner, U. C., Wilke, K., Steck, E., Korn, B., and Poustka, A. (1995) *Genomics* **29**, 725-731
77. De Smet, C., De Backer, O., Faraoni, I., Lurquin, C., Brasseur, F., and Boon, T. (1996) *Proc. Natl. Acad. Sci. U S A* **93**, 7149-7153
78. Lurquin, C., De Smet, C., Brasseur, F., Muscatelli, F., Martelange, V., De Plaen, E., Brasseur, R., Monaco, A. P., and Boon, T. (1997) *Genomics* **46**, 397-408

79. Jurk, M., Kremmer, E., Schwarz, U., Forster, R., and Winnacker, E. L. (1998) *Int. J. Cancer* **75**, 762-766
80. Irvine, R. A., and Coetzee, G. A. (1999) *Immunogenetics* **49**, 585
81. Bai, S., Grossman, G., Yuan, L., Lessey, B. A., French, F. S., Young, S. L., and Wilson, E. M. (2008) *Mol. Hum. Reprod.* **14**, 107-116
82. Karpf, A. R., Bai, S., James, S. R., Mohler, J. L., and Wilson, E. M. (2009) *Mol. Cancer Res.* **7**, 523-535

Figure 1-1. Schematic of AR Functional Domains. Diagram of human 919 amino acid residues comprised of the NH₂-terminal FXXLF motif (²³FQNLF²⁷), activation function 1 (AF1) (residues 142-337), DNA binding domain (DBD) (residues 559-623) and activation function 2 (AF2) in the ligand binding domain (LBD) (residues 671-919).

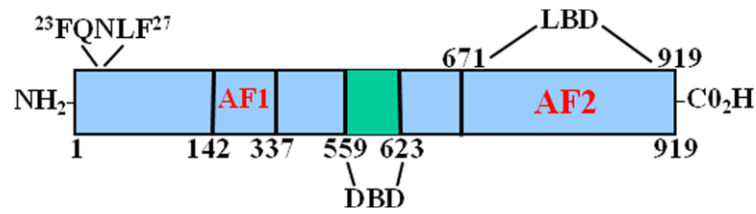


Figure 1-2. Testosterone (T) and Dihydrotestosterone (DHT). AR mediated gene expression is controlled by binding of the androgens, T and DHT. T has a double bond at the 4-5 carbons not present in DHT, the 5 α -reductase metabolite of T.

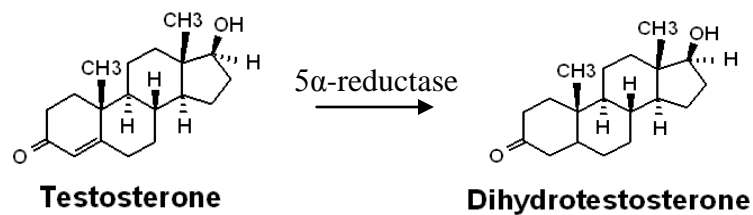
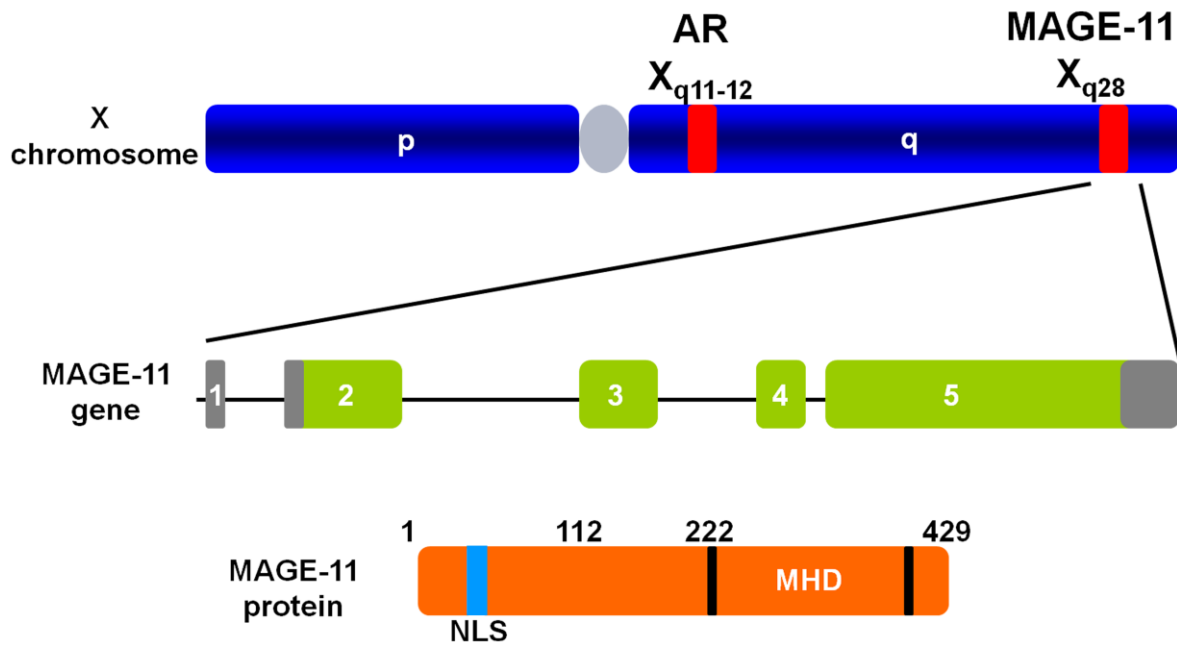


Figure 1-3. MAGE-11 Gene Structure and Protein. The MAGE-11 gene is on the long arm of the human X-chromosome (*blue*) at Xq28 and includes 5 exons, 4 of which are coding exons (*green*). The MAGE-11 gene translates into a 429 amino acid MAGE-11 protein (*orange*). Within the C-terminal region of MAGE-11 is the conserved MAGE homology Domain (MHD) (amino acids 222-421). MAGE also has an NH₂-terminal nuclear localization signal (NLS).



CHAPTER 2

MODULATION OF ANDROGEN RECEPTOR ACTIVATION FUNCTION 2 BY TESTOSTERONE AND DIHYDROTESTOSTERONE

Abstract

The androgen receptor (AR) is transcriptionally activated by high affinity binding of testosterone (T) or its 5α -reduced metabolite, dihydrotestosterone (DHT), a more potent androgen required for male reproductive tract development. The molecular basis for the weaker activity of T was investigated by determining T-bound ligand binding domain crystal structures of wild-type AR and a prostate cancer somatic mutant complexed with the AR FXXLF or coactivator LXXLL peptide. Nearly identical interactions of T and DHT in the AR ligand binding pocket correlate with similar rates of dissociation from an AR fragment containing the ligand binding domain. However, T induces weaker AR FXXLF and coactivator LXXLL motif interactions at activation function 2 (AF2). Less effective FXXLF motif binding to AF2 accounts for faster T dissociation from full-length AR. T can nevertheless acquire DHT-like activity through an AR helix-10 H874Y prostate cancer mutation. The Tyr-874 mutant side chain mediates a new hydrogen bonding scheme from exterior helix-10 to backbone protein core helix-4 residue Tyr-739 to rescue T-induced AR activity by improving AF2 binding of FXXLF and LXXLL motifs. Greater AR AF2 activity by improved core helix interactions is supported by the effects of melanoma antigen gene protein-11, an AR coregulator that binds the AR FXXLF motif and targets AF2 for activation.

We conclude that T is a weaker androgen than DHT because of less favorable T-dependent AR FXXLF and coactivator LXXLL motif interactions at AF2.

Introduction

The androgen receptor (AR) is a member of the nuclear receptor superfamily of ligand-activated transcription factors. Androgen activation of AR regulates prostate growth, bone and muscle mass, and spermatogenesis, and is a predisposing factor in prostate cancer. AR mediates transcriptional activity in response to two biologically active androgens that bind AR with similar high affinity (1). Testosterone (T) is the major circulating androgen secreted by the testis and the active androgen in muscle. Dihydrotestosterone (DHT), the 5 α -reduced metabolite of T, is a more potent androgen required for male reproductive tract development.

AR has a modular structure comprised of an NH₂-terminal transactivation domain, central DNA binding domain, linker hinge region and carboxyl-terminal ligand binding domain (LBD) (2). Like other nuclear receptor family members (3), AR has two major activation domains. Androgen induced AR transcriptional activity depends on activation function 1 in the largely un-structured NH₂-terminal region (2), and activation function 2 (AF2), a highly ordered hydrophobic surface in the LBD that requires androgen binding for its structural integrity (4).

The degree to which AF2 contributes to overall AR activity depends on multiple competing factors. Unlike other nuclear receptors, AR AF2 binds a number of LXXLL-related motifs. Important among these is the AR NH₂-terminal FXXLF motif ²³FQNL²⁷ that binds AF2 in an androgen dependent and specific manner. AR FXXLF motif binding to AF2 is the basis for the AR NH₂- and carboxyl-terminal N/C interaction (5-7) that contributes to

AR dimerization (8, 9) and is critical for AR regulation of androgen dependent genes (10-12). The functional significance of the AR N/C interaction *in vivo* is supported by the effects of several naturally occurring mutations that disrupt AR FXXLF motif binding and cause resistance to androgen without diminishing high affinity androgen binding (13-16). The androgen insensitivity syndrome results in varying degrees of incomplete masculinization of the external genitalia in genetic males depending on the extent to which the mutation disrupts AR function (17).

In addition to the AR FXXLF motif, multiple related motifs bind the AR AF2 site with relatively high affinity (18). FXXLF motifs are present in a number of putative AR coregulatory proteins and interact at AF2 (19, 20). Within the AR NH₂-terminal domain is a WXXLF motif that interacts with the AR AF2 site in the presence of androgen but with weaker affinity than the AR FXXLF motif (5, 10). Similar to other nuclear receptors, AR AF2 serves as the binding site for steroid receptor coactivator (SRC)/p160 coactivator LXXLL motifs. Crystal structures demonstrate overlapping binding sites for AR FXXLF and coactivator LXXLL motifs (4, 18). Based on peptide display screening (18, 20, 21) and binding affinity measurements (4), AR AF2 preferentially binds FXXLF motifs compared to coactivator LXXLL motifs. In addition, we have shown that androgen dependent AR FXXLF motif binding to AF2 in the AR N/C interaction competitively inhibits coactivator LXXLL motif binding (19).

The contribution of AF2 to AR transcriptional activity is also influenced by cell and tissue specific coactivators, some of which selectively increase accessibility of AF2 to coactivator recruitment. One mechanism proposed to increase AR AF2 activity in prostate cancer is higher levels of SRC/p160 coactivators that compete for the AR N/C interaction

and increase AR transcriptional activity through AF2 (10, 22). The AR coregulator melanoma antigen gene protein-11 (MAGE-11) of the MAGEA gene family binds the AR FXXLF motif to expose AF2 and increase coactivator recruitment (23). Naturally occurring AR somatic mutations in prostate cancer can increase AR activity by enhancing SRC/p160 coactivator recruitment to AF2 (7). The relative binding affinities and competitive relationships at the AF2 site suggest that high affinity androgen binding triggers sequential interactions of multiple coregulatory proteins.

In this report we provide biochemical and structural evidence that T is a less effective androgen than DHT because of weaker T dependent FXXLF and LXXLL motif binding at the AR AF2 surface. This conclusion is supported by a prostate cancer somatic mutation AR-H874Y that increases the transcriptional response to T in association with improved FXXLF and LXXLL motif binding at AF2. Crystal structure determination of T bound WT and H874Y AR LBD provided some insight into the possible differential molecular effects of T *versus* DHT. Receptor bound with T appears to induce isolated conformational heterogeneity at the AF2 surface. The AR H874Y mutation creates new direct hydrogen (H) bonds between core helix residues that probably contribute to the molecular basis for the described functional rescue by this prostate cancer mutant.

Materials and Methods

Plasmids—pCMVhAR vectors expressing full-length human AR with H874Y, E897K and K720A mutations (6, 14, 24) and AR507-919 which lacks the NH₂-terminal region (2) were described. Coding sequences for AR-(663-919) and AR-(663-919)-H874Y were inserted at the NdeI and BamHI sites of the pET-15b bacterial expression vector by PCR amplification of corresponding pCMVhAR mutant plasmids. GAL-AR-(658-919) and

H874Y, E897K and K720A mutants were created by PCR amplification of respective pCMVhAR plasmids and subcloning into Tth111I and XbaI digested pGAL0. GAL-AR-(640-919) was created by PCR amplifying the fragment from pCMVhAR and subcloning into NdeI and XbaI digested pGAL0. VP-AR-(1-660) (13), VP-TIF2-(624-1287) (VP-TIF2.1) (25), GAL-AR-(624-919) and H874Y, E897K and K720A mutants (7), prostate specific antigen-enhancer-luciferase (PSA-Enh-Luc) (26), mouse mammary tumor virus (MMTV)-Luc, 5XGAL4Luc3 (10) and pSG5-MAGE-11 coding for full-length MAGE-11 residues 1 to 429 (23) were described. All PCR amplified regions were verified by DNA sequencing.

Reporter Gene Assays—The CWR-R1 prostate cancer cell line derived from the CWR22 recurrent human prostate cancer xenograft (24, 27) was plated at 1.6 or 2×10^5 cells/well in 12 well plates in prostate cell growth medium containing Richter's improved minimal essential medium (Gibco) or Dulbecco's modified Eagle's medium (Gibco) supplemented with 5 ng/ml selenium, 10 mM nicotinamide, 5 μ g/ml insulin, 5 μ g/ml transferrin and 2% fetal bovine serum, and transfected using Effectene (Qiagen). Endogenous CWR-R1 cell AR-H874Y transcriptional activity was detected using 0.1 μ g/well MMTV-Luc reporter vector. AR AF2 activity was determined in CWR-R1 cells by transfecting 0.1 μ g WT or mutant GAL-AR-(624-919) or GAL-AR-(658-919) and 0.25 μ g 5XGAL4Luc3. For two-hybrid interaction assays, CWR-R1 cells were transfected with 50 ng VP-TIF2-(624-1287), WT or mutant GAL-AR-(624-919) and 0.1 μ g 5XGAL4Luc3. For 12 well plates, DNA was combined with (per well) 45 μ l transfection buffer (Qiagen) and 1 μ l Enhancer, vortexed and incubated for 5 min at room temperature. Effectene (1 μ l/well) was added, vortexed for 10 s, and incubated for 10 min at room temperature. Prostate cell growth

medium (0.2 ml) was added and vortexed, and 220 μ l DNA solution added to each well containing 1 ml of medium. The next day cells were washed with phosphate-buffered saline (PBS) and 1 ml phenol red-free, serum-free basic prostate medium containing Improved minimal essential Zinc Option medium (Invitrogen), and the indicated steroids were added per well. Cells were incubated at 37°C overnight, washed with PBS, and harvested in 0.25 ml lysis buffer containing 1% Triton X-100, 2 mM EDTA, and 25 mM Tris phosphate, pH 7.8. Cells were rocked at room temperature for 30 min in lysis buffer, and 0.1 ml cell lysate analyzed for luciferase activity using a Lumistar Galaxy (BMG Labtech) automated multiwell plate reader luminometer.

Human epithelial cervical carcinoma HeLa cells were maintained in Eagle's minimum essential medium supplemented with 10% fetal bovine serum (Gemini or HyClone), penicillin, streptomycin and 2 mM L-glutamine. For reporter gene assays, HeLa cells were plated at 5×10^4 cells/well in 12 well plates and 24 h later transfected using FuGENE-6 Transfection Reagent (Roche Applied Science) with 10 ng pCMVhAR or H874Y mutant and 0.25 μ g PSA-Enh-Luc reporter vector to determine androgen-induced AR transactivation. To measure AR AF2 activity, HeLa cells were transfected with 0.1 μ g GAL-AR-(658-919) and the H874Y mutant and 0.25 μ g 5XGAL4Luc3. For two-hybrid interaction assays, HeLa cells were transfected with 0.1 μ g 5XGAL4Luc3, 50 ng VP-AR-(1-660) or VP-TIF2-(624-1287), and 50 ng GAL-AR-(624-919), -(640-919), -(658-919), or GAL-AR-(624-919)-H874Y. DNA was added to 43 μ l serum-free medium and 0.6 μ l of FuGENE-6 reagent per well. After a 15 min incubation, 40 μ l of FuGENE/DNA mixture was added to each well containing 1 ml medium. The next day cells were washed with PBS, and 1 ml/well serum-free medium lacking phenol red containing the indicated steroids was added and incubated

overnight at 37°C. Twenty four hours later cells were washed with PBS and assayed for luciferase activity after harvesting in 0.25 ml lysis buffer as described above.

Monkey kidney CV1 cells were maintained in Dulbecco's modified Eagle's medium containing 10% bovine calf serum (HyClone), 2 mM L-glutamine, penicillin, streptomycin, and 20 mM Hepes, pH 7.2. Cells (4.2×10^5 /6 cm dish) were plated in medium containing 5% bovine calf serum and 24 h later transfected using calcium phosphate DNA precipitation (28). The effect of TIF2 on AR AF2 activity was determined by transfecting 5 µg 5XGAL4Luc3 and 0.1 µg GAL-AR-(624-919), GAL-AR-(658-919), or the H874Y mutants in the absence and presence of 2 µg pSG5-TIF2. The effect of MAGE-11 on AR transcriptional activity was determined by transfecting 0.1 µg of pCMVhAR or pCMVhAR-H874Y and 5 µg PSA-Enh-Luc in the absence and presence of 2 µg pSG5-MAGE-11 and 2 µg pSG5-TIF2. Cells were incubated overnight with and without the indicated androgens and the next day placed in serum-free medium in the absence and presence of androgen. After 24 h cells were washed with PBS, harvested in 0.25 ml lysis buffer, and assayed for luciferase activity as described.

Immunoblots—Relative expression levels of WT and mutant GAL-AR-(624-919), GAL-AR-(658-919), pCMVhAR, and pCMVhAR-(507-919) were determined by immunoblot analysis. COS-1 cells were plated at 2×10^6 cells/10 cm dish in 10% bovine calf serum (HyClone) in Dulbecco's modified Eagle's medium containing penicillin, streptomycin, 2 mM L-glutamine, and 20 mM Hepes, pH 7.2 and transfected using DEAE dextran (28). After 24 h, medium containing 1 µM MG132 (Sigma), a proteasome inhibitor, was added to cells expressing GAL-AR-(624-919) and GAL-AR-(658-919) and readed after an overnight incubation and incubated for 1 h. Cells were washed with 8 ml cold PBS,

harvested in 1 ml PBS, and solubilized in 0.1 ml RIPA buffer containing 1% Nonidet P-40, 0.5% sodium deoxycholate, 0.1% SDS, 1 mM dithiothreitol, 1 mM phenylmethylsulfonyl fluoride, and complete protease inhibitor mixture (Roche Applied Science). Protein concentrations were determined using the BioRad assay with bovine serum albumin as standard. Protein extracts were separated on a 10% acrylamide gel containing SDS and analyzed by immunoblot. GAL4 fusion proteins were detected using rabbit polyclonal anti-GAL antibody (Santa Cruz Biotechnology) at 1:500 dilution. AR was detected using rabbit polyclonal AR52 immunoglobulin G (29) at 2 µg/ml. Incubations with primary antibody were for 1 h at room temperature. Anti-rabbit horseradish peroxidase-conjugated secondary IgG antibody (Amersham Biosciences) was used at 1:10,000 dilution for 1 h at room temperature. Signals were detected using chemiluminescence (SuperSignal West Dura Extended Duration Substrate, Pierce).

Androgen Dissociation Rate Assays—Ligand dissociation rate studies were performed at 37°C in whole cell binding assays by plating 4×10^5 COS cells/well of 6-well plates and transfecting 1 or 2 µg pCMVhAR, pCMVhAR-(507-919), or H874Y mutant per well using DEAE-dextran (28). Transfected cells were incubated for 2 h at 37°C in 0.6 ml serum-free medium lacking phenol red and containing 5 nM [1,2,6,7-³H]T (78.5 Ci/mmol) or 3 nM [1,2,4,5,6,7-³H]DHT (124 Ci/mmol). Nonspecific binding was determined in parallel wells by adding 100 fold molar excess of unlabeled androgen. Timed dissociation rates were determined by amending to 50 µM T or 17 α -methyltrienolone (R1881) (PerkinElmer Life Sciences) to the labeling media added in 0.1 ml of medium. Cultured cell incubations at 37°C were terminated at different times and cells were washed with PBS, harvested in 0.5 ml lysis buffer containing 2% SDS, 10% glycerol and 20 mM Tris, pH 6.8, and radioactivity was

determined by scintillation counting. Dissociation half-times were determined as the mean \pm S.E. time required to reduce specific androgen binding by 50%.

Protein Preparation—Crystallography grade AR LBD (human AR residues 663-919) and AR-H874Y LBD with an NH₂-terminal His₆ tag and thrombin cleavage site were expressed from pET-15b in BL-21 DE3 *Escherichia coli*. Cells were grown overnight at 18°C in 2X YT bacterial growth medium (16 g/liter Tryptone-B, 10 g/liter yeast extract-B, 5 g/liter NaCl₂, Bio101 Systems, Q-Biogene) containing 0.1 g/liter carbenecillin (Sigma), 1 mM isopropyl thiogalactopyranoside, and 0.5 mM T added from a 347 mM stock in dimethyl sulfoxide. Cells resuspended in urea extraction buffer (50 ml of 25 mM Tris, pH 8.0, 0.3 M NaCl₂, and 2 M urea per 10 g cells) were lysed with an APV LAB 1000 homogenizer and centrifuged at 40,000 rpm for 45 min at 4°C. The supernatant was loaded onto a Ni²⁺-charged immobilized nickel metal affinity Sepharose column (ProBond, Invitrogen) equilibrated with 25 mM Tris, pH 8.0, 0.3 M NaCl₂, and 50 mM imidazole. A linear gradient to 1 M imidazole with 25 mM Tris, pH 8.0, and 0.3 M NaCl₂ was used to elute the AR LBD. Pooled fractions were amended with thrombin (5 NIH units/mg protein, Sigma) and NaCl₂ to ~0.4 M and dialyzed (15,000 molecular weight cut off, Spectra/Por membrane) overnight at 4°C against a buffer containing 10 μ M T, 25 mM Tris, pH 8.0, 0.4 M NaCl₂, 5 mM DTT, 2 mM EDTA, and 10% glycerol. The digested AR LBD was diluted 8-fold with 25 mM Hepes, pH 7.5, 50 mM NaCl₂, 5 mM DTT, 2 mM EDTA, and 10% glycerol and immediately loaded onto a 5 ml HiTrap SP-HP-Sepharose ion exchange column, washed with dilution buffer and eluted using a linear gradient to 1 M NaCl₂ with 25 mM Hepes, pH 7.5, 5 mM DTT, 2 mM EDTA, and 10% glycerol. Samples containing AR LBD were combined, amended to 10 μ M T and 0.5 M NaCl₂, and concentrated with a Centriprep centrifugal filter unit (Amicon) to <10 ml. Size

exclusion chromatography was performed on the concentrated pooled ion exchange chromatography purified fractions using a HiLoad Superdex S75 (26/60) size exclusion column (GE Healthcare). Purified AR LBD was eluted with buffer containing 10 μ M T, 25 mM Hepes, pH 7.5, 0.15 M Li_2SO_4 , 10 mM DTT, 0.5 mM EDTA, and 10% glycerol and concentrated to 2-4 mg/ml using a Centriprep centrifugal filter unit. The final sample buffer contained 10 μ M T, 25 mM HEPES, pH 7.5, 0.15 M Li_2SO_4 , 10 mM DTT, 0.5 mM EDTA, 10% glycerol, and 0.05% β -n-octoglucoside.

Fluorescence Polarization Measurements of Peptide Binding Affinity—Fluorescence binding studies were performed using WT AR LBD and AR-H874Y LBD expressed in *E. coli* in the presence of 0.5 mM T or 50 μ M DHT. Protein was purified as described above except AR LBD–DHT thrombin digestion and overnight dialysis were not performed, and DHT was not readded during purification. Protein was concentrated to 0.6-3 mg/ml using Centriprep centrifugal filter units in buffer containing 10 μ M T or DHT, 0.15 M Li_2SO_4 , 10 mM DTT, 0.5 mM EDTA, 10% glycerol, 0.05% β -n-octoglucoside, and 25 mM HEPES, pH 7.5. AR FXXLF and TIF2 LXXLL peptide binding affinities were determined by fluorescence polarization at room temperature for 1 h using 5-40 μ M AR LBD and AR-H874Y LBD purified in the presence of 10 μ M ligand and assayed with and without addition to 40 μ M DHT or T and 10 nM AR-20-30 fluorescein-RGAFQNLFQSV or TIF2 third LXXLL motif 732-756 fluorescein-QEPVSPKKKENALLRYLLDKDDTKD (Synpep, Dublin, CA). As a control, human estrogen receptor- β (ER β) LBD (residues 257-530) was analyzed in parallel in the presence of 40 μ M estradiol (E_2). Fluorescence polarization values were determined using an Envision (PerkinElmer Life Sciences) fluorescence plate reader with 485 nm

excitation and 520 nm emission filters. Binding isotherms were constructed and K_D values determined by nonlinear least-squares fit based on a 1:1 interaction (30).

Crystallization and Data Analysis—Concentrated solutions of purified AR-H874Y LBD and AR LBD complexed with T and amended with 2-3 M excess of AR-(20-30) FXXLF motif peptide RGAFQNLFQSV or TIF2-(740-753) LXXLL-III motif peptide KENALLRYLLDKDD were used to obtain diffraction grade crystals. Vapor diffused hanging drops at 22°C with a 1:1 (v/v) ratio of the AR complex and the precipitant solution produced ~150-200 μm crystals within 3-15 days. Salt solutions containing 0.6 M sodium-potassium tartrate and Bistris propane, pH 7.0 or Tris, pH 8.5, were used as precipitants. Prior to flash freezing in liquid N_2 , crystals were transiently mixed with a cryoprotectant solvent consisting of precipitant solution amended to 20% glycerol. X-ray diffraction data were collected at 100 K with an ADSC 210 detector at the IMCA-CAT, sector 17ID, or a MAR225 CCD detector at the SER-CAT, sector 22BM at the Advanced Photon Source synchrotron. Diffraction data were integrated and scaled with HKL2000 (31).

Structure Determination and Refinement—An initial model for the T-bound AR-H874Y LBD with AR-(20-30) peptide data was determined by molecular replacement with MolRep (32, 33) and the AR LBD coordinates from the AR-DHT structure (34) (Protein Data bank access code 1I37). The convincing solution contained a single AR LBD complex in the asymmetric unit that had excellent quality 1.8 \AA resolution electron density for T and the respective peptide. Multiple cycles of manual model building with COOT (35) and maximum likelihood restrained refinement with all hydrogens was performed with Refmac (36) in all cases. Initial models for the remaining data sets were determined and refined in a similar manner. Table 2-3 summarizes the crystallographic and refinement statistics.

Coordinate files with hydrogens were generated with MolProbity (37). To eliminate possible slight differences arising from variation in AF2 helix position, backbone heavy atoms for AR chain A LBD residues 680-890 were used for structure superimposition and performed with the CCP4i LSQAB utility using coordinates without hydrogens. Reported interatomic distances are between heavy atoms unless specified, and the angles with protons when necessary were measured with COOT or PyMol. Structure figures were generated with PyMol from Delano Scientific.

Results

AF2 Activation by T and DHT—To investigate the differential effects of T and DHT on AR AF2 activity, we performed studies using WT AR and a prostate cancer somatic mutant AR-H874Y that has an increased transcriptional response to T (7, 24). To optimize detection of AR AF2 activity, we varied the length of the hinge region of several AR LBD–GAL4-DNA binding domain fusion proteins expressed in several cell lines (Fig. 2-1A). In CV1 cells, T and DHT increased TIF2-dependent GAL-AR-(658-919) activity to a greater extent than GAL-AR-(624-919), indicating inhibition by hinge residues that include the AR nuclear targeting signal (38) (Fig. 2-1C). The H874Y mutation increased androgen sensitivity and overall transcriptional activity but remained dependent on ligand and coexpression of TIF2 (Fig. 2-1C).

Transcriptional activity of GAL-AR-(624-919), -(640-919) and -(658-919) was also low in HeLa cells without coexpression of TIF2 (Fig. 2-1D). In two-hybrid assays, GAL-AR-(640-919) and GAL-AR-(658-919) interacted to a greater extent than GAL-AR-(624-919) with VP-AR-(1-660) indicative of the AR N/C interaction and with VP-TIF2-(624-1287) reflecting coactivator LXXLL motif binding to AF2 (Fig. 2-1D) (4-8).

Androgen-dependent AF2 activity of GAL-AR-(658-919) was stronger in the CWR-R1 prostate cancer cell line and was detected independent of coexpressed TIF2 (Fig. 2-1E). Activity of GAL-AR-(658-919) was greater than GAL-AR-(624-919), and the H874Y mutation increased the response to T. Differences in transcriptional activity did not result from differences in protein expression (Fig. 2-1B) and was AF2-dependent since charge clamp mutants K720A and E897K eliminated the response (Fig. 2-1F).

Thus, differential effects of T and DHT on WT and H874Y AR AF2 activity were evident in CWR-R1 cells using GAL-AR-(658-919), which avoided the inhibitory effects of AR hinge residues ⁶²⁴MTLGARKLKKLGNLKL⁶³⁹ (39) (AR nuclear targeting signal underlined) (38).

Increased AR-H874Y AF2 Activation by T and Adrenal Androgens—The magnitude and dose response of GAL-AR-(658-919)-H874Y AF2 activity by T in CWR-R1 cells were similar to DHT but less than the WT with T (Figs. 2-1E and 2-2A). GAL-AR-(658-919)-H874Y activity was also greater with 4-androstene-3,17-dione compared to WT. Androstenediol activated WT and H874Y GAL-AR-(658-919) equivalent to WT with T.

In HeLa cells, the predominant effect of the H874Y mutation was also increased sensitivity to T (Fig. 2-2B), whereas GAL-AR-(658-919) and the H874Y mutant responded similarly to DHT. We noted a lack of transcriptional response by GAL-AR-(658-919) to androstenediol in HeLa cells, which contrasted equivalent activity by androstenediol and T in CWR-R1 cells. Two-hybrid studies suggested that the greater activity by androstenediol in CWR-R1 cells resulted from metabolism to an active androgen (data not shown).

Full-length endogenous AR-H874Y in CWR-R1 cells does not activate the PSA-Luc reporter (40) but activates MMTV-luciferase in response to T and DHT and higher

concentrations of androstenedione and androstanediol (Fig. 2-3A). Transiently expressed AR and AR-H874Y in CWR-R1 cells activate PSA-Luc in response to T and DHT, and adrenal androgens were more effective with AR-H874Y (data now shown). In HeLa cells, AR-H874Y lacked constitutive activity but increased the response to T with less differential effects by DHT, androstenedione, and androstanediol (Fig. 2-3B).

The results in both CWR-R1 and HeLa cell lines suggest that the predominant effect of the H874Y mutation is to increase the AF2 response to T. Our ability to detect AR AF2 activity in CWR-R1 cells but not HeLa or CV1 cells without coexpression of TIF2 likely reflects higher endogenous SRC/p160 coactivator levels in CWR-R1 cells that endogenously express the AR-H874Y mutant (40).

Preferential AF2 Activation by MAGE-11—MAGE-11 is an AR coregulator expressed in prostate cancer cell lines and in normal tissues of the human male and female reproductive tracts (23). MAGE-11 binds the AR NH₂-terminal FXXLF motif and increases AF2 by inhibiting the AR N/C interaction. To gain further evidence that AR-H874Y increases AF2 activity in response to T, we determined the effect of MAGE-11 with and without coexpression of TIF2 using a PSA-luciferase reporter.

Coexpression of TIF2 had minimal effects on AR and AR-H874Y activity (Fig. 2-4) in agreement with the inhibitory effects of the AR N/C interaction on coactivator recruitment by AF2 (28). Coexpression of MAGE-11 with and without TIF2 preferentially increased AR-H874Y activity in response to T compared to WT AR and AR-H874Y with DHT. AR-H874Y activity induced by T and DHT was nearly equal in the presence of MAGE-11 with or without TIF2. This contrasts WT AR where DHT induced greater activity than T in the presence of MAGE-11 with or without TIF2. Coexpression of MAGE-11 also increased

ligand independent activity of AR-H874Y more than WT AR. Differences in transcriptional activity were independent of differences in protein expression levels based on immunoblot analysis (see Fig. 2-6B). The preferential effects of MAGE-11 on T dependent AR-H874Y activity suggest that H874Y imparts DHT-like activity to T by increasing coactivator recruitment to AF2.

FXXLF and LXXLL Motif Binding Affinities—Binding isotherms calculated by fluorescence polarization indicate WT AR LBD–DHT binds the AR FXXLF peptide with ~2-fold higher affinity than WT AR LBD–T with no significant change by the H874Y mutation (Fig. 2-5; Table 2-1). Similar results were observed for the TIF2 LXXLL peptide except overall binding affinities were weaker than the FXXLF peptide. ER β LBD–E₂ bound the TIF2 LXXLL peptide with higher affinity than the FXXLF peptide as reported previously (4). The data suggest a direct differential effect of T and DHT on AF2 motif binding affinity that is not altered by the H874Y mutation.

T and DHT Dissociation Kinetics—The prostate cancer mutation H874Y slows the dissociation rate of synthetic androgen R1881 from AR and AR-(507-919), a carboxyl-terminal fragment that lacks the AR NH₂-terminal domain (7). To investigate the similar AR-H874Y AF2 activity induced by T and DHT, we determined androgen dissociation half-times from WT and H874Y full-length AR and AR-(507-919) containing the DNA binding domain and LBD, which expressed similarly on immunoblots (Fig. 2-6B).

T dissociates 3-4 times faster than DHT from full-length WT AR (Fig. 2-6A; Table 2-2) (1) but with a similar rate as DHT from AR-(507-919) (Table 2-2), suggesting similar steroid contacts in the ligand binding pocket. T dissociates 3-4 times slower from AR-H874Y than from WT AR at a rate similar to DHT dissociation from AR and AR-H874Y. The

dissociation rate of T and DHT from AR-(507-919)-H874Y was ~2 fold slower than from WT AR-(507-919).

The data indicate that slow dissociation of DHT from full-length WT AR results predominantly from interactions outside the ligand binding pocket, and H874Y has effects inside and outside the binding pocket. The similar half-time of T dissociation from AR-H874Y to DHT from AR and AR-H874Y parallel AF2 transcriptional activities (see Figs. 2-1 and 2-2) and provide further evidence that H874Y imparts DHT-like activity to T by increasing the transcriptional activity of AF2.

T-bound WT AR LBD and AR-H874Y LBD Structures—We determined the crystal structures of WT and H874Y AR LBD bound with T in the presence of the AR-(20-30) NH₂-terminal FXXLF motif peptide or TIF2 coactivator peptide TIF2-(740-753) third LXXLL motif. Crystallographic refinement data are provided in Table 2-3. Globally, all four structures conform to the canonical nuclear receptor LBD fold (Figs. 2-7A and 2-7B) and when superimposed are nearly identical based on r.m.s.d. statistics for the *xyz* displacement relative to the WT AR LBD–T–FXXLF coordinates (0.26Å for WT AR LBD–T–LXXLL, 0.14Å for AR-H874Y LBD–T–FXXLF, and 0.27Å for AR-H874Y LBD–T–LXXLL). Globally, the structures concur with previously reported structures for WT AR LBD bound to DHT and R1881 and prostate cancer mutants AR-T877A LBD and AR-W741L LBD bound to steroid and nonsteroid ligands (4, 18, 34, 41-45). Our WT AR LBD–T structures with AR FXXLF (Protein Data Base access code 2Q7I) or TIF2 LXXLL (Protein Data Base 2Q7J) peptide superimpose to the DHT-bound structures with FXXLF (Protein Data Base 1TR7) or LXXLL (Protein Data Base 1T63) peptide (see Fig. 2-9) with an r.m.s.d. of 0.27Å and 0.3Å and to WT AR LBD–S-1 (Protein Data Base 2AXA) and AR-W741L LBD–bicalutamide

(Protein Data Base 1Z95) with an r.m.s.d. of 0.37Å and 0.31Å, respectively. Consistent with the AR LBD–R1881 (4) and DHT peptide bound structures (18, 42), the LXXLL motif in the T-bound structures is carboxyl-terminally shifted along the helical axis relative to the FXXLF peptide, and Leu-745 and Leu-749 lie in register with Phe-23 and Phe-27 (Fig. 2-7A). The AR-(20-30) FXXLF peptide H-bonds to conserved charge clamp residues Glu-897 and Lys-720 required for AR AF2 activity (6). The NH₂-terminus of the LXXLL peptide fails to H-bond with Glu-897 and maintains the carboxyl-terminal shift, motif registry, and interaction to Lys-720 as shown for the AR LBD bound to R1881 (4) (Figs. 2-7A, 2-7B and 2-7C). The T-bound ligand binding pockets are essentially identical to each other and nearly identical to the DHT-bound AR LBD structures (34, 42) (Figs. 2-7C and 2-7D, and Table 2-4).

WT AR LBD–T–FXXLF and LXXLL–There were no major structural differences to thoroughly account for the noted physiologic differences between T and DHT. For both, the steroid A-ring lies near the side chain of Arg-752, a conserved helix-5 residue required for ligand binding (Fig. 2-8) (41, 43, 44). In the T-bound WT AR LBD–FXXLF structure, we observed a 3.0Å interatomic distance between the steroid 3-keto O and Arg-752 side chain atom N-η₂ and measured a 126° angle subtended by atoms Arg-752 N-η₂, H- η₂₂ and the T 3-keto O (Fig. 2-8A and Table 2-4). Although the 3.0Å distance supports the presence of a direct H-bond with Arg-752, the angular displacement is less than the optimal 180° angle and only slightly more favorable than the 110°, 3.0Å H-bond of DHT-AR LBD (Protein Data Base 1T63) (Figs. 2-8B and 2-8C).

Also located near the steroid A-ring is conserved structural water HOH1, which ideally could mediate up to 4 local H-bonds. However, 3 possible H-bond donors are side chain protons bonded to Arg-752 (N-η₁ and N-η₂) and Gln-711-A (N-ε₂). Three possible H-

bond acceptors are Gln-711 (A) (O- ϵ 1), the backbone carbonyl oxygen of Met-745 and the 3-keto O (Fig. 2-8A). Of these 6 atoms, the Arg-752 N- η 2, Gln-711 N- ϵ 2 and Met-745 backbone carbonyl oxygen align closest to 3 of 4 angles dictated by the tetrahedral geometry of water and leaves open the possibility for HOH1 to donate an H-bond to the T 3-keto O. The likelihood of an HOH1 to 3-keto O H-bond is indicated by the reduced interatomic distance of 3.2Å compared to 3.5Å in DHT-bound structures (Protein Data Base 1T63 and 1I37), the planar Δ 4,5 double bond of T which positions the 3-keto O closer to HOH1, and the more negative charge character to the 3-keto O than the nonpolar neutral 3-keto O of DHT. The HOH1 to 3-keto O C3 vector of 117° is nearly colinear to 120° sp^2 electrons on the 3-keto O in favor of the HOH1 O-H vector. Although invoking an HOH1 to T 3-keto O H-bond forms a narrow 80° angle between the 3-keto O, HOH1 O, and Met-745 carbonyl oxygen atoms that violates the ideal tetrahedral water geometry, the superior hydrophilic properties of the T A-ring relative to DHT increase the propensity of T to accept this second H-bond through the fourth coordination of HOH1. Better H-bonding by T appears to also slightly reduce the distance between HOH1 and the Met-745 backbone carbonyl (2.7Å) relative to DHT (2.9Å).

On the D-ring of T, the 17 β -hydroxyl group accepts an H-bond from the helix-10 Thr-877 side chain and donates an H-bond to helix-3 Asn-705 O- δ 1 (Figs. 2-7C and 2-9) as reported for DHT and R1881 (4, 34). The Asn-705 side chain amine in turn H-bonds to the backbone carbonyl of Glu-890 in the linker between helix-11 and 12 (not shown). In the vicinity of the A-B-ring juncture, the C-19 bridgehead methyl group of T divides the hydrophobic space between Met-745 and Trp-741 as in the AR LBD–DHT structures and

maintains the Trp-741 indole ring nitrogen rotated toward the conserved structural water (HOH3 in our WT AR structures) and residue 874.

Summarized here are amino acid residues in our T-bound structures where positive $3\sigma F_o - F_c$ electron density warranted the addition of a second side chain conformation or a sulfate ion. Occupancy for the A and B side chain conformers was to ~50% each, except for Gln-711, which was estimated as 80% A and 20% B at best: WT-T-FXXLF-Leu-712, Ser-740, Cys-806, Met-807, Ser-814, Ile-815, Met-895 and two sulfates; WT-T-LXXLL-Glu-678, Gln-711, Leu-712, Asn-727, Met-780, Cys-806, Ile-841, Met-895,, and one sulfate; H874Y-T-FXXLF-Gln-711, Leu-712, Met-780, Cys-806, Ile-841, Met-895 and two sulfates; H874Y-T-LXXLL-Glu-678, Glu-709, Leu-712, Arg-726, Cys-806 and Met-895. Most notable among these is helix-3 Gln-711 near HOH1, the next sequential residue to Leu-712 which contacts $i+1$ of the bound peptide motif, and helix-12 Met-895 which lies proximal to Leu-712 but more distal to the $i+1$ residue of the bound peptide and the steroid A-ring (Fig. 2-10). We also observed in each structure, but do not illustrate, a glycerol that derives from the protein buffer solution that binds above the Gln-711 side chain. It is unclear whether these alternate conformers are crystallization artifacts, or as for Gln-711, arise from the presence of glycerol. Others such as Leu-712 or Met-895 may represent conformational freedom arising from a protein- or ligand mediated mechanism.

AR H874Y LBD-T-FXXLF and LXXLL—We noted a more definitive structural change in our analysis of the AR-H874Y mutant LBD bound to T and AR FXXLF (Protein Data Base access code 2Q7K) or TIF2 LXXLL (Protein Data Base 2Q7L) peptide. Side chains of exterior helix-10 WT residue His-874 (Fig. 2-10A) and H874Y mutant residue Tyr-874 (Fig. 2-10B) occupy space in a second shell of residues that surround Met-742, a first shell interior

helix-5 residue that contributes to the hydrophobic core and whose side chain lies adjacent to the steroid C-ring in the binding pocket. Side chains for Met-742 and third shell AF2 helix residues Val-903, Ile-906, and Leu-907 located above residue 874 are virtually superimposed atom for atom in the WT and H874Y structures (Fig. 2-10D), and the Met-742 side chain clearly conforms to a single orientation for WT and H874Y AR. This overall WT AR configuration allows structural HOH3 to mediate an H-bond network from the His-874 side chain (N- ϵ 2) to the Met-742 backbone carbonyl and continues through HOH4 to the helix-4 Tyr-739 backbone carbonyl (Fig. 2-10A).

Despite the bulkier phenyl hydroxyl group, Tyr-874 in the H874Y mutant appears easily accommodated with no major rearrangement of neighboring helices or side chains (Figs. 2-10B and 2-10C). Tyr-874 supplies a larger side chain that extends more than 2Å further towards helix-5 and displaces HOH3 with its phenolic hydroxyl group and presents a definitive change in H-bonding scheme. The helix-10 Tyr-874 phenolic oxygen can accept a direct 3.4Å H-bond from the backbone amide of helix-5 Met-742 at a favorable angle of 120° (Tyr-874 C- ζ , O- η to Met-742 N) that closely aligns the Met-742 amide N-H bond vector to the assumed 120° sp^2 electrons of the Tyr-874 O- η atom. In turn the Tyr-874 hydroxyl proton donates a 2.8Å direct H-bond to the backbone carbonyl of helix-4 Tyr-739 at a favorable angle of 121° (Tyr-874 O- η to Tyr-739 O, C) that closely aligns with the assumed 120° sp^2 electrons of the Tyr-739 carbonyl O atom. It is noteworthy that helix-4 residue Tyr-739 is adjacent to Gln-738, a residue whose side chain lies adjacent to the $i+1$ residue and displays different conformations with induced fit binding to the FXXLF or LXXLL motif and can participate in an H-bond network that links the helix-4 Met-734 CO to Lys-905 through the Gln-738 and Gln-902 side chains (Fig. 2-10D). The Tyr-874 phenyl presents more favorable

side chain chemistry to engage C- δ 2 and C- ϵ 1 in hydrophobic interactions with Val-903 C- γ 2 (3.5Å) and Ile-906 C- δ 1 (3.4Å) than the heterocyclic imidazole ring of WT His-874 (4.0Å from C- δ 2 to Val-903 C- γ 2 and 3.7Å from C- ϵ 1 to Ile-906 C- δ 1) (Fig. 2-10D). The nearly identical T-bound crystal structures reveal that restored activation by T-bound AR-H874Y is not directly ligand mediated or accompanied by T-induced structural rearrangement and must be driven by the H874Y mutation.

Discussion

AR activation by T and DHT–AR is unique among the family of steroid hormone receptors by having two biologically active high affinity hormones that differ in physiological potency. DHT is a morphogen required for male sexual developmental, whereas T is the major androgen in muscle and is anabolic at puberty. Normal levels of T without conversion to DHT fail to stimulate complete male genital development of the human fetus. This is evident from the human 5 α -reductase syndrome caused by a genetic defect in the enzyme that converts T to DHT (46). Activity differences between T and DHT cannot be explained by differences in transcription targets since there is no compelling evidence for differentially regulated gene sets, nor are they explained by the often reported different AR binding affinities for T and DHT. True equilibrium binding conditions may not be uniformly established, because the ligand-free AR and AR bound to T are more susceptible to degradation than AR bound to DHT leading to over-estimation of T binding affinity. By measuring association and dissociation rate constants and accounting for AR instability in the absence and presence of ligand, T and DHT equilibrium binding affinities are similar (1). Nevertheless, a ~10 fold higher concentration of T is required to achieve the AR mediated transcriptional effects of DHT (47). A DHT-like transcriptional response by

higher concentrations of T is supported by the 5 α -reductase gene knockout mouse where a compensatory rise in circulating T levels results in masculinization at birth (48).

Masculinization in humans with 5 α -reductase deficiency occurs at puberty when circulating T levels increase (49).

In this study we sought to elucidate the molecular basis for the different activities of T and DHT. Our biochemical data show that relative to DHT, T is a less potent androgen because of weaker FXXLF and LXXLL motif interactions at AF2 which are increased by the H874Y mutation. T and DHT dissociate with similar rates from AR-(507-919) but T dissociates ~3 times faster than DHT from WT AR and considerably slower from AR-H874Y. These results indicate that weaker AR FXXLF motif binding to AF2 results in the more rapid dissociation of T. Conversely, stronger AR FXXLF motif binding slows DHT dissociation from WT AR and T and DHT dissociation from AR-H874Y. Weaker interactions at AF2 thus appear to explain the reduced androgenic activity of T.

The similar LBD crystal structures of T-bound WT AR LBD with AR FXXLF or TIF2 LXXLL peptide to that of DHT (18, 34, 42) provide only subtle clues how these chemically similar ligands transmit different signals to the AF2 surface. Our structural data suggest that differences in A-ring H-bonding alter the conformational freedom of neighboring AF2 floor residue Leu-712. Structures of T-bound AR-H874Y indicate a gain-of-function arising not from chemical differences between T and DHT or altered motif binding affinity, but from replacement of a water mediated H-bond network with direct H-bonds between external helix-10 Tyr-874 side chain and internal helix-4 Tyr-739 and helix-5 Met-742 backbone atoms. For both WT AR and AR-H874Y, small changes in H-bonding have measurable effects on motif binding at AF2 and ultimately AR transcriptional activity.

Chemical Properties of T and DHT—T is the major circulating male hormone and like DHT has 19 carbons and differs only by a $\Delta_{4,5}$ double bond in ring A. With two fewer protons than the saturated ring A of DHT, the $\Delta_{4,5}$ double bond of T polarizes the region and increases the negative charge at the 3-keto O and positive charge at carbon 5. Based on Coulomb's law for simple electrostatic interactions (50), these properties of T impart greater H-bonding potential that accounts for its 10 fold greater water solubility than DHT. However, water solubility and inherent hydrophilicity and hydrophobicity do not explain androgen retention times in the binding pocket because T, DHT, and R1881 dissociate with similar rates from an AR fragment containing the LBD, and R1881 dissociates from AR at a rate intermediate between T and DHT (7). Water solubility and dissociation rate of R1881 are further influenced by a 17-methyl group on ring D that introduces more hydrophobic character to a hydrophobic pocket near Met-780, Leu-704 and Leu-701.

In the same sense, the saturated non-polar ring A of DHT is more chemically compatible with the hydrophobic environment of proximal ligand binding pocket residues than the unsaturated polar A-ring of T. Phe-764 is a conserved hydrophobic residue among steroid receptors (41) along with Val-746, Met-749, Leu-704, and Leu-707 that contact the bound ligand. Compared to T, the greater hydrophobic character and complementary shape of the DHT A-ring cannot explain the slower dissociation rate of DHT from full-length AR since T and DHT dissociate with similar rates from AR-(507-919). On the other hand, the saturated A-ring of DHT may more effectively increase AR AF2 activity by stabilizing the LBD core for higher affinity motif interactions.

Counterintuitive Hypothesis for T and DHT Activity—Modulation of FXXLF or LXXLL motif binding at AF2 by T and DHT relies on a conserved H-bond between Arg-752

N- η 2 and the steroid 3-keto O which is influenced by the Δ 4,5 double bond in T that imposes a more planar nature to the double bond side of ring A. Our T structures display a 3.0Å H-bond heavy atom distance from the ring-A 3-keto O to Arg-752 the same as DHT, but an angle from the more planar A-ring of T (126°) that is slightly more favorable for H-bonding than the chair configuration in DHT (110°) (Figs. 2-8A, 2-8B and 2-8C). This contrasts a recent report indicating a better Arg-752 to 3-keto O H-bond for DHT than T (51).

Ring A chemistry also influences a network of H-bonds through structural water HOH1 that is centrally positioned between ring A of T and key residues in AF2 backbone helices 3 and 5. HOH1 can accept a proton from side chains of helix-5 Arg-752 (3.0Å) and helix-3 Gln-711 (2.6Å) and donate a proton to the backbone carbonyl of helix-5 Met-745 (2.7Å). Based on the distance and angular relationships, these H-bond interactions for bound T and DHT satisfy 3 of 4 possible tetrahedral coordinates to water (52). T appears more likely than DHT to also accept an H-bond from HOH1 because of the more planar Δ 4,5 double bond in ring A positions the 3-keto O of T 0.3Å closer to HOH1 and the greater negative charge centered on the 3-keto O of the dipolar A-ring. The 117° angle for the assumed HOH1 O-H bond vector of T aligns well with the 120° sp^2 3-keto O electrons compared to 100° for DHT (53). The polar nature and superior hydrophilic properties of the T A-ring over DHT may favor the coexistence of donated H-bonds from HOH1 to the 3-keto O and Met-745 despite formation of a non-ideal, constrained 80° angle (T 3-keto O, HOH1, Met-745 O) within the tetrahedral geometry of HOH1.

Our results suggest the counterintuitive hypothesis that greater H-bonding by T is detrimental to agonist activity. With shorter distances between HOH1 and the 3-keto O and Met-745 carbonyl and the negative charge character of its 3-keto O, the polarized A-ring of T

may over-constrain the geometry and introduce unfavorable hydrophilic character into the hydrophobic environment of the binding pocket. The T $\Delta_{4,5}$ polarized double bond is located in a hydrophobic region bounded by Met-745, Phe-764, Met-749, and Val-746, within 5Å of the Met-745 to Val-746 amide bond. This introduces a polar atom mismatch with the 3-keto O being 3.8Å to the Met-745 O and the presumably positive T C-5 atom within 5Å of the Val-746 NH. In contrast, through changes also not evident in the crystal structures, it was recently suggested that a novel high affinity nonsteroidal AR modulator may influence AF2 activity by engaging more favorable hydrophobic π -bonding to Phe-764 and alternative H-bonding to backbone residues in helices 3 and 5 (45).

For DHT, the nonpolar saturated boat-configured A-ring provides a neutral 3-keto O and increases the distance between HOH1 and the 3-keto O to 3.5Å, which weakens or eliminates a second HOH1 mediated H-bond. More relaxed A-ring geometry of DHT is further evident in the 0.2Å longer distance between HOH1 and the Met-745 O. The saturated A-ring of DHT eliminates the polarized atom mismatch and provides better hydrophobic interactions with neighboring residues listed above. Just exactly how T and DHT transmit these different signals to the AF2 surface is not clear, but in both cases the side chain of Met-745 lies above the steroid A-ring and projects towards Leu-712, a proximal residue that lies in the floor of AF2.

AF2 Residue Leu-712–Leu-712 establishes key hydrophobic contacts with $i+1$ Phe-23 of the AR F_{i+1} XXLF motif and $i+1$ Leu-745 of the TIF2 LXXLL motif. Physiological relevance for Leu-712 in AR activity is established by the L712F mutation that causes grade 3 partial androgen insensitivity without altering equilibrium androgen binding affinity (7, 54). Increased bulk by Phe-712 in AR-L712F may interfere at the $i+1$ motif binding site.

Low intensity difference map electron density indicates the Leu-712 side chain is equally positioned in two conformations in all of our T-bound crystal structures. Two conformers are also seen with Met-895, an AF2 helix-12 residue within $\sim 4\text{\AA}$ of Leu-712, but more distant to the $i+1$ and steroid A-ring binding sites. Notably, there were single conformers of Leu-712 and Met-895 for WT AR LBD bound to DHT with FXXLF or LXXLL peptide (18, 34, 42).

We cannot rule out the possibility that the two conformations of Leu-712 and Met-895 are crystallographic artifacts. On the other hand, the better interactions between the 3-keto O of T to HOH1 and HOH1 to Met-745 and the polarity mismatch in the hydrophobic region near steroid carbons C-4 and C-5 suggest a mechanism not directly discerned from the structure. The effects of T appear to transmit through Met-745 to nearest AF2 floor residue Leu-712, which contacts the $i+1$ residue of the bound peptide. Based on proximity to the A ring and HOH1, the signaling conduit transmits through Gln-711 and/or Met-745 to Leu-712. Of these, Met-745 is most likely since it lies above the T A-ring $\Delta 4,5$ double bond to directly transmit A-ring chemistry to the side chain position of Leu-712 (Fig. 2-8). Gln-711 (adjacent to Leu-712) is less likely because two conformers of Gln-711 were in only 2 of 4 T-bound structures and was possibly influenced by a spuriously bound buffer derived glycerol. More importantly, two conformers of Gln-711 were reported for WT AR bound to DHT and FXXLF peptide (18). Two conformations of Met-895 may be a more indirect contributor to AF2 or have a cross-helix influence from Leu-712. In contrast, DHT appears to impart greater structural integrity to Leu-712 and AF2 helix-12 Met-895 in and near AF2 allowing near maximum motif binding and AR transcriptional activity. Elimination of conformational heterogeneity in Leu-712 and Met-895 by DHT may be required for optimal AF2 activity.

There are examples where side chain conformations of ligand binding pocket residues are strongly influenced by chemical architecture of the bound ligand. The C19 methyl group of T (shown here) and DHT (34) direct the side chains of Met-745 and Trp-741 into identical positions relative to the binding pocket. The Trp-741 nitrogen in the T and DHT-bound structures may establish interactions with structural HOH3. In contrast, R1881 lacks a C19 methyl group, which allows Trp-741 the conformational freedom to adopt a position where the indole nitrogen is rotated away from HOH3 (4, 7) as shown in Fig. 2-11. Nonsteroid ligands such as bicalutamide (44) or its S-1 agonist analog (43) extend ether linked para-substituted phenyl groups into an open channel between the AF2 helix-12 Met-895 and helix-5 Met-742 and cause Trp-741 to adopt yet a third unique conformation (Fig. 2-11).

Prostate Cancer Mutant AR-H874Y-H874Y is an AR somatic mutation identified in the human CWR22 prostate cancer xenograft that was isolated from a hormone refractory bone marrow metastasis of a patient treated with flutamide and luteinizing hormone releasing hormone agonist (24) and in a bone marrow metastasis from another patient receiving similar treatment (55). AR-H874Y retains high affinity T and DHT binding (7, 56) but more effectively interacts with the FXXLF motif despite similar motif binding affinity to WT AR. Improved FXXLF motif binding contributes to the slower dissociation rate of T and nearly equivalent T-induced transcriptional response as DHT-bound WT AR. Optimal AR FXXLF motif binding and slow ligand dissociation are thus hallmarks of the fully stabilized AR consistent with properties of the AR N/C interaction (8, 57) and AR stabilization (7, 58). Greater AF2 activity of T-bound AR-H874Y is supported by the effects of MAGE-11, an AR coregulator that binds the AR FXXLF motif and targets AF2 for activation by SRC/p160 coactivators (23).

The nearly identical crystal structures of bound T and DHT and surrounding pocket residues indicate that the DHT-like activity of T-bound AR-H874Y is not strictly ligand-mediated. H874Y provides two direct H-bonds in the receptor core in place of 3 water-mediated H-bonds in WT AR LBD that can stabilize the interior core near helix-5 Met-742, helix-4 Tyr-739, and exterior helix-10 that underlies AF2 helix-12. This tethers Met-742, a key residue proximal to the ligand binding pocket, and Tyr-739 near key AF2 domain residues, with exterior helix-10 via the mutant Tyr-874. Direct H-bonding likely improves AF2 motif binding and increases the lifetime of bound T. Agonist-induced stabilization of helix-10 is supported by the activity of S-1 bicalutamide which may form an H-bond from its fluorine atom to HOH3, a structural water that interacts with His-874 and is functionally replaced by the Tyr-874 phenolic oxygen (see Fig. 2-11) (43). The proposed destabilizing effects of T are more than compensated by the structural stabilizing effects of the H874Y mutation. Increased activity by AR-H874Y was also recognized for hydroxyflutamide and other ligands (24, 43). AR mutations that cause the androgen insensitivity syndrome support the importance of stabilizing helix-10 for AR function as well (59).

Prostate cancer cell survival and tumor expansion is favored by mutations that increase AR response to T, particularly in recurrent prostate cancer where SRC/p160 coactivators can be overexpressed (22). Our studies provide support for recent findings that local androgen production increases AR transcriptional activity in prostate cancer. Greater circulating T levels correlate with prostate cancer development (60, 61) and unlike normal prostate following androgen deprivation (62), T levels persist in recurrent prostate cancer tissue (63).

H-bond Chemistry and Protein Structure—Subtle changes in water mediated H-bond chemistry that influence AR transcriptional activity may result from thermodynamic effects on protein structure and protein-ligand interactions (64). H-bonds between protein groups and buried water molecules can stabilize structure through compensatory changes in enthalpy and entropy (65) as might occur for the H-bonding projections of Gln-711, Arg-752, Met-745, His-874, and Tyr-874. Such water mediated H-bonds can provide favorable enthalpy but less favorable entropy than direct H-bonds in protein-ligand interactions (64, 66). Deeply buried structured water molecules engaged in multiple H-bonds increase protein flexibility and vibrational entropy, whereas direct protein-mediated H-bonds provide a more rigid structure with fewer degrees of freedom compared to water-mediated H-bonds (67). Replacement of structured water by direct H-bonds in AR-H874Y may reduce vibrational entropy and stabilize AF2 helix-12 for improved FXXLF and LXXLL motif binding (5, 7). Increased stabilization of AF2 helix-12 by direct H-bonding in AR-H874Y could increase the activity of T and weaker adrenal androgens. Nonsteroidal ligands such as bicalutamide or the S-1 analog have an extended *para*-phenyl substituent that binds in a channel between AF2 and His-874 that can directly H-bond to the same HOH3 through a fluorine atom (43, 44).

We conclude that T and DHT differentially modulate AR activity by altering the AR AF2 surface response towards AR FXXLF and coactivator LXXLL motif binding mediated through a network of water mediated H-bonds and hydrophobic interactions. T-bound WT AR acquires subtle conformational instability arising from the increased polarity of T, which decreases the effectiveness of AF2 to serve as an FXXLF and LXXLL motif-binding site. DHT-bound WT AR and prostate cancer mutant AR-H874Y bound to T or DHT fully engage the FXXLF and LXXLL motifs for maximal AR transcriptional activity. The biologically

active androgens T and DHT are examples of agonist-dependent modulation of AF2 transcriptional activity that has profound physiological consequences *in vivo*.

REFERENCES

1. Wilson, E. M., and French, F. S. (1976) *J. Biol. Chem.* **251**, 5620-5629
2. Simental, J. A., Sar, M., Lane, M. V., French, F. S., and Wilson, E. M. (1991) *J. Biol. Chem.* **266**, 510-518
3. Warnmark, A., Treuter, E., Wright, A. P., and Gustafsson, J. A. (2003) *Mol. Endocrinol.* **17**, 1901-1909
4. He, B., Gampe, R. T., Kole, A. J., Hnat, A. T., Stanley, T. B., An, G., Stewart, E. L., Kalman, R. I., Mingos, J. T., and Wilson, E. M. (2004) *Mol. Cell* **16**, 425-438
5. He, B., Kempainen, J. A., and Wilson, E. M. (2000) *J. Biol. Chem.* **275**, 22986-22994
6. He, B., and Wilson, E. M. (2003) *Mol. Cell. Biol.* **23**, 2135-2150
7. He, B., Gampe, R. T., Hnat, A. T., Faggart, J. L., Mingos, J. T., French, F. S., and Wilson, E. M. (2006) *J. Biol. Chem.* **281**, 6648-6663
8. Langley, E., Zhou, Z. X., and Wilson, E. M. (1995) *J. Biol. Chem.* **270**, 29983-29990
9. Schaufele, F., Carbonell, X., Guerbodot, M., Borngraeber, S., Chapman, M. S., Ma, A. A., Miner, J. N., and Diamond, M. I. (2005) *Proc. Natl. Acad. Sci. USA* **102**, 9802-9807
10. He, B., Lee, L. W., Mingos, J. T., and Wilson, E. M. (2002) *J. Biol. Chem.* **277**, 25631-25639
11. Li, J., Fu, J., Toumazou, C., Yoon, H. G., and Wong, J. (2006) *Mol. Endocrinol.* **20**, 776-785
12. Hsu, C. L., Chen, Y. L., Ting, H. J., Lin, W. J., Yang, Z., Zhang, Y., Wang, L., Wu, C. T., Chang, H. C., Yeh, S., Pimplikar, S. W., and Chang, C. (2005) *Mol. Endocrinol.* **19**, 350-361
13. Langley, E., Kempainen, J. A., and Wilson, E. M. (1998) *J. Biol. Chem.* **273**, 92-101
14. He, B., Kempainen, J. A., Voegel, J. J., Gronemeyer, H., and Wilson, E. M. (1999) *J. Biol. Chem.* **274**, 37219-37225
15. Quigley, C. A., Tan, J. A., He, B., Zhou, Z. X., Mebarki, F., Morel, Y., Forest, M., Chatelain, P., Ritzen, E. M., French, F. S., and Wilson, E. M. (2004) *Mech. Ageing Dev.* **125**, 683-695

16. Ghali, S. A., Gottlieb, B., Lumbroso, R., Beitel, L. K., Elhaji, Y., Wu, J., Pinsky, L., and Trifiro, M. A. (2003) *J. Clin. Endocrinol. Metab.* **88**, 2185-2193
17. Quigley, C. A., De Bellis, A., Marschke, K. B., El-Awady, M. K., Wilson, E. M., and French, F. S. (1995) *Endocrine Reviews* **16**, 271-321
18. Hur, E., Pfaff, S. J., Payne, E. S., Gron, H., Buehrer, B. M., and Fletterick, R. J. (2004) *PLoS Biol.* **2**, E274.
19. He, B., Minges, J. T., Lee, L. W., and Wilson, E. M. (2002) *J. Biol. Chem.* **277**, 10226-10235
20. Hsu, C. L., Chen, Y. L., Yeh, S., Ting, H. J., Hu, Y. C., Lin, H., Wang, X., and Chang, C. (2003) *J. Biol. Chem.* **278**, 23691-23698
21. Chang, C. Y., Abdo, J., Hartney, T., and McDonnell, D. P. (2005) *Mol. Endocrinol.* **19**, 2478-2490
22. Gregory, C. W., He, B., Johnson, R. T., Ford, O. H., Mohler, J. L., French, F. S., and Wilson, E. M. (2001) *Cancer Res.* **61**, 4315-4319
23. Bai, S., He, B., and Wilson, E. M. (2005) *Mol. Cell. Biol.* **25**, 1238-1257
24. Tan, J. A., Sharief, Y., Hamil, K. G., Gregory, C. W., Zang, D. Y., Sar, M., Gumerlock, P. H., deVere White, R. W., Pretlow, T. G., Harris, S. E., Wilson, E. M., Mohler, J. L., and French, F. S. (1997) *Mol. Endocrinol.* **11**, 450-459
25. Voegel, J. J., Heine, M. J., Tini, M., Vivat, V., Chambon, P., and Gronemeyer, H. (1998) *EMBO J.* **17**, 507-519
26. Huang, W., Shostak, Y., Tarr, P., Sawyers, C., and Carey, M. (1999) *J. Biol. Chem.* **274**, 25756-25768
27. Gregory, C. W., Johnson, R. T., Mohler, J. L., French, F. S., and Wilson, E. M. (2001) *Cancer Res.* **61**, 2892-2898
28. He, B., Bowen, N. T., Minges, J. T., and Wilson, E. M. (2001) *J. Biol. Chem.* **276**, 42293-42301
29. Lubahn, D. B., Joseph, D. R., Sar, M., Tan, J. A., Higgs, H. N., Larson, R. E., French, F. S., and Wilson, E. M. (1988) *Mol. Endocrinol.* **2**, 1265-1275
30. Stanley, T. B., Leesnitzer, L. M., Montana, V. G., Galardi, C. M., Lambert, M. H., Holt, J. A., Xu, H. E., Moore, L. B., Blanchard, S. G., and Stimmel, J. B. (2003) *Biochemistry* **42**, 9278-9287

31. Otwinowski, Z., and Minor, W. (1997) *Meth. Enzymol.* **276**, 307-326
32. Vagin, A., and Teplyakov, A. (1997) *J. Appl. Cryst.* **30**, 1022-1025
33. Collaborative Computational Project Number 4 (1994) *Acta Crystallogr. D. Biol. Crystallogr.* **50**, 760-763
34. Sack, J. S., Kish, K. F., Wang, C., Attar, R. M., Kiefer, S. E., An, Y., Wu, G. Y., Scheffler, J. E., Salvati, M. E., Krystek, S. R. Jr, Weinmann, R., and Einspahr, H. M. (2001) *Proc. Natl. Acad. Sci. USA* **98**, 4904-4909
35. Emsley, P., and Cowtan, K. (2004) *Acta Crystallogr. D. Biol. Crystallogr.* **60**, 2126-2132
36. Murshudov, G.N., Vagin, A.A., and Dodson, E.J. (1997) *Acta Crystallogr. D Biol. Crystallogr.* **53**, 240-255
37. Lovell, S. C., Davis, I. W., Arendall III, W. B., de Bakker, P. I. W., Word, J. M., Prisant, M. G., Richardson, J. S., and Richardson, D. C. (2003) *Prot.. Struc. Func. Genetics* **50**, 437-450
38. Zhou, Z. X., Sar, M., Simental, J. A., Lane, M. V., and Wilson, E. M. (1994) *J. Biol. Chem.* **269**, 13115-13123
39. Wang, Q., Lu, J., and Yong, E. L. (2001) *J. Biol. Chem.* **276**, 7493-7499
40. Gregory, C. W., Fei, X., Ponguta, L. A., He, B., Bill, H. M., French, F. S., and Wilson, E. M. (2004) *J. Biol. Chem.* **279**, 7119-7130
41. Matias, P. M., Donner, P., Coelho, R., Thomaz, M., Peixoto, C., Macedo, S., Otto, N., Joschko, S., Scholz, P., Wegg, A., Basler, S., Schafer, M., Egner, U., and Carrondo, M. A. (2000) *J. Biol. Chem.* **275**, 26164-26171
42. Estebanez-Perpina, E., Moore, J. M., Mar, E., Delgado-Rodrigues, E., Nguyen, P., Baxter, J. D., Buehrer, B. M., Webb, P., Fletterick, R. J., and Guy, R. K. (2005) *J. Biol. Chem.* **280**, 8060-8068
43. Bohl, C. E., Miller, D. D., Chen, J., Bell, C. E., and Dalton, J. T. (2005) *J. Biol. Chem.* **280**, 37747-37754
44. Bohl, C. E., Gao, W., Miller, D. D., Bell, C. E., and Dalton, J. T. (2005) *Proc. Natl. Acad. Sci. USA* **102**, 6201-6206
45. Ostrowski, J., Kuhns, J. E., Lupisella, J. A., Manfredi, M. C., Beehler, B. C., Krystek, S. R., Bi, Y., Sun, C., Seethala, R., Golla, R., Slep, P. G., Fura, A., An, Y., Kish, K. F., Sack, J. S., Mookhtiar, K. A., Grover, G. J., and Hamann, L. G. (2007)

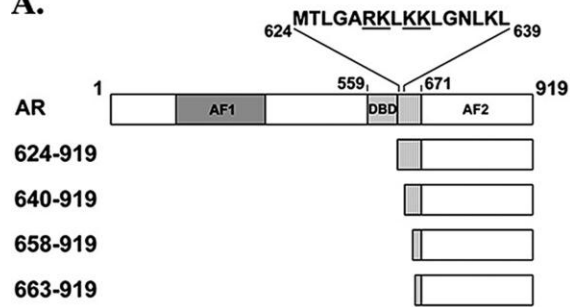
Endocrinology **148**, 4-12

46. Imperato-McGinley, J., Guerrero, L., Gautier T, and Peterson, R. E. (1974) *Science* **186**, 1213-1215
47. Grino, P. B., Griffin, J. E., and Wilson, J. D. (1990) *Endocrinology* **126**, 1165-1172
48. Mahendroo, M. S., Cala, K. M., Hess, D. L., and Russell, D. W. (2001) *Endocrinology* **142**, 4652-4662
49. Maes, M., Sultan, C., Zerhouni, N., Rothwell, S. W., and Migeon, C. J. (1979) *J. Steroid Biochem.* **11**, 1385-1392
50. Shan, S. O. and Herschlag, D. (1996) *Proc. Natl. Acad. Sci. USA* **93**, 14474-14479
51. Pereira de Jesus-Tran, K., Cote, P. L., Cantin, L., Blanchet, J., Labrie, F., and Breton, R. (2006) *Protein Sci.* **15**, 987-999
52. Matias, P. M., Carrondo, M. A., Coelho, R., Thomaz, M., Zhao, X. Y., Wegg, A., Crusius, K., Egner, U., and Donner, P. (2002) *J. Med. Chem.* **45**, 1439-1446
53. Baker, E. N., and Hubbard, R. E. (1984) *Prog. Biophys. Mol. Biol.* **44**, 97-179
54. Holterhus, P. M., Sinnecker, G. H., and Hiort, O. (2000) *J. Clin. Endocrinol. Metab.* **85**, 3245-3250
55. Taplin, M. E., Bublely, G. J., Shuster, T. D., Frantz, M. E., Spooner, A. E., Ogata, G. K., Keer, H. N., and Balk, S. P. (1995) *N. Engl. J. Med.* **332**, 1393-1398
56. Duff, J., and McEwan, I. J. (2005) *Mol. Endocrinol.* **19**, 2943-2954
57. Kempainen, J. A., Langley, E., Wong, C. I., Bobseine, K., Kelce, W. R., and Wilson, E. M. (1999) *Mol. Endocrinol.* **13**, 440-454
58. Zhou, Z. X., Lane, M. V., Kempainen, J. A., French, F. S., and Wilson, E. M. (1995) *Mol. Endocrinol.* **9**, 208-218
59. Ong, Y. C., Kolatkar, P. R., and Yong, E. L. (2002) *Mol. Hum. Reprod.* **8**, 101-108
60. Shaneyfelt, T., Husein, R., Bublely, G., and Mantzoros, C. S. (2000) *J. Clin. Oncol.* **18**, 847-853
61. Gann, P. H., Hennekens, C. H., Ma, J., Longcope, C., and Stampfer, M. J. (1996) *J. Natl. Cancer Inst.* **88**, 1118-1126

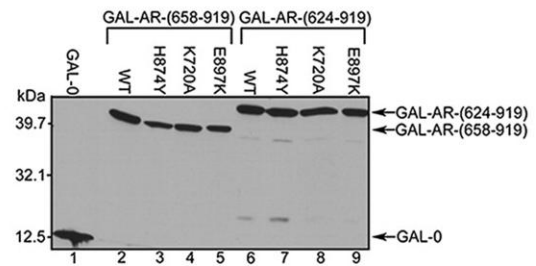
62. Page, S. T., Lin, D. W., Mostaghel, E. A., Hess, D. L., True, L. D., Amory, J. K., Nelson, P. S., Matsumoto, A. M., and Bremner, W. J. (2006) *J. Clin. Endocrinol. Metab.* **91**, 3850-3856
63. Mohler, J. L., Gregory, C. W., Ford, O. H., Kim, D., Weaver, C. M., Petrusz, P., Wilson, E. M., and French, F. S. (2004) *Clin. Can. Res.* **10**, 440-448
64. Sharrow, S. D., Edmonds, K. A., Goodman, M. A., Novotny, M. V., and Stone, M. J. (2005) *Protein Sci.* **14**, 249-256
65. Takano, K., Yamagata, Y., Kubota, M., Funahashi, J., Fujii, S., and Yutani, K. (1999) *Biochemistry* **38**, 6623-6629
66. Connelly, P. R., Aldape, R. A., Bruzzese, F. J., Chambers, S. P., Fitzgibbon, M. J., Fleming, M. A., Itoh, S., Livingston, D. J., Navia, M. A., Thomson, J. A., and Wilson, K. P. (1994) *Proc. Natl. Acad. Sci. USA* **91**, 1964-1968
67. Fischer, S., and Verma, C. S. (1999) *Proc. Natl. Acad. Sci. USA* **96**, 9613-9615

Figure 2-1. AF2 Activity in the AR LBD. (A) Schematic diagram of AR LBD deletion mutants. Full-length human AR (amino acid residues 1-919) contains activation function 1 (AF1, amino acid residues 142-337), DNA binding domain (DBD residues 559-623), hinge region residues 624-670, and LBD residues 671-919 that includes AF2. AR hinge region residues 624-639 contain the carboxyl-terminal portion of the bipartite AR nuclear targeting signal residues Arg-629, Lys-630, Lys-632, and Lys-633 (underlined) (38). AR-(624-919), -(640-919) and -(658-919) with WT and mutant sequence were expressed as GAL4 DNA binding domain fusion proteins. AR residues 663-919 and H874Y mutant were expressed for crystallography as His₆-tagged fusion proteins with intervening thrombin cleavage site. (B) Similar expression of GAL-AR-LBD fusion proteins. COS cells were transfected with 10 μg GAL-0 (*lane 1*), GAL-AR-(658-919) (*lanes 2-5*) and GAL-AR-(624-919) (*lanes 6-9*) with WT or mutant sequence. Protein extracts (60 μg of protein/lane) were separated on a 10% acrylamide gel containing SDS and the blot probed using an anti-GAL antibody. (C) Androgen-dependent activity of GAL-AR-(624-919), GAL-AR-(658-919) WT and H874Y mutants in CV1 cells requires coexpression of TIF2. CV1 cells plated in 6-cm dishes were transfected by calcium phosphate DNA precipitation with 5 μg 5XGAL4Luc3 reporter vector and 0.1 μg GAL-AR-(624-919) or GAL-AR-(658-919) with WT or H874Y sequence in the absence and presence of 2 μg pSG5-TIF2. Cells were treated with and without increasing concentrations of DHT (*D*) and T as indicated and luciferase activity was determined. Data are representative of three independent experiments. (D) Inhibition of the AR N/C and coactivator interactions by AR hinge residues 624-639. HeLa cells were transfected using FuGENE 6 by adding per well 0.1 μg 5XGAL4Luc, 50 ng VP16, VP-AR-(1-660), or VP-TIF2-(624-1287) with 0.1 μg GAL-AR-(624-919), -(640-919) or -(658-919). Cells were incubated with and without 0.1-10 nM DHT for 24 h as indicated and assayed for luciferase activity. Data are representative of three independent experiments. (E) Androgen-dependent transcriptional activity of GAL-AR-(624-919), GAL-AR-(658-919), and H874Y mutants in CWR-R1 cells. CWR-R1 cells (2×10^5 /well) were transfected using Effectene by adding per well 0.1 μg GAL-AR-(624-919), GAL-AR-(658-919) or H874Y mutants and 0.25 μg 5XGAL4Luc3. Cells were treated with and without increasing concentrations of T and DHT for 24 h as indicated, and luciferase activity was determined. Data are representative of three independent experiments. (F) Androgen dependent AF2 activity of GAL-AR-(658-919) in CWR-R1 cells. CWR-R1 cells (2×10^5 /well) were transfected using Effectene by adding per well 0.1 μg GAL-AR-(658-919) or H874Y, K720A or E897K mutants and 0.25 μg 5XGAL4Luc3. Lys-720 and Glu-897 are charge clamp residues in AF2. Cells were incubated with and without 0.1, 1, and 10 nM T for 24 h and luciferase activity was determined. Data are representative of at least three independent experiments.

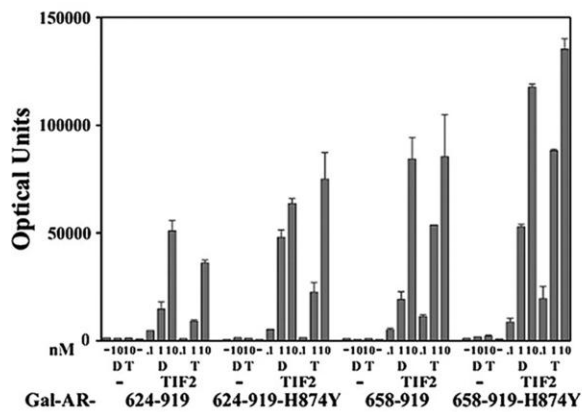
A.



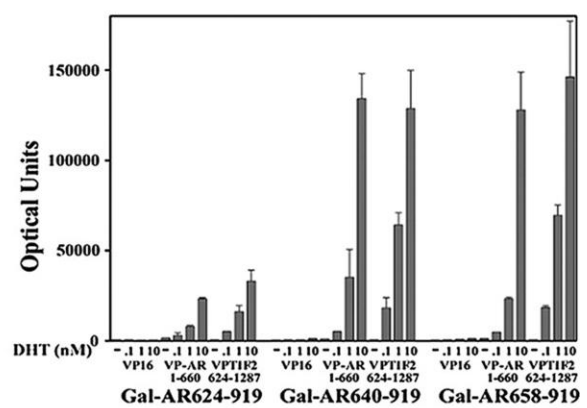
B.



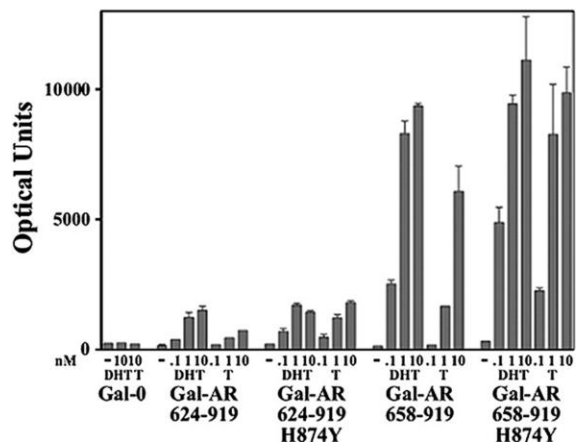
C. CV1



D. HeLa



E. CWR-R1



F. CWR-R1

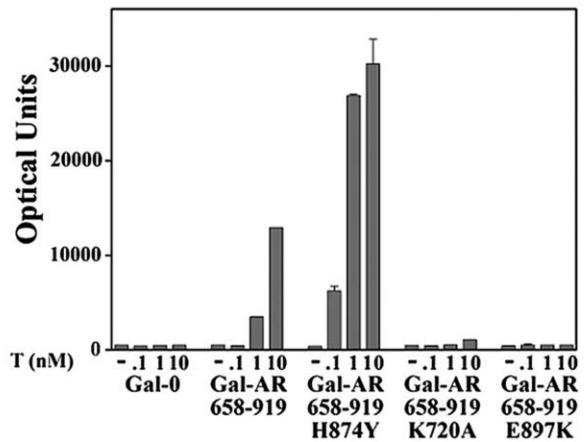


Figure 2-2. Increased AR-H874Y LBD AF2 Activity Response to T. (A) CWR-R1 prostate cancer cells (2×10^5 /well) were transfected using Effectene by adding per well 0.1 μg GAL-0, GAL-AR-(658-919), or H874Y mutant and 0.25 μg 5XGAL4Luc3. Cells were incubated in the absence and presence of 0.1, 1 and 10 nM 5α -androstane- $3\alpha,17\beta$ -diol (*Di*, *Diol*), androstenedione (*Dn*, *Dione*), T and DHT for 24 h as indicated, and luciferase activity was determined. (B) HeLa cells were transfected using FuGENE 6 by adding per well 0.1 μg GAL-0, GAL-AR-(658-919) or H874Y mutant and 0.25 μg 5XGAL4Luc3. Transfected cells were incubated with and without androgen as indicated for 24 h and assayed for luciferase activity. Data in A and B are representative of at least three independent experiments.

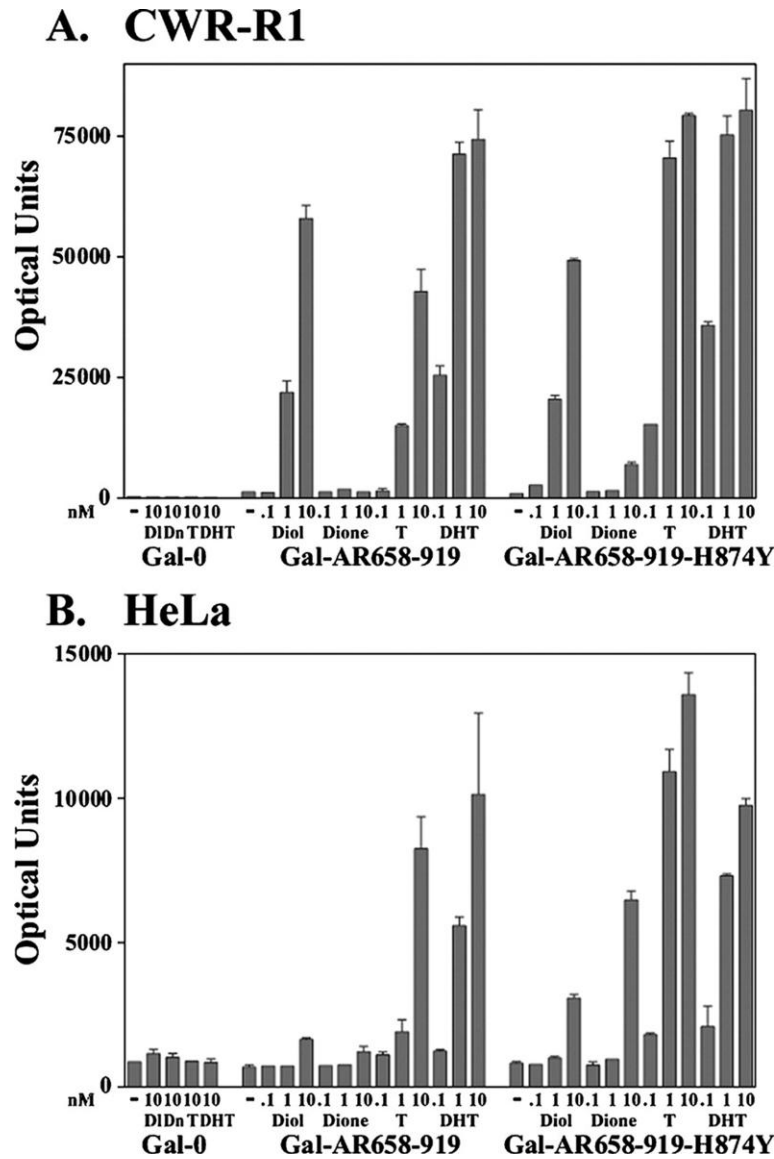


Figure 2-3. Increased Transcriptional Activity of AR-H874Y by T and Adrenal Androgens. (A) CWR-R1 cells (1.6×10^5 cells/well) were transfected with 0.1 μg MMTV-Luc/well of 12-well plates using Effectene. Cells were incubated in the absence and presence of increasing concentrations of DHT, T, androstenedione (*Dione*), and androstenediol (*Diol*) as indicated for 24 h and assayed for luciferase activity. (B) HeLa cells were transfected using FuGENE 6 by adding per well 10 ng pCMV5 empty vector (p5), pCMVhAR or the H874Y mutant and 0.25 μg PSA-Enh-Luc. Cells were incubated with and without 0.001 to 10 nM DHT (*D*) or T, and 0.1 to 10 nM androstenedione (*Dn*, *Dione*) or 5 α -androstane-3 α ,17 β -diol (*DI*, *Diol*) for 24 h before luciferase activity was determined. Data in A and B are representative of three independent experiments.

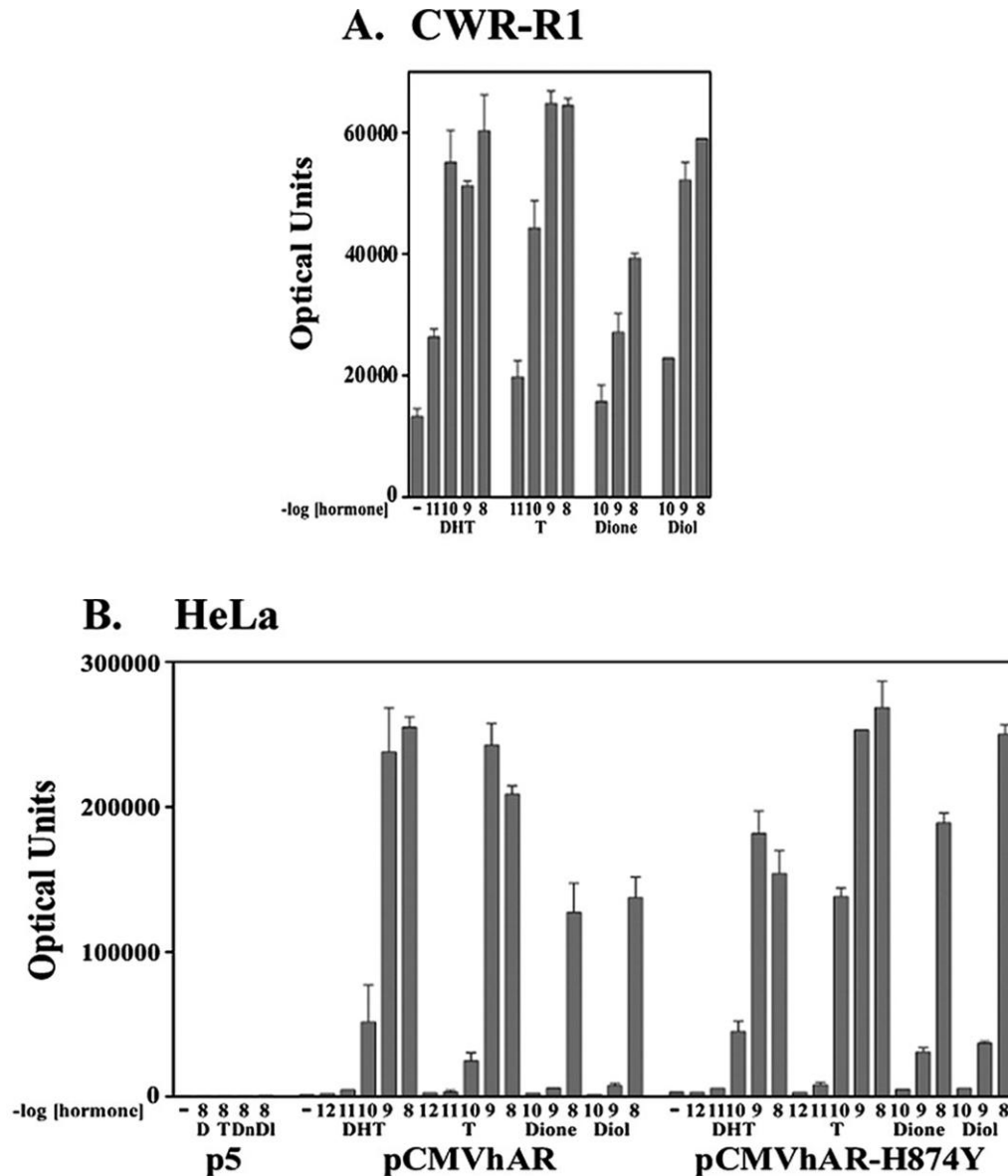


Figure 2-4. MAGE-11 Increases AR-H874Y Activity Response to T and DHT. CV1 cells plated in 6-cm dishes were transfected using calcium phosphate DNA precipitation by adding per dish 0.1 μ g of WT pCMVhAR (AR-WT) or H874Y mutant and 5 μ g PSA-Enh-Luc reporter in the absence and presence of 2 μ g pSG5-TIF2 and/or 2 μ g pSG5-MAGE-11-(1-429) (*MAGE*) as indicated. Cells were incubated with and without 0.1 nM T for 48 h before luciferase activity was determined. Data are representative of three independent experiments.

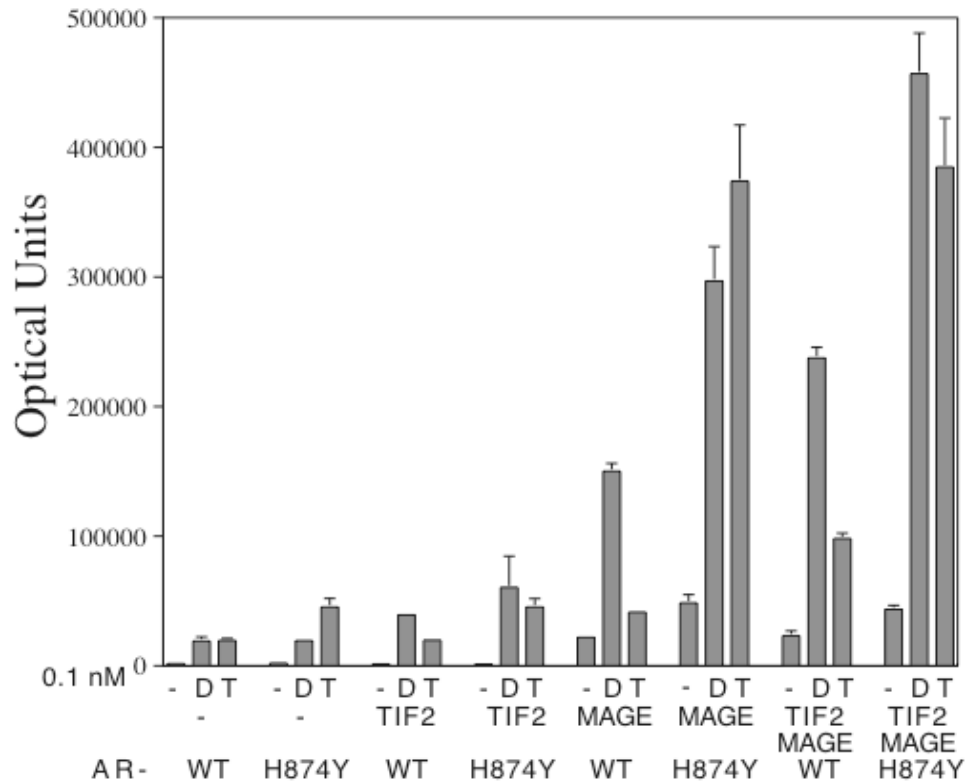


Figure 2-5. Fluorescence Binding Isotherms. (A) Increasing concentrations of AR LBD and AR-H874Y LBD purified in the presence of 10 μ M T or DHT, and ER β LBD in the presence of 40 μ M estradiol were incubated for 1 h at room temperature without further ligand addition with fluorescein-labeled AR FXXLF peptide as described under “Experimental Procedures”. (B) Increasing concentrations of purified WT AR LBD, AR-H874Y LBD, and ER β LBD purified in the presence of 10 μ M ligand were incubated for 1 h at room temperature in the presence of 40 μ M T, DHT or estradiol and fluorescein-labeled TIF2 LXXLL peptide as described under “Experimental Procedures”. Affinity binding constants for AR FXXLF and TIF2 LXXLL peptides are summarized in Table 2-1. The data are the mean \pm S.E. expressed as millipolarization units (*mP*) versus purified receptor LBD concentration.

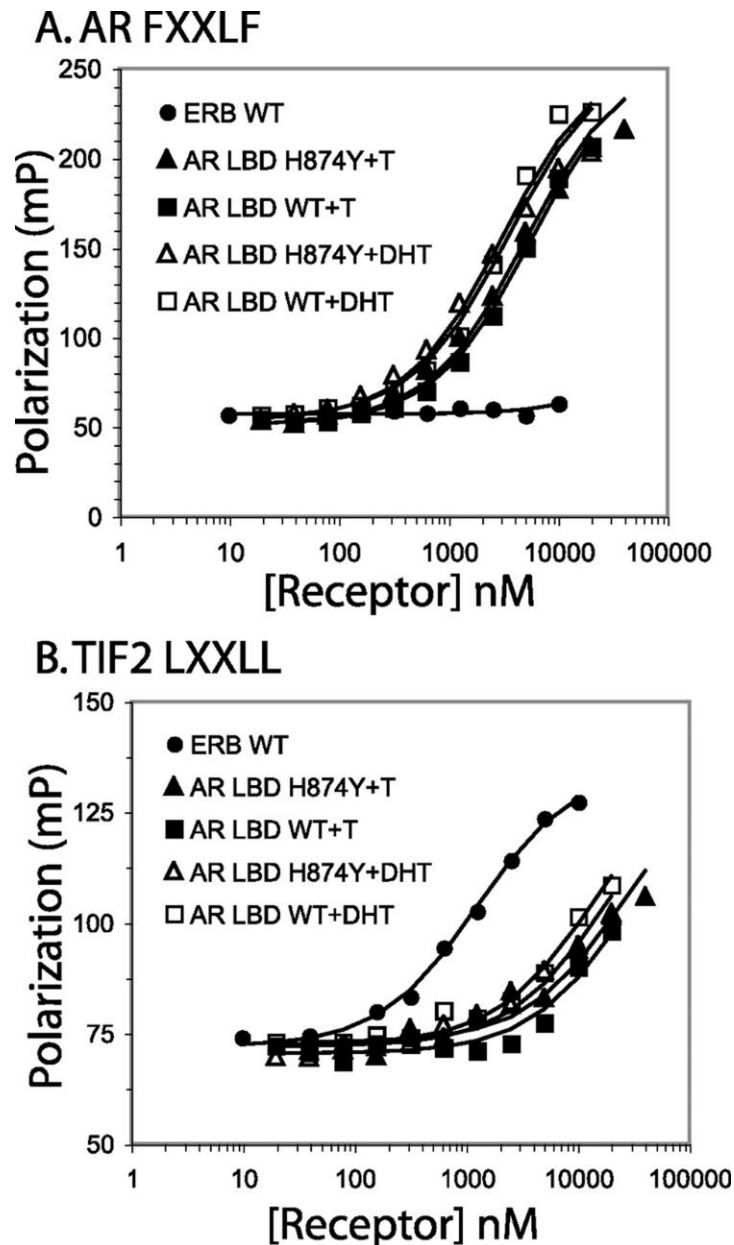


Figure 2-6. Kinetics of T and DHT Dissociation from AR and AR-H874Y. (A) Dissociation rates of [³H]T and [³H]DHT were determined as described under “Experimental Procedures” by transient transfection of COS cells with 2 μg pCMVhAR (AR) and 2 μg pCMVhAR-H874Y (AR-H874Y). Transfected cells in culture were incubated for 2 h at 37°C in the presence of 5 nM [³H]T and 3 nM [³H]DHT followed by a chase period with unlabeled 50 μM T or 50 μM R1881 and assayed at 30-min intervals up to 2.5 h. Pseudo-first order ligand dissociation allowed use of unlabeled R1881 to prevent rebinding of [³H]DHT and avoid the complications of low water solubility of DHT. Dissociation half-times were calculated as the time required at 37°C to reduce specific binding by 50%. Data are representative of three independent experiments. (B) Immunoblot of WT and H874Y AR and AR-(507-919) expression levels in COS cells. Cells transfected with 10 μg pCMVhAR, pCMVhAR-(507-919), and the corresponding H874Y mutants were incubated in serum free medium in the absence of hormone. Protein extracts (20 μg protein/lane) were separated on a 10% acrylamide gel containing SDS and the transferred protein blot probed using anti-AR antibody AR-52.

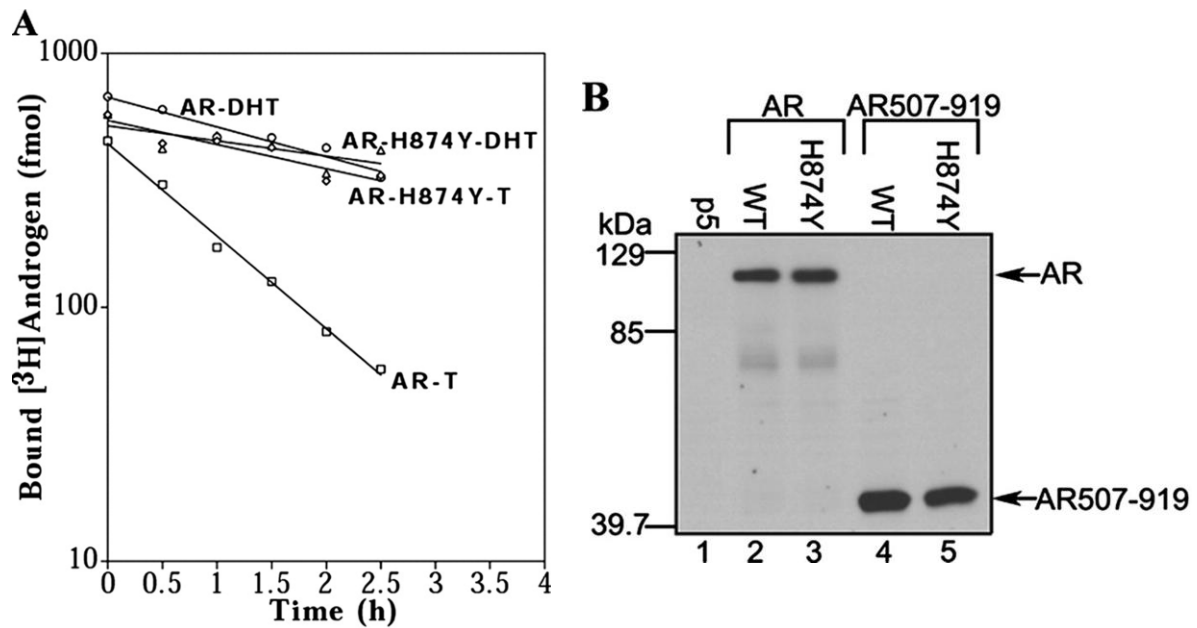


Figure 2-7. Crystal Structures of WT and H874Y AR LBD Bound with T and AR FXXLF or TIF2 LXXLL Peptide. (A) Global front view of superimposed structures of WT and H874Y AR LBD bound to T and AR-(20-30) FXXLF or TIF2-(740-752) LXXLL peptide. Shown are WT AR LBD–T–AR FXXLF peptide (*tan*, LBD ribbon; *magenta*, peptide), WT AR LBD–T–TIF2 LXXLL peptide (*lime green*, LBD ribbon; *cyan*, peptide), H874Y AR LBD–T–AR FXXLF peptide (*yellow*, LBD ribbon; *green*, peptide) and H874Y AR LBD–T–TIF2 LXXLL peptide (*lavender*, LBD ribbon; *blue*, peptide) and T (LBD ribbon color carbon, *red* oxygen). Human AR helix (*H*) and β -strand (*BS*) amino acid residues are H1 673-680; H2 not assigned; H3 697-721; H3' 725-727; H4 730-739; H5 741-756; BS3 761-765; BS4 768-771; H6 772-776; H7 780-797; H8 801-812; BS5 815-817; H9 824-842; H10 851-882; H11 884-887; H12 893-908; BS6 911-913. (B) Rotated view of (A) looking towards the carboxyl-terminal end of helix-5 and NH₂-terminal ends of helices 6 and 8. Residues 843-850 between H9 and H10 were devoid of electron density. (C) Detailed view of the T-bound ligand binding pocket and surrounding residues of WT and H874Y AR LBD bound with AR-(20-30) FXXLF or TIF2-(740-752) LXXLL peptide. In all four T-bound structures the ligand binding pockets are essentially identical to each other. A single conformation was observed for all the displayed side chains except for Leu-712 (50% A and B) and Gln-711 (80% A and 20% B in the WT AR LBD–T–LXXLL and AR-H874Y LBD–T–FXXLF structures). A buffer-derived glycerol molecule (not shown) near Gln-711 was present in all 4 WT and H874Y AR LBD–T structures. Color scheme as in (A) with nitrogen atoms in *blue* and oxygen atoms in *red*; *orange dashed lines* designate potential interactions with neighboring polar atoms. (D) Detailed view to display the molecular architecture from the ligand binding pocket to the AF2 peptide-binding site and *i*+1 side chain of Phe-23 of bound AR-(20-30) FXXLF peptide and Leu-745 of bound TIF2 LXXLL peptide. Different conformers of Met-734 and Tyr-739 correlate with the induced fit binding of the FXXLF or LXXLL motif. The WT and H874Y AR LBD bound to T and AR FXXLF or TIF2 LXXLL peptide are superimposed and use the color scheme of (A). Side chains for Leu-712 and Met-895 are distributed equally into two rotamers.

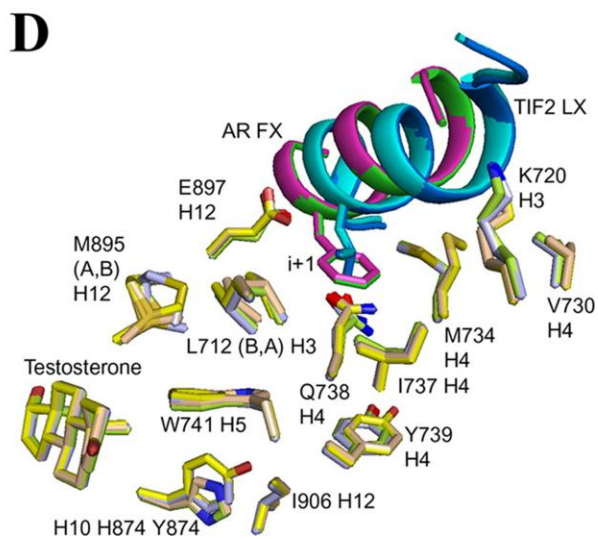
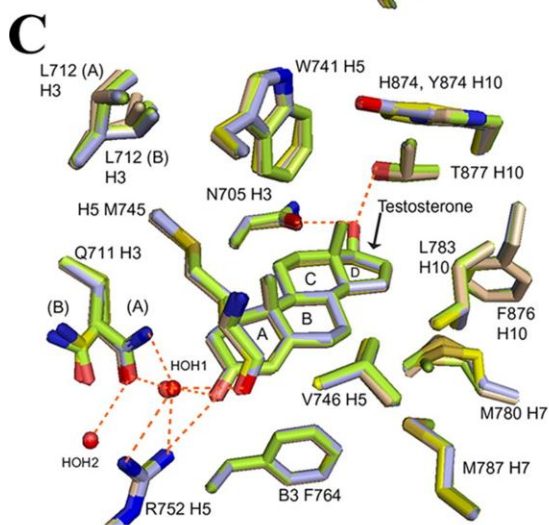
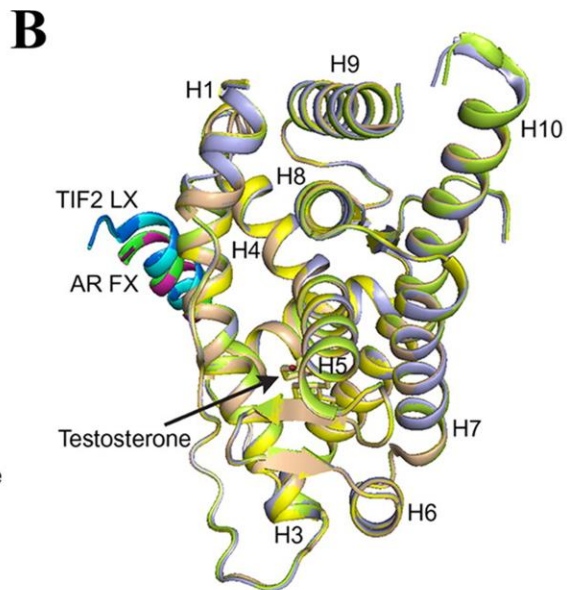
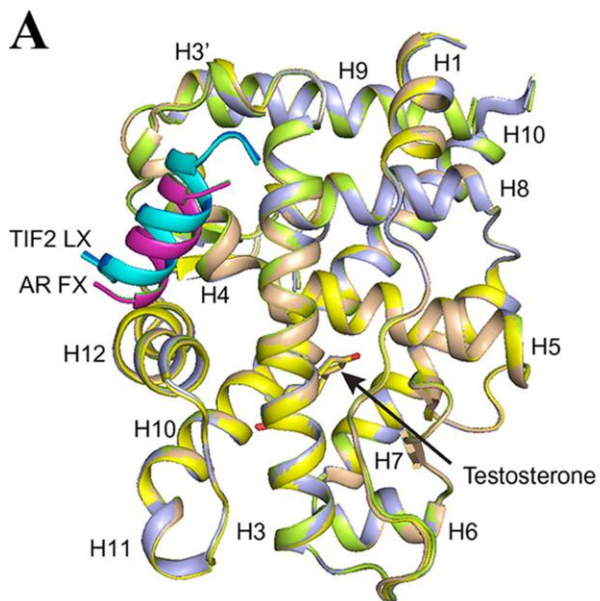


Figure 2-8. Potential A-ring and Water mediated H-bonding Schemes for T and DHT. Predicted A-ring H-bond distances and angles are shown based on the tetrahedral geometry of conserved structural water HOH1 (see Table 2-4). *Arrowhead black dashed lines* indicate the direction of donated H-bonds and *orange dashed lines* designate potential interactions with neighboring polar atoms of WT AR LBD bound to T and AR-(20-30) FXXLF peptide (*tan*) (A); WT AR LBD bound to DHT and GRIP-1-(740-752) LXXLL peptide (*green*) (42) (B); and the superimposition of A and B (C). Superior hydrophilic properties and a shorter distance are thought to enhance the HOH1 to T 3-keto O H-bond over that in DHT.

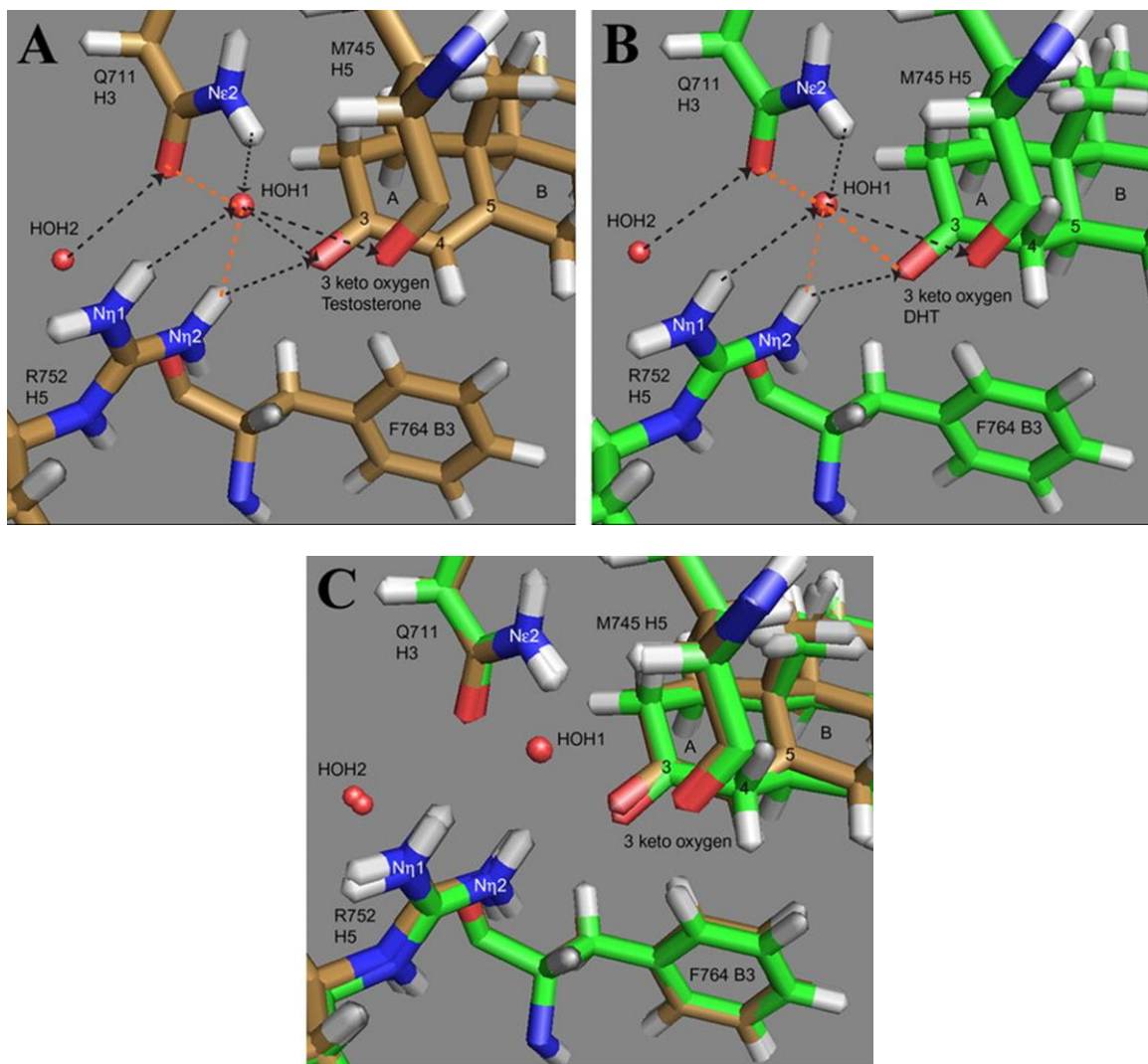


Figure 2-9. Comparison of WT AR LBD–T–AR FXXLF and WT AR LBD–DHT–LXXLL. Detailed view shows nearly identical molecular architecture of T and DHT-bound AR LBD from the ligand binding pocket to AF2 peptide-binding site. Shown here for WT AR LBD–T–AR-(20-30) FXXLF peptide (*tan*) but seen in all of our T-bound AR LBD structures are the two side chain conformations for Leu-712 and Met-895. By comparison with previously reported WT AR LBD–DHT (*green*) with GRIP1-(740-752) LXXLL peptide (IT63, 42) or FXXLF (not shown, ITR7, 18), those side chains were conformed into a single rotamer. The *i*+1 motif residues, Phe-23 (*magenta*) of the AR FXXLF peptide and Leu-745 (*cyan*) of the GRIP-1 LXXLL peptide, are shown. *Orange dashed lines* designate potential interactions with neighboring polar atoms. Portions of the LBD backbone are transparently displayed.

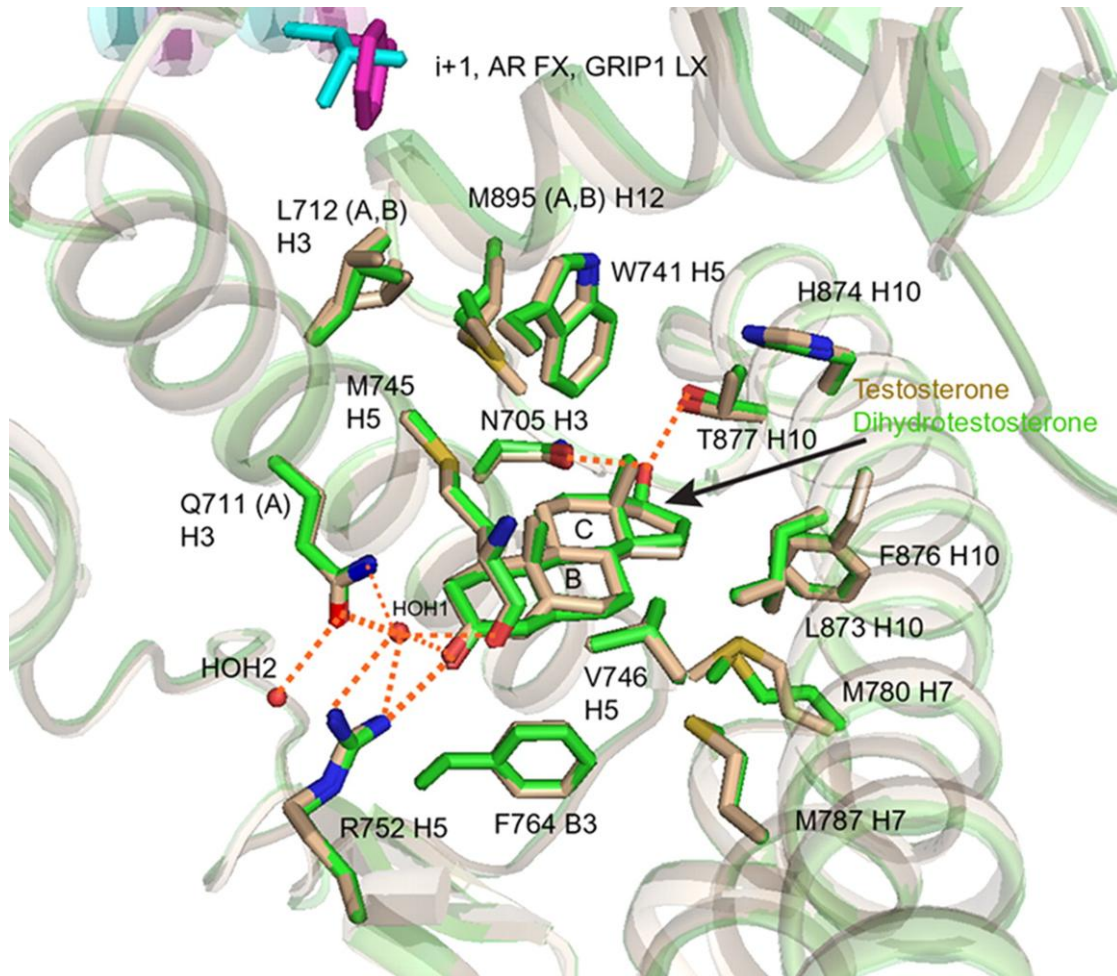


Figure 2-10. Detailed Crystal Structure Comparison of WT and H874Y AR LBD Bound to T and AR FXXLF Peptide. (A) Detailed view of WT AR LBD bound to T and AR-(20-30) FXXLF peptide showing a water mediated H-bond network from His-874 (*tan*) nitrogen (*blue*) through HOH3 (*red sphere*) to the helix-5 Met-742 amide and HOH4 to the helix-4 Tyr-739 backbone carbonyl. These conserved receptor core structural waters link His-874, which lies beneath helix-12, to Tyr-739. *Black dashed arrowhead lines* indicate the direction of donated H-bonds; *orange dashed lines* designate potential interactions with neighboring polar atoms; interatomic distances are reported in Angstroms; T rings labeled A-D. (B) Detailed view of AR-H874Y LBD–T–AR-20-30 FXXLF peptide. Note the extended phenolic hydroxyl of AR H874Y prostate cancer mutation Tyr-874 displaces structural water HOH3 and provides direct H-bonds to the backbone amide of helix-5 Met-742 and the carbonyl of helix-4 Tyr-739 (*yellow*). H-bonds labeled as in (A) with HOH4 shown as *blue sphere*. (C) Superposition of (A) and (B) showing how the phenolic hydroxyl group of helix-10 mutant Tyr-874 of AR-H874Y nearly extends to the same position as HOH3 in the WT AR LBD structure with conservation of backbone positions for Try-739, Trp-741, and Arg-752. (D) Superposition of WT AR LBD (*tan*) bound to T and AR-(20-30) FXXLF (*i+1* Phe-23, *green*) and AR-H874Y LBD (*yellow*) bound to T and AR-(20-30) FXXLF (*i+1* Phe-23, *magenta*). TIF2-(740-752) LXXLL *i+1* residue Leu-745 (*cyan*) is shown for comparison. Direct H-bonding by Tyr-874 to the backbone of Tyr-739 displaces HOH3 and could further stabilize another H-bonding network represented with *orange dashed lines* that links Met-734 CO to Gln-738, Gln-902, and Lys-905.

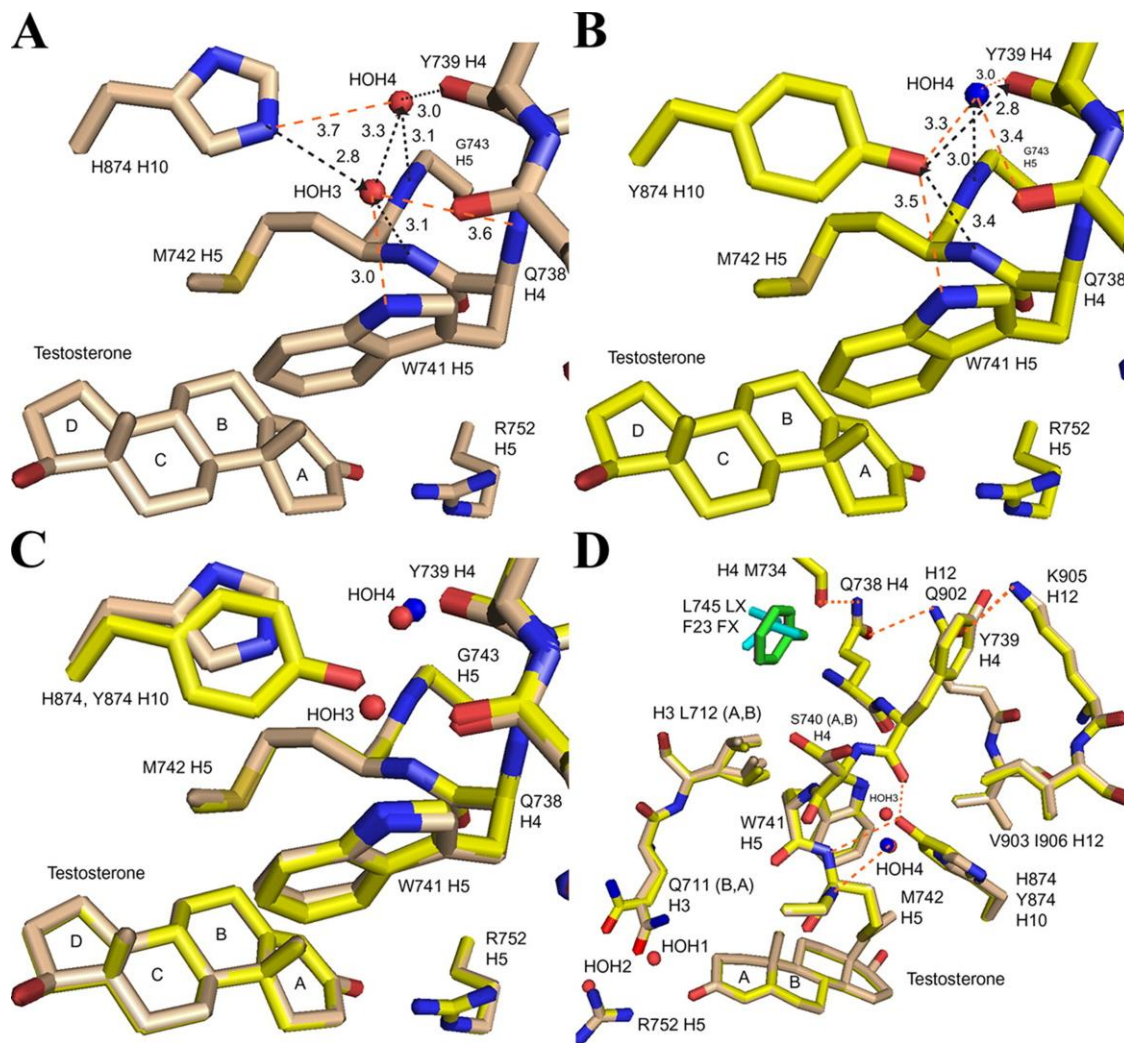


Figure 2-11. Structural Differences Between the Steroid and Nonsteroidal Ligand Binding Pockets. Superimposition of WT AR LBD crystal structures bound with an FXXLF peptide and T (*brown*), DHT (*green*) (18), R1881 (*magenta*) (4), and S-1 bicalutamide agonist analog (*cyan*) (43) and AR-H874Y LBD bound to the AR FXXLF peptide and T (*yellow*). The C-19 bridgehead methyl group on T and DHT forces the Met-745 and Trp-741 side chains away from the steroid A-ring. For R1881 and S-1, the absence of an equivalent methyl group allows these side chains to adopt different rotamers that fill the vacated space above ring-A. The *para*-fluoro phenyl group on S1 extends into the space between helix-12 Met-895 and helix-5 Met-742 and directs Trp-741 to a third unique conformation. Appropriate *para*-phenyl substituents are thought to stabilize the AR LBD core by interacting with HOH3 (43).

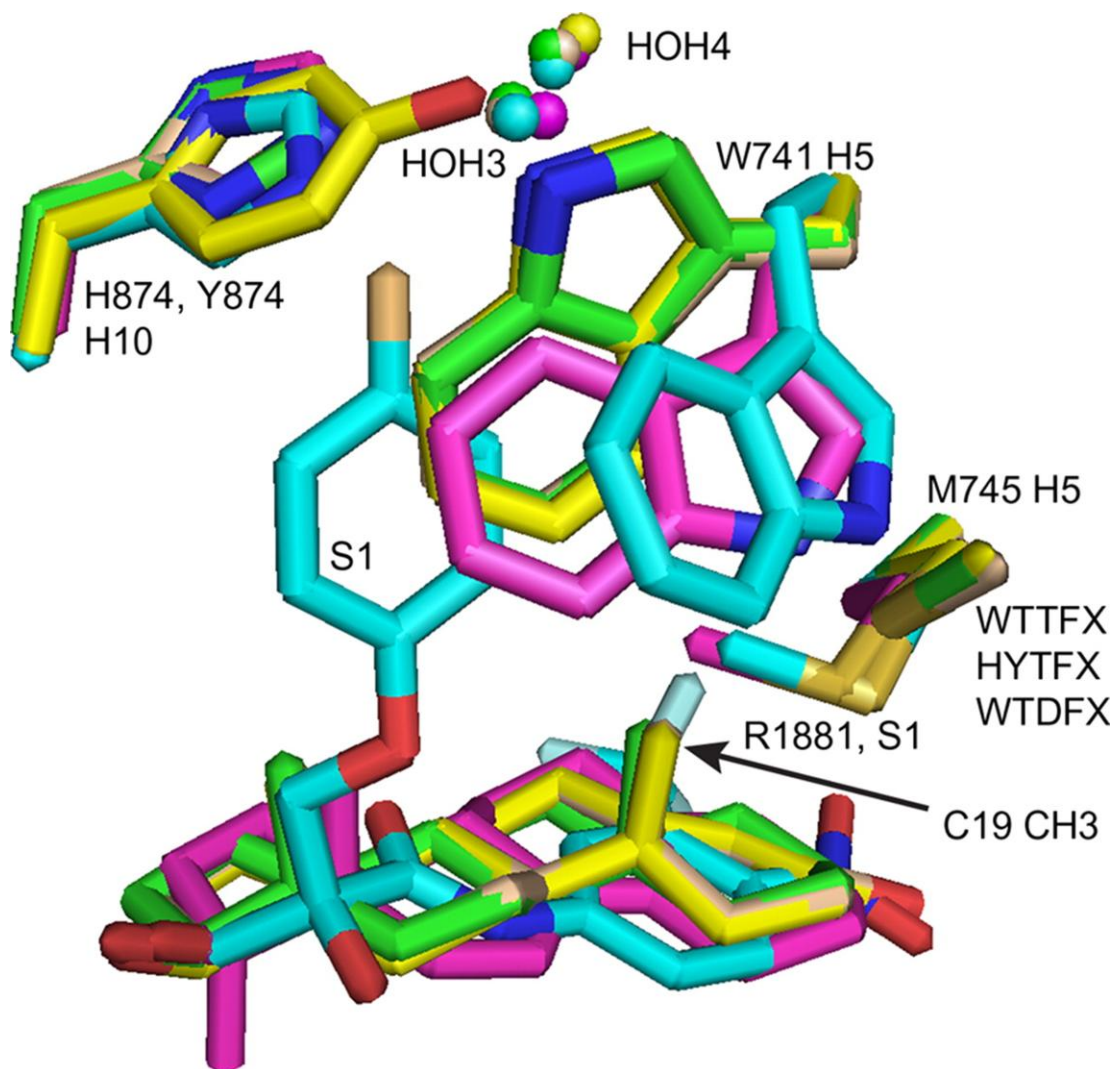


Table 2-1. Androgen Dependent AR LBD and AR-H874Y LBD Binding Affinities for AR FXXLF and TIF2 LXXLL Peptides. Fluorescence polarization measurements were determined using fluorescein-labeled peptides as described under “Experimental Procedures” for 1 h at room temperature for purified AR LBD, AR-H874Y LBD, and ER β LBD containing 10 μ M T, 10 μ M DHT, or 40 μ M estradiol as indicated without further ligand addition.

AR and ERβ LBD Binding Affinities (Kd, μM) for FXXLF and LXXLL Peptides			
	<u>T</u>	<u>DHT</u>	<u>E₂</u>
<u>FXXLF</u>			
AR-LBD	5.5 \pm 0.3	3.0 \pm 0.4	–
AR-LBD-H874Y	4.9 \pm 0.6	3.5 \pm 0.6	–
ER β -LBD	–	–	>30
<u>LXXLL</u>			
AR-LBD	27 \pm 4	13.1 \pm 1.5	–
AR-LBD-H874Y	25 \pm 5	17.2 \pm 2.1	–
ER β -LBD	–	–	1.2 \pm 0.1

Table 2. Dissociation Half-times of [³H]T and [³H]DHT. Dissociation rates of [³H]T and [³H]DHT from AR, AR-(507-919), and the corresponding H874Y mutants expressed from pCMV5 were determined in transfected COS cells at 37°C as described under “Experimental Procedures”. Dissociation half-times were calculated as the mean \pm S.E. from at least three independent assays.

Dissociation half-times of [³H]T and [³H]DHT (min at 37°C)		
	<u>T</u>	<u>DHT</u>
AR	55 \pm 6	188 \pm 36
AR-H874Y	197 \pm 27	268 \pm 51
AR507-919	25 \pm 3	32 \pm 4
AR507-919-H874Y	49 \pm 4	87 \pm 6

Table 2-3. Crystallographic Data and Refinement Statistics. ^a $R_{\text{sym}} = \sum |I_{\text{avg}} - I_i| / \sum I_i$ is the data consistency where I_{avg} is the mean observed intensity and I_i is the observed intensity. ^b $R_{\text{factor}} = \sum |F_{\text{obs}} - F_{\text{calc}}| / \sum F_{\text{obs}}$, where F_{obs} and F_{calc} are the observed and calculated structure factors. R_{free} is calculated from 3.2% of randomly selected reflections excluded in refinement and R_{factor} calculations. ^cReported as the r.m.s.d. from ideal geometry. ^dStructure coordinates and structure factor files are available at the Protein Data Bank website.

Crystal	AR H874Y T AR20-30	AR H874Y T TIF2-III	AR WT T	AR WT T TIF2-III
X-ray source / λ (Å)	APS-22BM / 0.98	APS-17BM / 0.98	APS-17BM / 0.98	APS-17BM / 0.98
Resolution (Å)	50.0 - 1.80	25.0 - 1.92	24.0 - 1.87	27.0 - 1.90
Space group	P2 ₁ 2 ₁ 2 ₁			
Unit cell (Å)	a=55.9 b=66.1 c=70.7	a=54.4 b=66.8 c=69.9	a=56.0 b=66.4 c=70.8	a=54.8 b=66.9 c=70.2
Unique reflections	24,591	20,085	22,190	20,937
Complete (%) (last shell)	98.5 (87.4)	99.5 (98.1)	98.6 (87.8)	99.9 (100.0)
I/ σ (last shell)	41.1 (3.8)	41.6 (3.0)	41.9 (2.4)	47.4 (3.8)
R_{sym} ^a (%) (last shell)	4.2 (29.9)	4.7 (54.6)	4.4 (60.0)	4.4 (52.6)
Refinement	Refmac	Refmac	Refmac	Refmac
Resolution range	42.7 - 1.8	20.5 - 1.92	20.5 - 1.87	20.6 - 1.90
R factor ^b / R free ^b (%)	18.0 / 20.9	18.2 / 22.1	17.3 / 21.7	18.0 / 22.0
Bond lengths ^c (Å)	0.008	0.009	0.008	0.009
Bond angles ^c (degrees)	1.07	1.15	1.17	1.13
Mean B value	23.7	30.4	28.0	28.7
Non-hydrogen atoms:	2265	2303	2275	2330
protein / peptide	2058	2125	2055	2140
ligand	21	21	21	21
solvent / other	170 / 16	151 / 6	183 / 16	158 / 11
RCSB access code ^d	2Q7K	2Q7L	2Q7I	2Q7J

Table 2-4. Hydrogen Bond Distances and Angles for WT AR LBD Bound with T and AR FXXLF Peptide or DHT and LXXLL Peptide. Gln-711 N is oriented up for WT AR LBD–T with AR-(20-30) FXXLF peptide (Protein Data Bank 2Q7I) and WT AR LBD–DHT with ARA70 FXXLF peptide (Protein Data Bank 1T63) (42) consistent with the original AR LBD–DHT structure (34). Distances and angles were measured by PyMol from heavy atom (H), proton (P), carbonyl oxygen (CO), carbonyl oxygen, or carbon (C), heavy atom to heavy atom (H2H), heavy atom to proton (H2P). Ideal water geometry is tetrahedral with $\sim 109^\circ$ angles.

WT AR LBD-T-FXXLF									
BOND DISTANCE (Å)					BOND ANGLE (°)				
	ATOM	ATOM	H2H	H2P	ATOM	ATOM	ATOM	H2H2H	H2P2H
H - bonds	HOH1	M745O	2.7	–	HOH1	M745O	M745C	–	117
	R752Nη2	T-O3	3.0	2.3	R752Nη2	H	T-O3	126	–
	HOH1	T-O3	3.2	–	HOH1	T-O3	T-C3	–	117
	R752Nη1	HOH1	3.0	2.0	HOH1	H	R752Nη1	151	–
	Q711Nε2	HOH1	2.6	1.8	Q711Nε2	H	HOH1	142	–
	HOH2	Q711O	3.0	–	HOH2	Q711O	Q711C	–	146
Alternate	R752Nη2	HOH1	3.1	2.2	R752Nη2	H	HOH1	145	–
Potential	HOH1	Q711O	3.4	–	HOH1	Q711O	Q711C	–	77
Interactions	HOH2	F764O	2.7	–	HOH2	F764O	F764C	–	143
	Q711Nε2	T-O3	3.7	3.0	Q711Nε2	H	T-O3	127	–
								H2H	H2P (P2P*)
HOH1 Geometry				3-keto O	HOH1	R752Nη1	102	112	
				R752Nη1	HOH1	Q711Nε2	117	128*	
				Q711Nε2	HOH1	T-O3	78	67	
				Q711Nε2	HOH1	M745O	124	112	
				M745O	HOH1	R752Nη1	117	119	
				M745O	HOH1	T-O3	80	–	

WT AR LBD-DHT-LXXLL									
BOND DISTANCE (Å)				BOND ANGLE (°)					
	ATOM	ATOM	H2H	H2P	ATOM	ATOM	ATOM	H2H2H	H2P2H
	HOH1	M745O	2.9	–	HOH1	M745O	M745O	–	117
H - bonds	R752Nη2	T-O3	3.0	2.5	R752Nη2	H	T-O3	110	–
	R752Nη1	HOH1	3.1	2.2	R752Nη2	H	HOH1	151	–
	Q711Nε2	HOH1	2.7	1.9	Q711Nε2	H	HOH1	135	–
	HOH2	Q711O	3.1	–	HOH2	Q711O	Q711C	–	137
Alter-nate	R752Nη2	HOH1	3.0	2.1	R752Nη1	H	HOH1	145	–
Poten-tial	HOH1	Q711O	3.4	–	HOH1	Q711O	Q711C	–	79
Interac-tions	HOH1	T-O3	3.5	–	HOH1	T-O3	T-C3	–	100
	HOH2	F764O	2.9	–	HOH2	F764O	F764C	–	143
	Q711Nε2	T-O3	4.0	3.3	Q711Nε2	H	T-O3	128	–
								H2H	H2P (P2P*)
HOH1 Geometry					M745O	HOH1	R752Nη1	116	116
					R752Nη1	HOH1	Q711Nε2	121	134*
					Q711Nε2	HOH1	M745O	122	108
					Q711Nε2	HOH1	T-O3	79	68
					M745O	HOH1	T-O3	79	–
					R752Nη1	HOH1	T-O3	98	109

CHAPTER 3

MELANOMA ANTIGEN GENE PROTEIN-A11 (MAGE-11) F-BOX LINKS THE ANDROGEN RECEPTOR NH₂-TERMINAL TRANSACTIVATION DOMAIN TO p160 COACTIVATORS

Abstract

Androgen-dependent transcriptional activity by the androgen receptor (AR) and its coregulators is required for male reproductive development and function. In humans and other primates, melanoma antigen gene protein-A11 (MAGE-11) is an AR selective coregulator that increases AR transcriptional activity. Here we show that the interaction between AR and MAGE-11 is mediated by AR NH₂-terminal FXXLF motif binding to a highly conserved MAGE-11 F-box in the MAGE homology domain, and is modulated by serum-stimulation of mitogen-activated protein kinase phosphorylation of MAGE-11 Ser-174. The MAGE-11-dependent increase in AR transcriptional activity is mediated by a direct interaction between MAGE-11 and transcriptional intermediary factor 2 (TIF2) through the NH₂-terminal region of TIF2, and by a MAGE-11 FXXIF motif interaction with an F-box-like region in activation domain 1 of TIF2. The results suggest that MAGE-11 functions as a bridging factor to recruit AR co-activators through a novel FXX(L/I)F motif-F-box interaction paradigm.

Introduction

The androgen receptor (AR) is a ligand-activated transcription factor that mediates the biological effects of testosterone (T) and dihydrotestosterone (DHT). High affinity binding of

androgen targets AR to the nucleus where it interacts with coregulators and androgen response element DNA associated with androgen-regulated genes. Naturally occurring functional knockouts of AR in the human population caused by AR gene mutations result in the androgen insensitivity syndrome, and demonstrate the functional importance of AR in male sex development and maturation (1). Gain-of-function AR somatic mutations identified in clinical specimens of prostate cancer support a critical role for AR during tumor progression to castration-recurrent growth (1–4). The multidomain structure of AR includes the carboxyl-terminal ligand binding domain with activation function 2 (AF2), a hydrophobic interaction surface structurally dependent on bound androgen (5). AR AF2 binds LXXLL motifs of steroid receptor p160 coactivators (SRC), but interacts preferentially with the FXXLF motif in the AR NH₂ terminus (6, 7). AR activation function 1 (AF1) in the unstructured NH₂-terminal region interacts with multiple coregulatory proteins (8, 9).

AR undergoes an androgen-dependent NH₂- and COOH-terminal (N/C) interaction mediated by the AR NH₂-terminal FXXLF motif (²³FQNLF²⁷) binding to AF2 in the ligand binding domain (5, 10–14). The ligand-dependent AR N/C interaction stabilizes AR and underlies the potency differences between testosterone and DHT (2, 11, 13–15). The AR N/C interaction coordinates transcriptional activity between AF1 and AF2, in part by competitively inhibiting the SRC/p160 coactivator LXXLL motif binding to AF2 (15). The regulatory effect of the AR N/C interaction is modulated by melanoma antigen gene protein-A11 (MAGE-11), a MAGE gene family member and AR coregulator that binds the AR NH₂-terminal FXXLF motif, competes with the AR N/C interaction, and enhances AR transcriptional activity by increasing accessibility of AF2 for SRC/p160 coactivator recruitment (16).

MAGE-11 expression is limited to human and nonhuman primates (17, 18), suggesting it arose during mammalian evolution as an additional control mechanism in the AR signaling network. Post-translational modification of MAGE-11 by phosphorylation of Thr-360, and subsequent monoubiquitinylation of Lys-240 and Lys-245 within the MAGE homology domain, a highly conserved region of the MAGE gene family, is induced by epidermal growth factor (EGF) and stabilizes the interaction with AR (19). The increase in MAGE-11 levels in castration-recurrent prostate cancer during androgen deprivation therapy by DNA hypomethylation at the transcriptional start site supports the concept that MAGE-11 increases AR signaling in prostate cancer (20).

To understand the molecular mechanisms whereby MAGE-11 enhances AR transactivation, we pursued observations that MAGE-11 acts coordinately with transcriptional intermediary factor 2 (TIF2), one of the SRC/p160 coactivators implicated in AR signaling (16, 19). Previous studies have shown that TIF2 can associate with the NH₂-terminal region of AR, although the sites of interaction were not well defined (8, 10, 21). We considered the possibility that MAGE-11 enhances AR activity from AF1 through a direct interaction between MAGE-11 and TIF2.

The present study provides evidence that the AR NH₂-terminal FXXLF motif interacts with a highly conserved MAGE-11 F-box (residues 329–369) in the MAGE homology domain, and that the interaction is modulated by mitogen-activated protein (MAP) kinase phosphorylation of MAGE-11 Ser-174 in response to serum stimulation. MAGE-11 also interacts directly with the NH₂-terminal region of TIF2, and with the TIF2 AD1 region through a MAGE-11 FXXIF motif (²⁶⁰FPEIF²⁶⁴). The results suggest AR-mediated gene

transcription involves a novel protein interaction paradigm of the FXX(L/I)F motif binding to the F-box.

Materials and Methods

Plasmids—Expression plasmids include pCMV-AR (22), FLAG-AR (16), pCMV-AR-(1–660) (23), pCMV-AR Δ 120–472 (19), VP-AR-(1–660) (6), GAL-AR-(16–36) and -(4–52) (24), pSG5-MAGE-(1–429) (pSG5-MAGE), GAL-MAGE-(2–429) (GAL-MAGE), VP-MAGE-(2–429) (VP-MAGE), FLAG-MAGE-(2–429) (FLAG-MAGE) (16), pSG5-HA-MAGE-(2–429) and -(112–429), GAL-MAGE-K236A, -K240A,K245A, and -T360A, VP-MAGE-K236A,K240A,K245A and T360A (19), GAL-TIF2.0-(1–627), 2.1-(624–1287), 2.2-(1288–1464), 2.3-(624–1287), 2.3m123-(624–1179-L644E,L645A,L693A, L694A,L748A,L749A), 2.8-(1011–1179) and 2.12-(940–1131), VP-TIF2.0-(1–627), and pSG5-TIF2 (25).

Reporter vectors include prostate-specific antigen (PSA) enhancer luciferase (PSA-Enh-Luc) (26), mouse mammary tumor virus-luciferase (MMTV-Luc), MMTV Δ -(–421––364)-Luc, which contains a deletion of a negative response element (27–29), and 5 \times GAL4Luc3 (30). MMTV Δ -(–421––364)-Luc was created by PCR mutagenesis of MMTV-Luc (31), with the XhoI/BamHI fragment inserted at the same sites of MMTV-Luc. GST-TIF2-(1–627), -(624–1141), -(1180–1464), and -(1288–1464) were created by PCR amplifying corresponding regions of pSG5-TIF2 and inserting the EcoRI/XhoI-digested fragments into similarly digested pGEX-4T-1. FLAG-TIF2 vectors were constructed by a triple ligation: TIF2-(1–569) was PCR amplified from pSG5-TIF2 and digested with EcoRI/NdeI to obtain TIF2-(1–370); TIF2-(370–1464) was obtained by digesting the parent template with NdeI/XbaI; both fragments were ligated into EcoRI/XbaI sites of pCMV5-

FLAG-b. VP-TIF2.0-I336A, Y337A, pCMV-AR Δ 120–472-V33E, -K720A, -E897K, and -L26A,F27A, MAGE-11 alanine mutants, and phosphomimetics were created using QuikChange site-directed mutagenesis (Stratagene).

pSG5-HA-MAGE-(112–307), -(112–298), -(112–276), -(165–307) and -(Δ 329–369) were created by PCR amplification using primers containing EcoRI/SalI ends and ligation into pSG5-HA. Additional MAGE-11 F-box deletion mutants were created by double PCR mutagenesis to create an EcoRI/XhoI MAGE Δ 329–369 fragment that was inserted into the same sites of pSG5-HA to make pSG5-HA-MAGE Δ 329–369, and into EcoRI/SalI sites of FLAG-b to make FLAG-MAGE Δ 329–369.

GAL-MAGE-(85–205) and -(112–205) were created by PCR amplifying pSG5-MAGE and inserting EcoRI/XhoI-digested fragments into GAL0 digested with EcoRI and SalI. GAL-MAGE-(112–170) was created by PCR amplifying the parent template and ligating the EcoRI/SalI-digested fragment into the same sites of GAL0. GAL-MAGE-(251–272) wild-type and F260A,F264A mutant were created by cloning a small DNA insert into EcoRI and SalI sites of GAL0. All PCR-amplified regions were verified by DNA sequencing.

DNA Transfection-CWR-R1 prostate cancer cells were maintained and transfected using Effectene (Qiagen) as described (2, 32). CWR-R1 cells (1.6×10^5 cells/well) were transfected in 12-well plates with 0.1 μ g/well of MMTV-Luc or MMTV Δ (-421--364)-Luc in the absence and presence of 0.1 μ g of pSG5-MAGE-11 and/or 0.1 μ g of pSG5-TIF2. Medium was replaced 24 h later with serum-free, phenol red-free medium in the absence and presence of DHT and/or EGF and incubated at 37 °C overnight.

For small interfering RNA (siRNA) studies, CWR-R1 cells (4×10^5 /well) in 6-well plates were plated in 1 ml of antibiotic-free medium without EGF and transfected using Lipofectamine 2000 reagent (Invitrogen) in antibiotic-free medium with 0.1 μ g of MMTV Δ (-421--364)-Luc and 0.2 μ g of pSG5 or pSG5-MAGE with and without 4 nM TIF2 siRNA-3 (GAUCAGAAGUGACUAUUA) or siCONTROL nontargeting siRNA pool (Dharmacon RNA Technologies). After 48 h at 37 °C, cells were transferred to serum-free, phenol red-free medium containing antibiotics in the absence and presence of 0.1 DHT and 0.01 μ g/ml of EGF. After 24 h cells were lysed in 0.25 ml of buffer containing 1% Triton X-100, 2 mM EDTA, and 25 mM Tris phosphate, pH 7.8 (19). Luciferase activity was measured using an automated Lumistar Galaxy multiwell plate luminometer (BMG Labtech). Luciferase data are representative of at least three independent experiments, with the graphs showing the mean \pm S.E.

COS cells (4×10^5 /6-cm dish) were transfected in antibiotic-free medium using Lipofectamine 2000 with pSG5-MAGE, pSG5-TIF2, pCMV-AR, or empty parent vector in the absence and presence of 1 nM siRNA targeting MAGE-11, TIF2, AR, or nonspecific siCONTROL. The next day cells were placed to serum-free medium, and 24 h later extracts were analyzed by immunoblot as described below.

For inhibition of endogenous PSA mRNA expression, CWR-R1 cells (10^6 /6-cm dish) were transfected using Lipofectamine 2000 in 2% charcoal-stripped serum medium without antibiotics with 4 nM MAGE-11 siRNA-2 (GCACUGAUCCUGCAUGCUAUU), MAGE-11 siRNA-3 (CAACUGCUCUUUGGCAUUGUU), AR siRNA-3 (UCAAGAACUCGAUCGUAUUU), TIF2 siRNA-3, and siCONTROL nonspecific siRNA (Dharmacon RNA Technologies). After 48 h cells were treated for 6 h in fresh medium with

and without 10 nM DHT and 10 ng/ml of EGF. RNA was extracted in 1 ml of TRIzol (Invitrogen) and analyzed by quantitative reverse transcription-PCR using SuperScript II reverse transcriptase (Invitrogen), 4 µg of RNA reverse transcription-PCR, CTCATCCTGTCTCGGATTGT and AGAAACAGGCTGTGCCGAC PSA primers (amplify a 189-bp fragment spanning amino acids residues 20–82), and control peptidylprolyl isomerase A primers ATCTTGTCATGGCAAATGC and GCCTCCACAATATTCATGCC (amplify a 134-bp fragment spanning amino acids residues 97–141). Reactions were performed using a Roche LightCycler in 20 µl containing 0.4 µg of cDNA, 10 µl of 2× QuantiTect SYBR PCR Master Mix (Qiagen), and 2 µl of 2 µM primers at 95 °C for 15 min followed by 55 cycles of 94 °C for 15 s, 58 °C (PSA) or 55 °C (peptidylprolyl isomerase A) for 30 s, 72 °C for 30 s, and 79 °C for 8 s. A no template control was included in each run using standard curves for PSA and peptidylprolyl isomerase A (33).

LAPC-4 human prostate cancer cells were cultured in RPMI 1640 medium (Invitrogen) supplemented with 2 mM l-glutamine, penicillin, streptomycin, 10% fetal bovine serum, and 1 nM methyltrienolone (R1881) (34). LAPC-4 cells (5×10^5 cells/well) in 6-well plates containing 1 ml of antibiotic-free medium without R1881 were transfected the following day using Lipofectamine 2000 with 0.1 µg/well of MMTV Δ (-421--364)-Luc in the absence and presence of 3 nM siRNA. After 48 h at 37 °C, cells were transferred to serum-free, phenol red-free medium containing antibiotics in the absence and presence of 0.1 nM DHT and 0.1 µg/ml of EGF, and luciferase activity was measured 24 h later.

Human endometrial Ishikawa cells (10^5 cells/well) were transfected in 12-well plates using FuGENE 6 (Roche Applied Science) (19, 33) with 0.1 µg/well of PSA-Enh-Luc and 0.1 µg of pSG5 empty vector, wild-type, and mutant pSG5-MAGE. The next day medium

was replaced with serum-free, phenol red-free medium in the absence and presence of 1 nM DHT with and without 0.1 µg/ml EGF. Twenty-four h later, luciferase activity was measured.

Monkey kidney CV1 cells (4.2×10^5 /6-cm dish) were transfected using calcium phosphate (15) with 0.05 or 0.1 µg of wild-type or mutant pCMV-AR and the indicated amounts of pSG5-TIF2, pSG5-MAGE, MMTV-Luc, or PSA-Enh-Luc. Immediately after transfection and 24 h later, cells were placed in serum-free, phenol red-free medium in the absence and presence of 1 nM DHT, incubated for 24 h at 37 °C, and luciferase activity was measured.

Mammalian two-hybrid assays were performed in human HeLa epithelial cervical carcinoma cells (5×10^4 cells/well) transfected using FuGENE 6 (2) in 12-well plates with 0.1 µg/well of 5×GAL4Luc3, 0.05 µg of wild-type or mutant GAL-MAGE, GAL-TIF2, GAL-AR-(4–52), or GAL-AR-(16–36) with 0.1 µg of wild-type or mutant VP-AR-(1–660), VP-MAGE, or VP-TIF2.0. The day after transfection, cells were transferred to serum-free medium and incubated overnight at 37 °C before luciferase activity was measured.

Immunochemistry-Immunoblotting and immunoprecipitation were performed by transfecting each 10-cm dish with 2–4 dishes/group, $1.8\text{--}2.5 \times 10^6$ monkey kidney COS-1 cells and 6×10^6 human embryonic kidney 293 cells using DEAE dextran (2, 7), 2.0×10^6 CV1 cells using 450 µl of H₂O, 75 µl of CaCl₂, and 675 µl of 2× HBS added to 8 ml of medium/10-cm dish (2× HBS = 0.28 M NaCl, 0.05 M Hepes, and 1.5 mM Na₂HP0₄, pH 7.1). HeLa cells (7.5×10^5) and 4.4×10^5 Ishikawa cells were transfected using 8 µl of FuGENE 6 and 160 µl of medium in 6 ml of medium. Twenty-four h after transfection, cells were transferred to serum-free, phenol red-free medium in the absence and presence of 0.1 µg/ml of EGF, 10 nM DHT, and/or 1 µM MG132, a proteasome inhibitor. After 24 h, cells were

harvested in phosphate-buffered saline. For siRNA experiments, COS-1 cells (4×10^5 cells/well) plated in antibiotic-free medium in 6-well plates were transfected using Lipofectamine 2000 reagent with pSG5, pSG5-MAGE, pSG5-TIF2, or pCMV-AR in the absence and presence of siRNA.

For phosphorylation studies, COS cells (2×10^6 /10-cm dish) were transfected using DEAE dextran and extracted in immunoprecipitation (IP) lysis buffer containing 0.15 M NaCl, 0.5% Nonidet P-40, 10% glycerol, 50 mM Tris-HCl, pH 7.5, Complete protease inhibitor mixture (Roche), 1 mM dithiothreitol, and 1 mM phenylmethylsulfonyl fluoride. Protein concentration was measured using the Bio-Rad assay and bovine serum albumin as standard. Cell extracts were incubated in the absence and presence of 800 IU of λ -phosphatase (New England Biolabs) for 1 h at 4 °C. For immunoblots, cells were solubilized in immunoblot (IB) lysis buffer containing 0.15 M NaCl, 1% Triton X-100, 0.1% SDS, 1% sodium deoxycholate, 0.5 mM EDTA, 50 mM Tris-HCl, pH 7.5, 1 mM phenylmethylsulfonyl fluoride, 1 mM dithiothreitol, and Complete protease inhibitor mixture (Roche). For inhibition of MAP kinase, U0126 (Promega) was added immediately after transfection to serum-containing medium. Cells were transferred 24 h later to serum-free medium with and without the same concentration of U0126 and 1 μ m MG132. The next day cells were solubilized in IB lysis buffer containing Phosphatase Mixture Inhibitors 1/2 (Sigma). Protein extracts were combined with 0.2 volumes of 6 \times sample buffer containing 10% SDS, 30% glycerol, 30% 2-mercaptoethanol, and 0.35 M Tris-HCl, pH 6.8.

Immunoprecipitation was performed using 2–4 10-cm dishes/group of transfected COS-1 or HEK293 cells harvested in phosphate-buffered saline and pooled (15). Cells were solubilized in IP lysis buffer containing 0.05 M sodium fluoride. Lysates were precleared

using 0.1 ml of agarose (Sigma) by rotating for 1 h at 4 °C. Samples were transferred to 15 µl of anti-FLAG M2 affinity-agarose (Sigma) and incubated at 4 °C for 1 h or overnight. Samples were washed 3 times with IP lysis buffer, and protein was resuspended in 0.05 ml of 2× SDS sample buffer containing 3.3% SDS, 10% 2-mercaptoethanol, 10% glycerol, and 0.12 M Tris-HCl, pH 6.8. Immunoprecipitates, protein extracts, and EZ-Run Prestained Rec protein ladder (Fisher Bioreagents) were separated on 8, 10, or 12% acrylamide gels containing SDS and transferred overnight to nitrocellulose membranes at 4 °C.

Immunoblots were probed using the following antibodies: rabbit anti-HA tag (1:2500, Abcam, ab9110), mouse anti-β-actin (1:5000, Abcam), rabbit anti-GAL (1:500, Santa Cruz Biotechnology, sc-577), rabbit anti-VP16 activation domain (1:2000, Abcam, ab4809), mouse anti-FLAG M2 monoclonal antibody (1:2000, Sigma, F3165), mouse anti-TIF2 (1:275, BD Transduction Laboratories, 610985), rabbit anti-Skp1 (1:400, Abcam, ab10546), rabbit AR32 immunoglobulin G (22) (0.4 µg/ml), rabbit AR52 immunoglobulin G (5 µg/ml) (35, 36), rabbit anti-MAGE-11 peptide antibodies MagAb-(13–26), -(59–79), and -(94–108) immunoglobulin G (6–10 µg/ml) (33), and rabbit polyclonal FLAG-MAGE antibody (10 µg/ml) raised against purified baculovirus-expressed FLAG-tagged human MAGE-11. Incubations with primary antibody were performed for 1 h at room temperature or overnight at 4 °C, and with anti-mouse and anti-rabbit horseradish peroxidase-conjugated secondary IgG antibodies (1:10,000, Amersham Biosciences) at room temperature for 1 h. Signals were detected using chemiluminescence (SuperSignal West Dura Extended Duration Substrate, Pierce).

In Vitro Binding and Kinase Assays-Glutathione S-transferase (GST) affinity matrix binding assays were performed with GST-TIF2 fusion proteins and ³⁵S-labeled MAGE-11

expressed from pSG5-MAGE-11 using the TnT T7 Quick Coupled transcription-translation system (Promega) (6, 10). GST empty vector pGEX-4T-1 and GST-TIF2 fusion proteins were expressed in XL1-Blue *Escherichia coli* by incubating in the presence of 1 mM isopropyl 1-thio- β -D-galactopyranoside for 3 h at 37 °C. Cell pellets were resuspended in GST binding buffer containing 0.5% Nonidet P-40, 1 mM EDTA, 0.1 M NaCl, 20 mM Tris-HCl, pH 8.0, with 1 mM dithiothreitol, 1 mM phenylmethylsulfonyl fluoride, and protease inhibitor mixture (Sigma). Protein expression was normalized by Coomassie Blue staining of a mini-gel. Fusion proteins were incubated with glutathione-Sepharose 4B beads (Amersham Biosciences) for 1.5 h at 4 °C, washed in GST binding buffer, and combined with ³⁵S-labeled MAGE-11 prepared using 25 μ Ci/sample of [³⁵S]methionine (PerkinElmer Life Sciences) and incubated for 2 h at 4 °C. Beads were washed, eluted using 2 \times SDS sample buffer, and analyzed on a 10% gel containing SDS.

In vitro kinase assays were performed as described (19) except using full-length recombinant active extracellular signal-regulated kinase 1 (ERK1) expressed from baculovirus in Sf9 cells (BioVision, 0.1 μ g/ μ l, specific activity 383 nmol/min/mg) and GST-MAGE-¹⁷¹PPQSPQEES¹⁷⁹, GST-MAGE-¹⁷¹PPQAPQEES¹⁷⁹, and GST-APRTPGGRR ERK1 peptide substrates modeled after myelin basic protein (37). GST fusion proteins were expressed from pGEX-4T-1 by cloning short inserts into EcoRI/XhoI (MAGE-11) and EcoRI/SalI sites (ERK1 control peptide) designed to disrupt the cloning site for rapid clone identification. GST-peptide-Sepharose bead suspensions (50 μ l) were washed in kinase buffer (1 mM EGTA, 0.4 mM EDTA, 5 mM MgCl₂, 0.05 mM dithiothreitol, and 5 mM MOPS, pH 7.2) and incubated in kinase buffer containing 5 μ l of 0.25 mM ATP and 0.16 μ Ci/ μ l of [γ -³²P]ATP (10 mCi/ml, 3000 Ci/mmol, PerkinElmer Life Sciences) for 30 min at

30 °C. Samples were separated on an 8–16% gradient minigel containing SDS (Invitrogen). Dried gels were exposed to x-ray film for 16 h and rehydrated for protein staining using Coomassie Blue.

Results

Dependence of AR Transactivation on MAGE-11 and TIF2-The ability of MAGE-11 to function as an AR coregulator in association with TIF2 was evaluated in CWR-R1 prostate cancer cells where the response to DHT was maximal at 0.1 nM DHT. Expression of MAGE-11 enhanced the dose-dependent increase in AR transactivation in CWR-R1 cells in response to DHT, and DHT and EGF, to a greater extent than TIF2 (Fig. 3-1A). Coexpression of MAGE-11 and TIF2 increased both ligand-dependent and ligand-independent AR activity to a greater extent than MAGE-11 or TIF2 alone.

TIF2 siRNA-3 inhibited TIF2 expression (Fig. 3-1B), and the MAGE-11-dependent increase in AR transcriptional activity in CWR-R1 cells (Fig. 3-1C), supporting the synergistic effects of MAGE-11 and TIF2. In LAPC-4 prostate cancer cells, the DHT and EGF-dependent increase in AR transactivation was inhibited by MAGE-11 siRNA-2, but not siRNA-3 (Fig. 3-1D), consistent with their relative inhibitory effects on MAGE-11 expression (Fig. 3-1B).

In CWR-R1 cells, endogenous AR was readily detected on immunoblots (Fig. 3-1E), whereas endogenous MAGE-11 was evident ~14 h after inducing quiescent cells to enter the cell cycle by treating with DHT and EGF (Fig. 3-1E, *upper panel*). The results suggest that endogenous MAGE-11 levels are low and cell cycle regulated, which may have hindered our attempts to coimmunoprecipitate endogenous MAGE-11 with AR or TIF2. However, we were able to demonstrate that siRNA knockdown of AR, MAGE-11, or TIF2 in CWR-R1

cells decreased the DHT and EGF-stimulated increase in PSA, an endogenous AR-regulated gene (Fig. 3-1E, *lower panel*). The results suggest that MAGE-11 functions coordinately with TIF2 to increase AR transactivation.

Identification and Function of a MAGE-11 F-box-The carboxyl-terminal region of MAGE-11 contains sites of EGF-dependent phosphorylation and ubiquitinylation required for MAGE-11 to interact with AR (Fig. 3-2A) (16, 19). Examination of the MAGE-11 sequence revealed a predicted α -helical F-box-like sequence

IPEE Ψ ₃X Ψ ₂X₂ Ψ X Ψ X₇ Ψ ₂X₆ Ψ X₈ Ψ ₂ similar to cyclin F, where Ψ is a hydrophobic residue and X is any amino acid. Sequence similarity with the F-box of cyclin F was noted throughout the MAGE gene family (Fig. 3-2B). The functional significance of MAGE-11 F-box residues 329–369 was supported by the presence of the EGF-dependent Thr-360 Chk1 phosphorylation site within the F-box (*underlined* in Fig. 3-2B), because phosphorylation at Thr-360 is required for MAGE-11 to interact with AR (16, 19).

The functional properties of the MAGE-11 F-box were investigated by creating alanine point mutations at conserved hydrophobic residues (Fig. 3-2C) and testing their effect on AR transactivation in Ishikawa cells, a human endometrial cell line that responds to EGF (Fig. 3-2D). The MAGE-11 F-box mutations reduced or eliminated the MAGE-11-dependent increase in AR transcriptional activity in response to DHT, and DHT and EGF.

Coimmunoprecipitation of AR with FLAG-MAGE in the absence and presence of DHT and EGF was not eliminated by the single or double mutations within the MAGE-11 F-box (data not shown), although deletion of the F-box inhibited the coimmunoprecipitation of MAGE-11 with FLAG-AR (Fig. 3-2E). The results suggest that a MAGE-11 F-box dependent interaction increases AR transcriptional activity.

Synergistic Effects of TIF2 on AR AF2 Activity Depend on the MAGE-11 F-box-The MAGE-11 and TIF2-dependent increase AR transcriptional activity that derives from AF2 in the ligand binding domain was investigated using full-length AR and AR Δ 120–472, a deletion mutant in which the AR NH₂-terminal AF1 region was deleted (Fig. 3-3B, *lower panel*). AR Δ 120–472 retains the AR NH₂-terminal FXXLF motif (²³FQNLF²⁷) that interacts with MAGE-11 and AR AF2. Androgen-dependent transcriptional activity of AR Δ 120–472 depends entirely on AF2.

In agreement with results in Fig. 3-2D, MAGE-11 F-box mutants, as shown for MAGE-L358A, L359A, eliminated the MAGE-11 and TIF2-dependent increase in AR transactivation (Fig. 3-3A). The ability of MAGE-11 and TIF2 to increase androgen-dependent AR Δ 120–472 activity (Fig. 3-3, B and C) demonstrates the synergistic effects of MAGE-11 and TIF2 on AF2 activity.

The dependence of AR Δ 120–472 transactivation on TIF2 binding to AF2 was demonstrated by the loss of activity caused by introducing the AR AF2 K720A or E897K charge clamp mutation that prevents TIF2 binding to AF2 (Fig. 3-3B), and by a TIF2 LXXLL motif mutant unable to bind AF2 (data not shown) (10). Transcriptional activity of AR Δ 120–472 was also eliminated by V33E, an AR mutation that inhibits AR FXXLF motif binding to MAGE-11 but not to AF2 (16) (Fig. 3-3B). This demonstrates that MAGE-11 binding to AR Δ 120–472 is required to relieve repression of AF2 activity caused by the AR N/C interaction.

The inhibitory effect of the AR N/C interaction on AF2 transcriptional activity was also indicated by the TIF2- dependent increase in AR Δ 120–472-FXXAA activity (Fig. 3-3B, *L26A,F27A*). In this case, mutations in the AR FXXLF motif inhibit binding to both AF2 and

MAGE-11 (6, 16), allowing TIF2 activation of AF2. AR Δ 120–472 activity in the presence of TIF2 was also inhibited by the double and most of the single mutations in the MAGE-11 F-box (Fig. 3-3, C and D). The results indicate that the MAGE-11 F-box is required for the synergistic effects of MAGE-11 and TIF2 on AR AF2 transcriptional activity.

MAGE-11 F-box Binds the AR FXXLF Motif and Skp1-Mammalian two-hybrid assays provide evidence that the MAGE-11 F-box interacts with the AR FXXLF motif (Fig. 3-4). A series of single F-box mutations in GAL-MAGE eliminated the interaction with VP-AR-(1–660), an AR NH₂-terminal fragment that contains the AR FXXLF motif and DNA binding domain (Fig. 3-4A). The AR FXXLF motif-dependent interaction with MAGE-11 was shown by loss of the interaction with VP-AR-(1–660)-FXXAA (LFAA) as reported previously (16). Interaction of the AR FXXLF motif with MAGE-11 was also eliminated by the MAGE-T360A mutation that disrupts a Chk1 phosphorylation site within the MAGE-11 F-box, and by mutations at monoubiquitinylation sites outside the F-box region (19).

To further characterize MAGE-11 F-box binding to the AR FXXLF motif, VP-MAGE single residue F-box mutants were coexpressed with GAL-AR-(4–52) or GAL-AR-(16–36), two short AR NH₂-terminal FXXLF motif peptides. VP-MAGE F-box mutations inhibited the interaction with the AR NH₂-terminal peptides (Fig. 3-4, B and C). The interaction was also influenced by a mutation at a potential MAP kinase phosphorylation site at MAGE-11 Ser-174, which lies outside the F-box. VP-MAGE binding to GAL-AR-(4–52) or GAL-AR-(16–36) decreased with the MAGE-11 S174A mutation, but was unchanged by the S174D phosphomimetic.

MAGE-11 also interacted with Skp1 based on coimmunoprecipitation of endogenous Skp1 with FLAG-MAGE in HEK293 cells (Fig. 3-4D). This suggests an additional and more classical function of the MAGE-11 F-box.

The results indicate a MAGE-11 F-box interaction with the AR FXXLF motif that is influenced by phosphorylation at Thr-360 within the F-box, and potential phosphorylation at Ser-174 NH₂-terminal to the F-box. MAGE-11 also interacts with Skp1, which suggests the MAGE-11 F-box serves as a binding site for Skp1, and MAGE-11 may associate with a Skp1-cullin-based E3 ubiquitin ligase complex.

Serum Stimulation of MAP Kinase Phosphorylation of MAGE-Ser-174-The MAGE-11 sequence flanking Ser-174 contains several potential Ser-Pro phosphorylation sites that include the MAP kinase consensus sequence ¹⁷²PQSP¹⁷⁵ (Fig. 3-5A). This, together with evidence that the S174A mutation inhibited MAGE-11 interaction with the AR FXXLF motif peptides, led us to investigate whether MAGE-11 is phosphorylated at Ser-174 by MAP kinase.

GAL-MAGE-(112–205) is a fusion protein that contains the MAGE-(168–182) Ser-Pro region and migrates as a double band before, and single band after treatment with λ-phosphatase (Fig. 3-5B, *lanes 1* and *2*), which suggests GAL-MAGE-(112–205) is phosphorylated. Evidence that Ser-174 is a phosphorylation site was obtained from GAL-MAGE-(112–205)-S174A, which migrated as a single band of similar mobility before and after treatment with λ-phosphatase (Fig. 3-5B, *lanes 3* and *4*). GAL-MAGE-(112–205)-S181A or -S117A mutants maintained the double band migration, which was eliminated by treatment with λ-phosphatase (Fig. 3-5B, *lanes 5* and *9*). The GAL-MAGE-(112–205)-S174A,S181A double mutant (Fig. 3-5B, *lanes 7* and *8*), and GAL-MAGE-(112–170), which

lacks Ser-174 (Fig. 3-5B, lanes 11 and 12), migrated as single bands before and after treatment with λ -phosphatase. The results point to Ser-174 as a phosphorylation site in MAGE-11. Based on the MAP kinase consensus sequence at Ser-174, and decreased binding of AR FXXLF motif peptides to MAGE-S174A but not the MAGE-S174D phosphomimetic, we investigated whether a MAP kinase inhibitor or hormone stimulation would influence phosphorylation of MAGE-Ser-174.

Increasing concentrations of U0126, a MEK1 inhibitor that prevents activation of ERK1/2 (38), eliminated the double band migration of GAL-MAGE-(112–205), but had no effect on GAL-MAGE-(112–205)-S174A (Fig. 3-5C). Neither treatment with EGF (0.1 μ g/ml) nor dibutyryl cyclic AMP (10 mM) altered the double band migration of GAL-MAGE-(112–205) (data not shown). However, addition of 10% serum to quiescent cells caused a time-dependent increase in intensity of the slower migrating band (Fig. 3-5D). In addition, introducing the MAGE-S174A mutation eliminated *in vitro* ERK1 phosphorylation of a GST-MAGE-(171–179) fusion peptide (Fig. 3-5E). The results suggest that serum stimulation of ERK1 phosphorylation at MAGE-Ser-174 modulates the MAGE-11 F-box interaction with the AR FXXLF motif.

Interaction Between MAGE-11 and TIF2-The studies suggested that MAGE-11 and TIF2 act synergistically to increase AR transactivation through AF2 (Figs. 3-1 and 3-3), but it remained unclear whether MAGE-11 could increase TIF2-dependent AR transcriptional activity independent of AF2. To address this, we made use of AR-(1–660), a constitutively active AR NH₂-terminal fragment that contains AF1, but lacks the AR ligand binding domain and AF2.

The relatively low activity of AR-(1–660) increased ~2-fold with the coexpression of TIF2 (Fig. 3-6A). This agrees with previous evidence that AR activation by TIF2 in the absence of MAGE-11 depends largely on TIF2 LXXLL motif binding to AR AF2 (6). AR-(1–660) activity increased to a greater extent with the expression of MAGE-11, and increased further with the coexpression of MAGE-11 and TIF2. The MAGE-11 and TIF2-dependent increase in AR-(1–660) activity was inhibited by MAGE-11 F-box mutations that interfere with MAGE-11 binding to the AR-(1–660) FXXLF motif (Fig. 3-6B).

The results raised the possibility of a direct interaction between MAGE-11 and TIF2 that could increase AR transcriptional activity in the absence and presence of androgen. An interaction between endogenous MAGE-11 and TIF2 in CWR-R1 or LAPC-4 cells could not be observed, possibly due to the low level cell cycle-dependent expression of MAGE-11 (Fig. 3-1E). Furthermore, the association between MAGE-11 and TIF2 may be transient like AR and MAGE-11 in the presence of DHT (16). However, an interaction between TIF2 and MAGE-11 was demonstrated by coimmunoprecipitation of HA-MAGE with FLAG-TIF2 (Fig. 3-7A), and by the coimmunoprecipitation of TIF2 with FLAG-MAGE (Fig. 3-7B). A direct interaction between MAGE-11 and TIF2 was supported by *in vitro* affinity matrix binding studies. MAGE-11 interacted to the greatest extent with the TIF2 NH₂-terminal region present in GST-TIF2.0-(1–627), and to a lesser extent with TIF2 carboxyl-terminal fragments, some of which contain AD1-(1011–1179) (Fig. 3-7C). The results suggest that MAGE-11 interacts directly with TIF2 to increase AR transcriptional activity.

MAGE-11 and TIF2 Interacting Domains-Mapping the interaction regions between MAGE-11 and TIF2 was performed initially using MAGE-11 deletion mutants (Fig. 3-8A). The requirement for MAGE-11 residues 112–298 was shown by coimmunoprecipitation of

MAGE-(112–429), -(112–307), and -(112–298) with FLAG-TIF2, compared with weaker interactions with MAGE-(112–276) and -(165–307) (Fig. 3-8B). Further resolution of the MAGE-11 interaction domains for TIF2 was limited by poor expression of the smaller MAGE-11 fragments.

In agreement with the *in vitro* binding results (Fig. 3-7C), regions in TIF2 (see diagram, Fig. 3-9A) that interacted with MAGE-11 included TIF2 NH₂-terminal 1–627 and AD1 1011–1179 residues. This was evident by the coimmunoprecipitation of HA-MAGE and HA-MAGE-(112–429) with FLAG-TIF2 (Fig. 3-8C, *top panel, lanes 3 and 4*), FLAG-TIF2.0-(1–627) (*lanes 5 and 6*), and FLAG-TIF2.8-(1011–1179), which contains AD1 (*lanes 7 and 8*). The MAGE-(112–307) region NH₂-terminal to F-box residues 329–369 was sufficient to interact with the NH₂-terminal region of TIF2 (Fig. 3-8D). Interaction between MAGE-11 and the NH₂-terminal region of TIF2 was also demonstrated in mammalian two-hybrid assays using VP-TIF2.0-(1–627) and GAL-MAGE-(85–205) (Fig. 3-8E). The GAL-MAGE-(85–205)-S174D phosphomimetic of MAP kinase site Ser-174 had greater inherent transcriptional activity than wild-type GAL-MAGE-(85–205) or the S174A mutant. However, the fold-increase in the presence of VP-TIF2.0-(1–627) and GAL-MAGE-(85–205) or the S174A and S174D mutants was similar relative to the VP16 empty vector controls. This suggests that phosphorylation at Ser-174 does not influence the interaction between MAGE-11 and TIF2.

Interaction between MAGE-11 and the AD1 region of TIF2 was also demonstrated by the ability of MAGE-11 to increase the transcriptional activity of GAL-TIF2 fusion proteins (Fig. 3-9A). Both full-length MAGE-11 and MAGE-(112–429) increased the transcriptional activity of GAL-TIF2.1-(624–1287) and GAL-TIF2.3-(624–1179)-m123, where the latter

contains mutations at each of the three TIF2 LXXLL motifs (Fig. 3-9B). These results support the *in vitro* binding and coimmunoprecipitation evidence that MAGE-11 interacts directly with TIF2 independent of the TIF2 LXXLL motifs.

Evidence that transcriptional activity arising from the MAGE-11 interaction with TIF2 requires the TIF2 AD1 region was supported by the absence of a MAGE-dependent increase in GAL-TIF2.0-(1–627) activity (Fig. 3-9B), even though the TIF2 NH₂-terminal region, which lacks AD1, interacts with MAGE-11 (see Figs. 3-7C and 3-8E). Full-length MAGE-11 and the MAGE-(112–429) fragment also increased the activity of GAL-TIF2.8-(1011–1179) and GAL-TIF2.12-(940–1131), TIF2 fragments with only AD1 in common (Fig. 3-9A and 3-9C).

Mutations in the MAGE-11 F-box inhibited the ability of MAGE-11 to increase the AD1 activity of GAL-TIF2.8 (Fig. 3-9D). This appears to reflect a decreased transcriptional response of GAL-TIF2.8 AD1 to p300, which is known to interact with TIF2. Alone, p300 resulted in a small increase in GAL-TIF2.8 activity. In the presence of MAGE-11, p300 increased TIF2 AD1 activity in a MAGE-11 F-box-dependent manner (Fig. 3-9E). The results indicate that the MAGE-(165–298) region interacts with the NH₂-terminal and AD1 regions of TIF2, and that the MAGE-11 F-box influences TIF2 AD1 activation by p300.

MAGE-11 FXXIF Motif-Within the MAGE-(165–298) region that interacts with TIF2 is a predicted α -helical FXXIF motif with the sequence ²⁶⁰FPEIF²⁶⁴ flanked by charged residues similar to the AR FXXLF motif sequence ²³FQNLF²⁷ (Fig. 3-10A). The AD1 region of TIF2 also contains a predicted α -helical sequence with spacing of hydrophobic residues similar to the F-box in cyclin F, Skp2, and MAGE-11 (Fig. 3-10B). We therefore

investigated whether the MAGE-11 FXXIF motif contributes to the interaction with TIF2 AD1.

Interaction between MAGE-11 and the AD1 region of TIF2 was indicated by the coimmunoprecipitation of HA-MAGE-(112–429) with FLAG-TIF2.8-(1011–1179) (Fig. 3-11A, *top panel, lane 2*). Coimmunoprecipitation of TIF2-AD1 and MAGE-11 was not eliminated by single F260A and F264A mutations in the ²⁶⁰FPEIF²⁶⁴ region of HA-MAGE-(112–429) (Fig. 3-11A, *lanes 3 and 4*) or HA-MAGE-(112–276) (data not shown). However, the MAGE-11-dependent increase in GAL-TIF2.1-(624–1287), and the increase in GAL-TIF2-(624–1179)-m123 activity, was inhibited by the F260A or F264A mutations in MAGE-11 (Fig. 3-11B). These same mutations also inhibited the TIF2-dependent increase in AR (Fig. 3-11C) and AR Δ 120–472 transcriptional activity (Fig. 3-11D). In mammalian two-hybrid assays, interaction between GAL-MAGE-(251–272), a short fusion peptide that contains the MAGE-11 FXXIF motif, and VP-TIF2.1-(624–1287), but not VP-TIF2.2-(1288–1464) (Fig. 3-11E), provided evidence that the MAGE-11 FXXIF motif mediates an interaction with TIF2.

Discussion

Interaction Between MAGE-11 and TIF2-MAGE-11 increases AR transcriptional activity in part by increasing the recruitment of SRC/p160 coactivators (10, 21, 39). In the absence of MAGE-11, the AR N/C interaction competitively inhibits SRC/p160 coactivator binding to AF2, which shifts the dominant activation function from AF2 to AF1 (5) (Fig. 3-12A). MAGE-11 relieves the AR N/C interaction-induced repression of AR AF2 activity by binding the AR FXXLF motif and increasing AF2 accessibility for SRC/p160 coactivator

binding. Here we show that MAGE-11 also interacts directly with TIF2 to increase both ligand-dependent and ligand-independent AR activity.

The results suggest that MAGE-11 functions as a bridging factor to stabilize and recruit SRC/p160 coactivators in a manner less dependent on AR binding of androgen. MAGE-11 interacts with the NH₂-terminal region of TIF2, and with TIF2 AD1 through a MAGE-11 FXXIF motif (Fig. 3-12B). TIF2, SRC1, and TRAM1 each increases the activity of the AR-(1–660) NH₂-terminal and the DNA binding domain fragment to a greater extent in the presence of MAGE-11. SRC/p160 coactivator interaction with the AR NH₂-terminal region (10, 21) may be facilitated by their interaction with MAGE-11.

MAGE-11 is an F-box Protein-MAGE-11 is a member of a multigene MAGE family whose functions are largely uncharacterized. MAGE- 11 is expressed in the human male and female reproductive tracts, and undergoes phosphorylation and monoubiquitinylation to interact with the AR FXXLF motif (16, 19, 33). Well characterized steroid receptor coactivator interaction motifs include the LXXLL motifs of SRC/p160 coactivators (40), FXXLF motifs of putative AR coactivators (7), bromodomains, and others (41). MAGE-11 residues 329–369 function as an F-box interaction site for the AR FXXLF motif (Fig. 3-12), and a MAGE-11 FXXIF motif interacts with an F-box-like sequence in the AD1 region of TIF2.

The ~40 amino acid F-box, named for a weakly conserved hydrophobic repeat first identified in cyclin F (42), is present in the S-phase kinase-associated protein Skp2, which interacts with Skp1 in the Skp1-cullin-Skp2-F-box (SCF) E3 ubiquitin ligase complex (42–44). About 70 F-box proteins identified in humans are involved in phosphorylation-dependent ubiquitination (42, 45). F-box proteins generally lack intrinsic activity (43, 46)

and are classified by their carboxyl-terminal substrate recognition motifs that recruit target proteins involved in gene regulation (44, 47–49). FBWs (FBXW) have WD40 repeats, FBLs (FBXL) have leucine-rich repeats, and FBXs (FBXO) lack these motifs or have other protein interaction motifs (45). F-box proteins include Skp2 of the SCF complex (48, 50, 51), and FBW7 (FBXW7 in humans, hCdc4 in *Saccharomyces cerevisiae*), a tumor suppressor that mediates the ubiquitinylation and degradation of cell cycle regulatory proteins such as c-Myc (52–54).

Based on our studies, MAGE-11 and its family members are F-box proteins that may function as components of the SCF complex. MAGE-11 would be in the FBX class of F-box proteins because it lacks a WD40 LxGH...D/N(X)₅(W/F/Y)(D/N) repeat sequence (55). MAGE-11 shares size and sequence similarity with Skp2, but lacks the repeating leucine-rich β -strand and α -helix arrangement of Skp2 (56). The carboxyl-terminal position of the MAGE-11 40-amino acid F-box (amino acids 329–369) in the conserved MAGE homology domain differs from the NH₂-terminal position of the F-box in components of the SCF complex. On the other hand, poxvirus ankyrin repeat proteins interact with Skp1 and have a 30-residue F-box-like sequence in the carboxyl-terminal region (57). The conserved nature of the MAGE-11 F-box across the MAGE family, the MAGE-11 F-box interaction with the AR FXXLF motif, the F-box requirement for the MAGE-11-dependent increase in GAL-TIF2 transcriptional activity, and evidence that MAGE-11 interacts with Skp1, suggest that the MAGE-11 F-box has multiple binding partners involved in domain sharing.

F-box proteins have functions other than as bait for the SCF complex (47). For example, the F-box protein MoKA is a KLF7 coregulator independent of the SCF complex and ubiquitination (58). MAGE-11 binding to the AR FXXLF motif is associated with

increased AR transcriptional activity and increased degradation of AR and MAGE-11 (15, 16, 19, 59). Agonist-induced down-regulation of other steroid receptors (49, 60–63) occurs for AR through its association with MAGE-11. Like Skp2, MAGE-11 is expressed at low levels in a cell cycle-dependent manner, although MAGE-11 levels increase in human endometrium during the window of receptivity to implantation, and in castration-recurrent prostate cancer (20, 33).

Whether the phosphorylation and monoubiquitinylation-dependent MAGE-11 F-box interaction with the AR FXXLF motif involves the action of an SCF ubiquitin E3 ligase complex remains to be established. Substrates such as c-Myc and cyclin E, which bind the FBXW7 F-box protein that binds Skp1 in the SCF complex, are targeted for ubiquitinylation by phosphorylation within a phosphodegron (64). MAGE-11 is phosphorylated within the F-box by checkpoint kinase Chk1, which triggers monoubiquitinylation at lysines 240 and 245 (19), and by MAP kinase in response to serum. Monoubiquitinylation, which has been shown to mediate interactions between regulatory components of the proteasome required for transcription (65), may be required for an SCF function of MAGE-11.

MAGE-11 F-box binding to the AR FXXLF motif, and MAGE-FXXIF motif binding to an F-box-like sequence in AD1 of TIF2, suggests a novel F-box-FXX(L/I)F protein interaction paradigm. Selectivity for the MAGE-11 F-box-AR FXXLF motif interaction is supported by the lack of MAGE-11 binding to FXXLF motifs present in other AR coactivators, even though these same FXXLF motifs interact with AR AF2 (7, 16). Single amino acid mutations disrupt the MAGE-11 F-box-AR FXXLF motif and MAGE-11 FXXIF-TIF2 AD1 interactions, although these same mutations did not eliminate

coimmunoprecipitation of the complex. This suggests that the protein structure outside the region to some extent compensates for single residue F-box mutations.

The FXX(L/I)F motifs in AR and MAGE-11, and the uncharacterized FXXIY motif in TIF2, are each flanked by charged residues that may facilitate protein-protein interactions by increasing the solubility of the hydrophobic region. AR FXXLF motif binding to AF2 is influenced by complementary charged clusters that surround the AF2 region of AR (24). The TIF2 FXXIY motif ³³³FSQIY³³⁷ and Skp1 FXXIL motif ¹⁰¹FELIL¹⁰⁵ within the interaction region for Skp2 (Fig. 3-10A) are also flanked by charged residues (43). Although functions for the TIF2 and Skp1 FXXLF-like motifs have not yet been demonstrated, the presence of flanking charged residues support a role in mediating protein-protein interactions. The ubiquitinylation-dependent interaction between the AR FXXLF motif and the MAGE-11 F-box may be relevant to other MAGE gene family members with sequence homology within the MAGE-11 F-box.

Post-translational Regulation by Phosphorylation-Phosphorylation of steroid receptors and their coactivators has been linked to ubiquitinylation and subsequent degradation (41, 63, 66–68). AR signaling is regulated by its own phosphorylation (29, 69, 70), which includes EGF-dependent MAP kinase phosphorylation at AR Ser-515 (29), and MAP kinase phosphorylation of SRC/p160 coregulators (41, 67, 68, 71). MAP kinase signaling was also implicated in AR activity based on the inhibitory effects of U0126, a MAP kinase MEK1 inhibitor (29, 72, 73).

MAGE-11 Thr-360 phosphorylation by checkpoint kinase Chk1 within the MAGE-11 F-box is required for its interaction with the AR FXXLF motif. AR FXXLF motif binding to MAGE-11 is modulated by serum stimulation of MAP kinase phosphorylation at MAGE-

Ser-174, although mutation of Ser-174 did not eliminate the ability of MAGE-11 to increase AR transcriptional activity (19). MAGE-11 Ser-174 appears to be a post-translational regulatory site phosphorylated by ERK1, based on the inhibitory effect of the S174A mutation in the context of shorter AR NH₂-terminal fragments (19), and the greater transcriptional activity of GAL-MAGE-11 fusion proteins containing the S174D phosphomimetic. Conformational changes in nuclear receptor coregulators are regulated by peptidyl-prolyl isomerase 1 (Pin1), which targets phosphorylated Ser/Thr-Pro residues (74, 75). Pin1, which is highly expressed in metastatic prostate cancer, may exert regulatory effects on MAGE-11 mediated by MAP kinase phosphorylation at Ser-174.

AR Reactivation in Prostate Cancer-AR becomes reactivated during androgen deprivation therapy and prostate cancer progression to castration-recurrent growth (76, 77). This involves mechanisms that include increases in mitogen signaling, SRC/p160 coactivator levels (32), sensitivity to low levels of androgen (19, 32, 73, 78), and local tissue androgen synthesis (79). Of the coregulators that interact with AR (80), both the SRC/p160 coactivators and MAGE-11 levels increase in castration-recurrent prostate cancer (20, 81, 82). MAGE-11 mRNA levels can increase by ~1000-fold in clinical specimens of castration-recurrent prostate cancer compared with benign prostate, and by ~50-fold in the castration-recurrent CWR22 human prostate cancer xenograft (20). Increased expression of MAGE-11 in prostate cancer during androgen deprivation therapy is associated with DNA hypomethylation at CpG sites in the MAGE-11 promoter and may also result from increased cyclic AMP signaling. The ability of MAGE-11 to increase AR transcriptional activity by interacting with TIF2 suggests that increased levels of both coactivators contribute to AR reactivation in castration-recurrent prostate cancer.

REFERENCES

1. Quigley, C. A., De Bellis, A., Marschke, K. B., El-Awady, M. K., Wilson, E. M., and French, F. S. (1995) *Endocrine Reviews* **16**, 271–321
2. Askew, E. B., Gampe, R. T., Stanley, T. B., Faggart, J. L., and Wilson, E. M. (2007) *J. Biol. Chem.* **282**, 25801–25816
3. He, B., Gampe, R. T., Hnat, A. T., Faggart, J. L., Minges, J. T., French, F. S., and Wilson, E. M. (2006) *J. Biol. Chem.* **281**, 6648–6663
4. Newmark, J. R., Hardy, D. O., Tonb, D. C., Carter, B. S., Epstein, J. I., Isaacs, W. B., Brown, T. R., and Barrack, E. R. (1992) *Proc. Natl. Acad. Sci. USA* **89**, 6319–6323
5. He, B., Gampe, R. T., Kole, A. J., Hnat, A. T., Stanley, T. B., An, G., Stewart, E. L., Kalman, R. I., Minges, J. T., and Wilson, E. M. (2004) *Mol. Cell* **16**, 425–438
6. He, B., Kempainen, J. A., and Wilson, E. M. (2000) *J. Biol. Chem.* **275**, 22986–22994
7. He, B., Minges, J. T., Lee, L. W., and Wilson, E. M. (2002) *J. Biol. Chem.* **277**, 10226–10235
8. Lavery, D. N., and McEwan, I. J. (2008) *Biochemistry* **47**, 3352–3359
9. Lavery, D. N., and McEwan, I. J. (2008) *Biochemistry* **47**, 3360–3369
10. He, B., Kempainen, J. A., Voegel, J. J., Gronemeyer, H., and Wilson, E. M. (1999) *J. Biol. Chem.* **274**, 37219–37225
11. Langley, E., Kempainen, J. A., and Wilson, E. M. (1998) *J. Biol. Chem.* **273**, 92–101
12. Langley, E., Zhou, Z. X., and Wilson, E. M. (1995) *J. Biol. Chem.* **270**, 29983–29990
13. Wong, C. I., Zhou, Z. X., Sar, M., and Wilson, E. M. (1993) *J. Biol. Chem.* **268**, 19004–19012
14. Zhou, Z. X., Lane, M. V., Kempainen, J. A., French, F. S., and Wilson, E. M. (1995) *Mol. Endocrinol.* **9**, 208–218
15. He, B., Bowen, N. T., Minges, J. T., and Wilson, E. M. (2001) *J. Biol. Chem.* **276**, 42293–42301
16. Bai, S., He, B., and Wilson, E. M. (2005) *Mol. Cell. Biol.* **25**, 1238–1257

17. Chomez, P., De Backer, O., Bertrand, M., De Plaen, E., Boon, T., and Lucas, S. (2001) *Cancer Res.* **61**, 5544–5551
18. Rogner, U. C., Wilke, K., Steck, E., Korn, B., and Poustka, A. (1995) *Genomics* **29**, 725-731
19. Bai, S., and Wilson, E. M. (2008) *Mol. Cell. Biol.* **28**, 1947–1963
20. Karpf, A. R., Bai, S., James, S. R., Mohler, J. L., and Wilson, E. M. (2009) *Mol. Cancer Res.* **7**, 523–535
21. Bevan, C. L., Hoare, S., Claessens, F., Heery, D. M., and Parker, M. G. (1999) *Mol. Cell. Biol.* **19**, 8383–8392
22. Lubahn, D. B., Joseph, D. R., Sar, M., Tan, J., Higgs, H. N., Larson, R. E., French, F. S., and Wilson, E. M. (1988) *Mol. Endocrinol.* **2**, 1265–1275
23. Simental, J. A., Sar, M., Lane, M. V., French, F. S., and Wilson, E. M. (1991) *J. Biol. Chem.* **266**, 510–518
24. He, B., and Wilson, E. M. (2003) *Mol. Cell. Biol.* **23**, 2135–2150
25. Voegel, J. J., Heine, M. J., Tini, M., Vivat, V., Chambon, P., and Gronemeyer, H. (1998) *EMBO J.* **17**, 507–519
26. Huang, W., Shostak, Y., Tarr, P., Sawyers, C., and Carey, M. (1999) *J. Biol. Chem.* **274**, 25756–25768
27. Giffin, W., Torrance, H., Rodda, D. J., Préfontaine, G. G., Pope, L., and Hache, R. J. (1996) *Nature* **380**, 265–268
28. Gottlieb, T. M., and Jackson, S. P. (1993) *Cell* **72**, 131–142
29. Ponguta, L. A., Gregory, C. W., French, F. S., and Wilson, E. M. (2008) *J. Biol. Chem.* **283**, 20989–21001
30. He, B., Lee, L. W., Minges, J. T., and Wilson, E. M. (2002) *J. Biol. Chem.* **277**, 25631–25639
31. Zhou, Z. X., Sar, M., Simental, J. A., Lane, M. V., and Wilson, E. M. (1994) *J. Biol. Chem.* **269**, 13115–13123
32. Gregory, C. W., Johnson, R. T., Mohler, J. L., French, F. S., and Wilson, E. M. (2001) *Cancer Res.* **61**, 2892–2898

33. Bai, S., Grossman, G., Yuan, L., Lessey, B. A., French, F. S., Young, S. L., and Wilson, E. M. (2008) *Mol. Hum. Reprod.* **14**, 107–116
34. Craft, N., Shostak, Y., Carey, M., and Sawyers, C. L. (1999) *Nature Med.* **5**, 280–285
35. Quarmby, V. E., Yarbrough, W. G., Lubahn, D. B., French, F. S., and Wilson, E. M. (1990) *Mol. Endocrinol.* **4**, 22–28
36. Tan, J. A., Joseph, D. R., Quarmby, V. E., Lubahn, D. B., Sar, M., French, F. S., and Wilson, E. M. (1988) *Mol. Endocrinol.* **2**, 1276–1285
37. Erickson, A. K., Payne, D. M., Martino, P. A., Rossomando, A. J., Shabanowitz, J., Weber, M. J., Hunt, D. F., and Sturgill, T. W. (1990) *J. Biol. Chem.* **265**, 19728–19735
38. Favata, M. F., Horiuchi, K. Y., Manos, E. J., Daulerio, A. J., Stradley, D. A., Feeser, W. S., Van Dyk, D. E., Pitts, W. J., Earl, R. A., Hobbs, F., Copeland, R. A., Magolda, R. L., Scherle, P. A., and Trzaskos, J. M. (1998) *J. Biol. Chem.* **273**, 18623–18632
39. Onate, S. A., Boonyaratanakornkit, V., Spencer, T. E., Tsai, S. Y., Tsai, M. J., Edwards, D. P., and O'Malley, B. W. (1998) *J. Biol. Chem.* **273**, 12101–12108
40. Heery, D. M., Kalkhoven, E., Hoare, S., and Parker, M. G. (1997) *Nature* **387**, 733–736
41. Han, S. J., Lonard, D. M., and O'Malley, B. W. (2009) *Trends Endocrinol. Metab.* **20**, 8–15
42. Bai, C., Sen, P., Hofmann, K., Ma, L., Goebel, M., Harper, J. W., and Elledge, S. J. (1996) *Cell* **86**, 263–274
43. Schulman, B. A., Carrano, A. C., Jeffrey, P. D., Bowen, Z., Kinnucan, E. R., Finnin, M. S., Elledge, S. J., Harper, J. W., Pagano, M., and Pavletich, N. P. (2000) *Nature* **408**, 381–386
44. Zheng, N., Schulman, B. A., Song, L., Miller, J. J., Jeffrey, P. D., Wang, P., Chu, C., Koepf, D. M., Elledge, S. J., Pagano, M., Conaway, R. C., Conaway, J. W., Harper, J. W., and Pavletich, N. P. (2002) *Nature* **416**, 703–709
45. Jin, J., Cardozo, T., Lovering, R. C., Elledge, S. J., Pagano, M., and Harper, J. W. (2009) *Genes Dev.* **18**, 2573–2580
46. Westbrook, T. F., Hu, G., Ang, X. L., Mulligan, P., Pavlova, N. N., Liang, A., Leng, Y., Maehr, R., Shi, Y., Harper, J. W., and Elledge, S. J. (2008) *Nature* **452**, 370–374
47. Hermand, D. (2006) *Cell Div.* **1**, 30

48. Jackson, P. K., and Eldridge, A. G. (2002) *Mol. Cell* **9**, 923–925
49. von der Lehr, N., Johansson, S., Wu, S., Bahram, F., Castell, A., Cetinkaya, C., Hydbring, P., Weidung, I., Nakayama, K., Nakayama, K. I., Söderberg, O., Kerppola, T. K., and Larsson, L. G. (2003) *Mol. Cell* **11**, 1189–1200
50. Craig, K. L., and Tyers, M. (1999) *Prog. Biophys. Mol. Biol.* **72**, 299–328
51. Nie, L., Wu, H., and Sun, X. H. (2008) *J. Biol. Chem.* **283**, 684–692
52. Onoyama, I., and Nakayama, K. I. (2008) *Cell Cycle* **7**, 3307–3313
53. Welcker, M., and Clurman, B. E. (2008) *Nat. Rev. Cancer* **8**, 83–93
54. Yada, M., Hatakeyama, S., Kamura, T., Nishiyama, M., Tsunematsu, R., Imaki, H., Ishida, N., Okumura, F., Nakayama, K., and Nakayama, K. I. (2004) *EMBO J.* **23**, 2116–2125
55. van der Voorn, L., and Ploegh, H. L. (1992) *FEBS Lett.* **307**, 131–134
56. Hao, B., Zheng, N., Schulman, B. A., Wu, G., Miller, J. J., Pagano, M., and Pavletich, N. P. (2005) *Mol. Cell* **20**, 9–19
57. Sonnberg, S., Seet, B. T., Pawson, T., Fleming, S. B., and Mercer, A. A. (2008) *Proc. Natl. Acad. Sci. USA* **105**, 10955–10960
58. Smaldone, S., Laub, F., Else, C., Dragomir, C., and Ramirez, F. (2004) *Mol. Cell. Biol.* **24**, 1058–1069
59. Chandra, S., Shao, J., Li, J. X., Li, M., Longo, F. M., and Diamond, M. I. (2008) *J. Biol. Chem.* **283**, 23950–23955
60. Dennis, A. P., Haq, R. U., and Nawaz, Z. (2001) *Front. Biosci.* **6**, D954–959
61. Muratani, M., and Tansey, W. P. (2003) *Nat. Rev. Mol. Cell. Biol.* **4**, 192–201
62. Verma, S., Ismail, A., Gao, X., Fu, G., Li, X., O'Malley, B. W., and Nawaz, Z. (2004) *Mol. Cell. Biol.* **24**, 8716–8726
63. Wu, R. C., Feng, Q., Lonard, D. M., and O'Malley, B. W. (2007) *Cell* **129**, 1125–1140
64. Nash, P., Tang, X., Orlicky, S., Chen, Q., Gertler, F. B., Mendenhall, M. D., Sicheri, F., Pawson, T., and Tyers, M. (2001) *Nature* **414**, 514–521

65. Archer, C. T., Burdine, L., Liu, B., Ferdous, A., Johnston, S. A., and Kodadek, T. (2008) *J. Biol. Chem.* **283**, 21789–21798
66. Hoang, T., Fenne, I. S., Cook, C., Børud, B., Bakke, M., Lien, E. A., and Mellgren, G. (2004) *J. Biol. Chem.* **279**, 49120–49130
67. Rowan, B. G., Garrison, N., Weigel, N. L., and O'Malley, B. W. (2000) *Mol. Cell. Biol.* **20**, 8720–8730
68. Rowan, B. G., Weigel, N. L., and O'Malley, B. W. (2000) *J. Biol. Chem.* **275**, 4475–4483
69. Gioeli, D., Ficarro, S. B., Kwiek, J. J., Aaronson, D., Hancock, M., Catling, A. D., White, F. M., Christian, R. E., Settlage, R. E., Shabanowitz, J., Hunt, D. F., and Weber, M. J. (2002) *J. Biol. Chem.* **277**, 29304–29314
70. Lopez, G. N., Turck, C. W., Schaufele, F., Stallcup, M. R., and Kushner, P. J. (2001) *J. Biol. Chem.* **276**, 22177–22182
71. Zhou, Z. X., Kempainen, J. A., and Wilson, E. M. (1995) *Mol. Endocrinol.* **9**, 605–615
72. AgoulNIK, I. U., Bingman, W. E., Nakka, M., Li, W., Wang, Q., Liu, X. S., Brown, M., and Weigel, N. L. (2008) *Mol. Endocrinol.* **22**, 2420–2432
73. Gregory, C. W., Fei, X., Ponguta, L. A., He, B., Bill, H. M., French, F. S., and Wilson, E. M. (2004) *J. Biol. Chem.* **279**, 7119–7130
74. Chen, S. Y., Wulf, G., Zhou, X. Z., Rubin, M. A., Lu, K. P., and Balk, S. P. (2006) *Mol. Cell. Biol.* **26**, 929–939
75. Yi, P., Wu, R. C., Sandquist, J., Wong, J., Tsai, S. Y., Tsai, M. J., Means, A. R., and O'Malley, B. W. (2005) *Mol. Cell. Biol.* **25**, 9687–9699
76. Gregory, C. W., Hamil, K. G., Kim, D., Hall, S. H., Pretlow, T. G., Mohler, J. L., and French, F. S. (1998) *Cancer Res.* **58**, 5718–5724
77. Yuan, X., and Balk, S. P. (2009) *Urol. Oncol.* **27**, 36–41
78. Culig, Z., Hobisch, A., Cronauer, M. V., Radmayr, C., Trapman, J., Hittmair, A., Bartsch, G., and Klocker, H. (1994) *Cancer Res.* **54**, 5474–5478
79. Mohler, J. L., Gregory, C. W., Ford, O. H., Kim, D., Weaver, C. M., Petrusz, P., Wilson, E. M., and French, F. S. (2004) *Clin. Cancer Res.* **10**, 440–448
80. Heemers, H. V., and Tindall, D. J. (2007) *Endocr. Rev.* **28**, 778–808

81. Agoulnik, I. U., Vaid, A., Nakka, M., Alvarado, M., Bingman, W. E., Erdem, H., Frolov, A., Smith, C. L., Ayala, G. E., Ittmann, M. M., and Weigel, N. L. (2006) *Cancer Res.* **66**, 10594–10602
82. Gregory, C. W., He, B., Johnson, R. T., Ford, O. H., Mohler, J. L., French, F. S., and Wilson, E. M. (2001) *Cancer Res.* **61**, 4315–4319

Figure 3-1. Dependence of AR Transactivation on MAGE-11 and TIF2. (A) CWR-R1 cells were transfected with 0.1 μ g of MMTV-Luc with or without 0.1 μ g of pSG5-MAGE-11 or pSG5-TIF2. Cells were incubated in the absence and presence of DHT (shown as -log DHT concentration) and 0.1 μ g/ml of EGF. (B) COS cells were transfected using Lipofectamine 2000 with 1 μ g of pSG5 or pSG5-MAGE (*top panel*), 1 μ g of pSG5 or pSG5-TIF2 (*middle panel*), and 0.5 μ g of pCMV5 or pCMV-AR (*bottom panel*) in the absence and presence of 1 nm nonspecific (*NS*) siRNA, MAGE-11 siRNA-2 and -3, TIF2 siRNA-3, and AR siRNA-3. Cell extracts were analyzed by immunoblot for MAGE-11 (10 μ g of protein/lane), TIF2 (40 μ g/lane), AR (30 μ g/lane), and β -actin. (C) CWR-R1 cells were transfected with 0.1 μ g of MMTV Δ (-421--364)-Luc, 0.2 μ g of pSG5 or pSG5-MAGE in the absence and presence of 4 nm nonspecific or TIF2 siRNA-3, and incubated in the absence and presence of 0.1 nm DHT and 0.01 μ g/ml of EGF. (D) LAPC-4 cells were transfected with 0.1 μ g of MMTV Δ (-421--364)-Luc and 3 nm siRNA and incubated in the absence and presence of 0.1 nm DHT and 0.1 μ g/ml EGF. (E) *top panel*, CWR-R1 cells incubated for 48 h in serum-free medium were treated for the indicated times with 0.1 nm DHT and 10 ng/ml of EGF. Cell extracts in IB lysis buffer (200 μ g of protein/lane) (*lanes 2–8*) were analyzed by immunoblot using 10 μ g/ml of MAGE-Ab-(13–26), -(59–79), and -(94–108) antibodies overnight at 4 $^{\circ}$ C, and AR32 and β -actin antibodies (33). Extracts of COS cells expressing pCMV-AR (30 μ g of protein) and pSG5-MAGE (0.25 μ g of protein) served as controls (*lane 1*). *Bottom panel*, CWR-R1 cells were transfected with 4 nm siRNA and incubated for 6 h with or without 10 nm DHT and 10 ng/ml of EGF. RNA was extracted and analyzed by quantitative reverse transcription-PCR as described under “Experimental Procedures” for endogenous PSA mRNA relative to peptidylprolyl isomerase A.

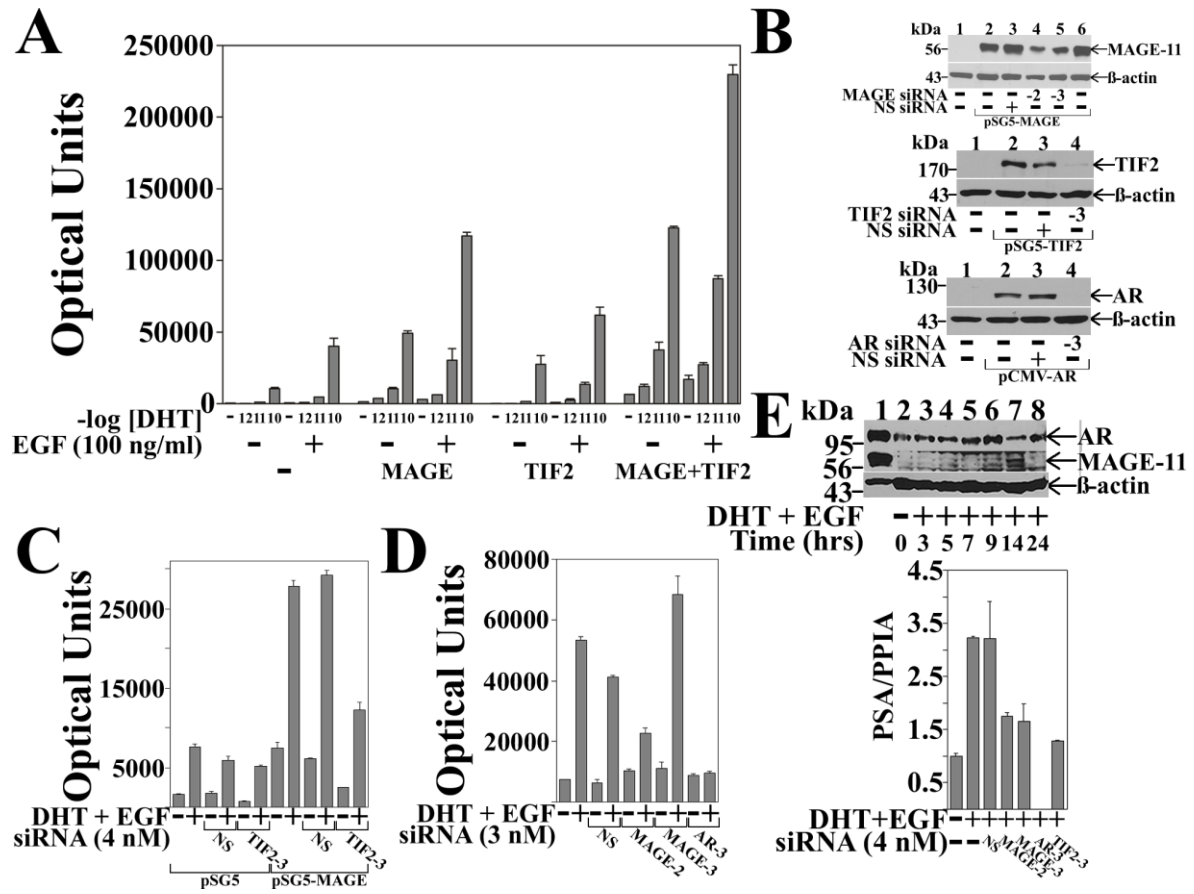


Figure 3-3. Requirement for MAGE-11 F-box in AR Transactivation by TIF2. (A) CV1 cells were transfected with 0.1 μg of pCMV-AR and 5 μg of MMTV-Luc, 2 μg of pSG5-TIF2, 2 μg of pSG5-MAGE wild-type (WT) or L358A/L359A F-box mutant, and incubated in the absence and presence of 1 nM DHT. (B) CV1 cells were transfected with 5 μg of MMTV-Luc and 0.1 μg of pCMV-AR Δ 120–472 WT or the indicated mutant, 2 μg of pSG5-TIF2 (*pSG5-T*) and/or 2 μg of pSG5-MAGE (*pSG5-M*). Cells were incubated in the absence and presence of 1 nM DHT. *Inset*, pCMV-AR Δ 120–472 WT and mutants (5 μg) were expressed in COS cells because expression was too low in CV1 cells. Cell extracts (30 μg of protein/lane) were analyzed on immunoblots probed with AR52 antibody. *Bottom panel*, schematic diagram of full-length human AR amino acid residues 1–919 with the NH₂-terminal FXXLF motif ²³FQNLF²⁷, activation function 1 (AF1), DNA binding domain (DBD), activation function 2 (AF2) in the ligand binding domain (LBD), and the AR Δ 120–472 deletion mutant that lacks AF1. (C) pCMV-AR Δ 120–472 (0.1 μg) was expressed in CV1 cells with 5 μg of MMTV-Luc, 2 μg of pSG5-TIF2 and/or 2 μg of pSG5-MAGE WT or the indicated F-box mutant. Cells were incubated in the absence and presence of 1 nM DHT. (D) pCMV-AR Δ 120–472 (0.1 μg) was expressed in CV1 cells with 5 μg of MMTV-Luc in the absence and presence of 2 μg of pSG5-TIF2 and/or 2 μg of pSG5-MAGE WT or single residue F-box mutant. Cells were incubated in the absence and presence of 1 nM DHT. *Bottom panel*, CV1 cells were transfected with pSG5 (8 μg /10-cm dish) (—), pSG5-MAGE WT or the indicated single residue F-box mutant. Cell extracts in IB lysis buffer (95 μg of protein/lane) were analyzed on immunoblots probed with antibody raised against FLAG-tagged MAGE-11.

Figure 3-4. Interaction Between MAGE-11 F-box and AR FXXLF Motif. (A) GAL-MAGE wild-type (*WT*), F-box mutant, or GAL-MAGE-K236A/K240A/K245A (*KA*) (0.05 μ g) were transfected in HeLa cells with 0.1 μ g of 5 \times GAL4Luc3 and 0.1 μ g of VP16 empty vector (—), VP-AR-(1–660) or VP-AR-(1–660)-L26A,F27A (LFAA) with a mutation in the AR FXXLF motif. *Bottom panel*, GAL-MAGE F-box or *KA* mutants, *WT* and GAL0 (—) (2 μ g/10-cm dish) were expressed in HeLa cells. Cell extracts prepared in IB lysis buffer (150 μ g of protein/lane) were analyzed on immunoblots probed using GAL antibody (1:100 dilution). (B) HeLa cells were transfected with 0.1 μ g of 5 \times GAL4Luc3, 0.05 μ g of GAL-AR-(4–52), and 0.1 μ g of VP16 (—), VP-MAGE *WT*, or the indicated mutant. *Bottom panel*, HeLa cells were transfected with VP-MAGE mutants (*lanes 1–8*), VP-MAGE *WT* (*lane 9*), and VP16 empty vector (—) (*lane 10*) (2 μ g/10-cm dish). Cell extracts in IB lysis buffer (100 μ g of protein/lane) were analyzed by immunoblot using VP16 antibody. (C) HeLa cells were transfected with 0.05 μ g of GAL-AR-(4–52) or GAL-AR-(16–36), 0.1 μ g of 5 \times GAL4Luc3 and 0.1 μ g of VP16 empty vector (—) or VP-MAGE *WT* or the indicated mutant. *D*, coimmunoprecipitation of endogenous Skp1 with FLAG-MAGE. FLAG empty vector (—) (3 μ g), FLAG-MAGE (3 μ g), and FLAG-MAGE-(112–429) (6 μ g) were expressed in HEK293 cells. The next day cells were treated for 24 h with 100 ng/ml of EGF and 1 μ M MG132. IP of an overnight incubation and cell extracts (35 μ g of protein/lane) were analyzed using FLAG and Skp1 antibodies.

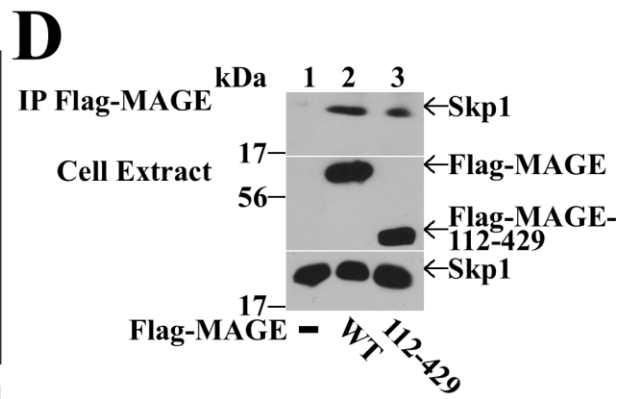
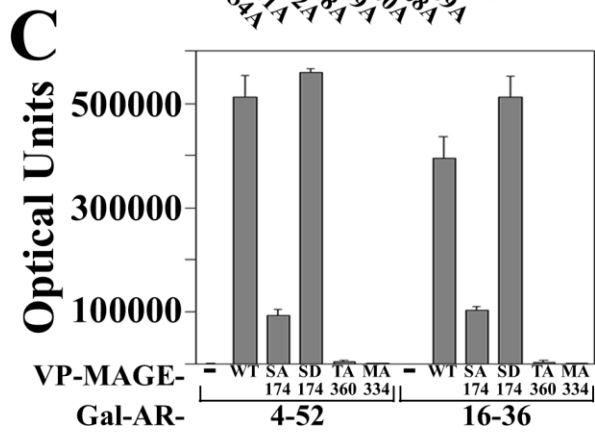
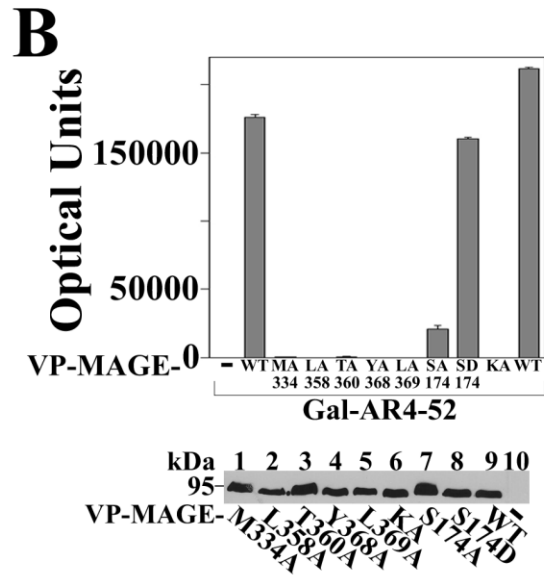
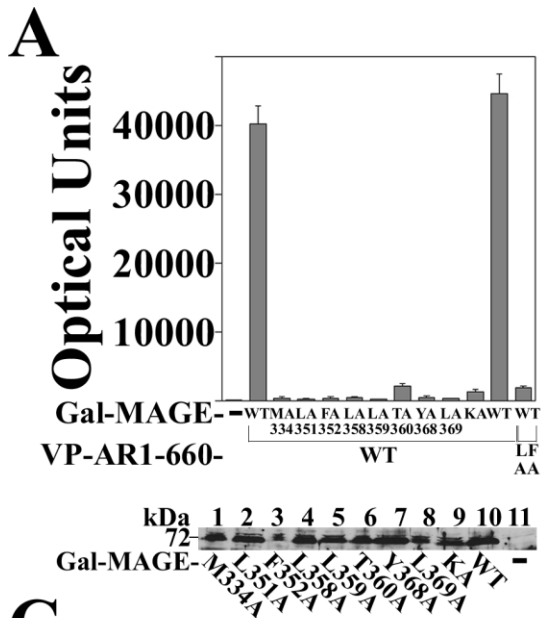


Figure 3-5. Serum Stimulation of MAP Kinase Phosphorylation of MAGE-11 Ser-174.

(A) MAGE-11 Ser-Pro sites Ser-168, Ser-170, Ser-174, and Ser-181 (*underlined*) include consensus MAP kinase site 172 PQSP 175 . (B) GAL-MAGE-(112–205) wild-type (WT) and mutants and GAL-MAGE-(112–170) (5 μ g) were expressed in COS cells. Cell extracts in IP lysis buffer without sodium fluoride (35 μ g) were incubated in the absence and presence of 800 IU of λ -phosphatase for 1 h at 4 $^{\circ}$ C, and the immunoblot probed with GAL antibody. (C) GAL0 (—), GAL-MAGE-(112–205) WT, or S174A mutant (5 μ g) were expressed in COS cells. Immediately after transfection and the next day, serum-free medium containing 1 μ M MG132 and U0126 was added. Cells were extracted in IB lysis buffer containing phosphatase mixture inhibitors 1/2. Protein extracts (35 μ g of protein/lane) were analyzed on immunoblots probed using GAL and β -actin antibodies. (D) GAL-MAGE-(112–205) (5 μ g) was expressed in COS cells incubated in the absence (*lanes 1, 3, 5, and 7*) or presence of 10% fetal bovine serum (*lanes 2, 4, 6, and 8*). Cells were harvested at 0, 30, 60, and 120 min in IB lysis buffer. Cell extracts (35 μ g of protein/lane) were analyzed by immunoblots probed with GAL and β -actin antibodies. (E) ERK1 *in vitro* phosphorylation of MAGE-11 Ser-174. *In vitro* kinase assay (*top panel*) was performed as described (19) at 30 $^{\circ}$ C for 30 min with 0.16 μ Ci/ μ l of [γ - 32 P]ATP, 0.1 μ g of active ERK1 kinase and purified GST0 (*lane 1*), GST-MAGE-(171–179) WT (*lane 2*), and S174A mutant (*lane 3*), and ERK1 substrate modeled after myelin basic protein (37) (*lane 4*). The dried gel was exposed to x-ray film for 16 h, and rehydrated for Coomassie Blue staining to demonstrate equivalent protein loading (*bottom panel*).

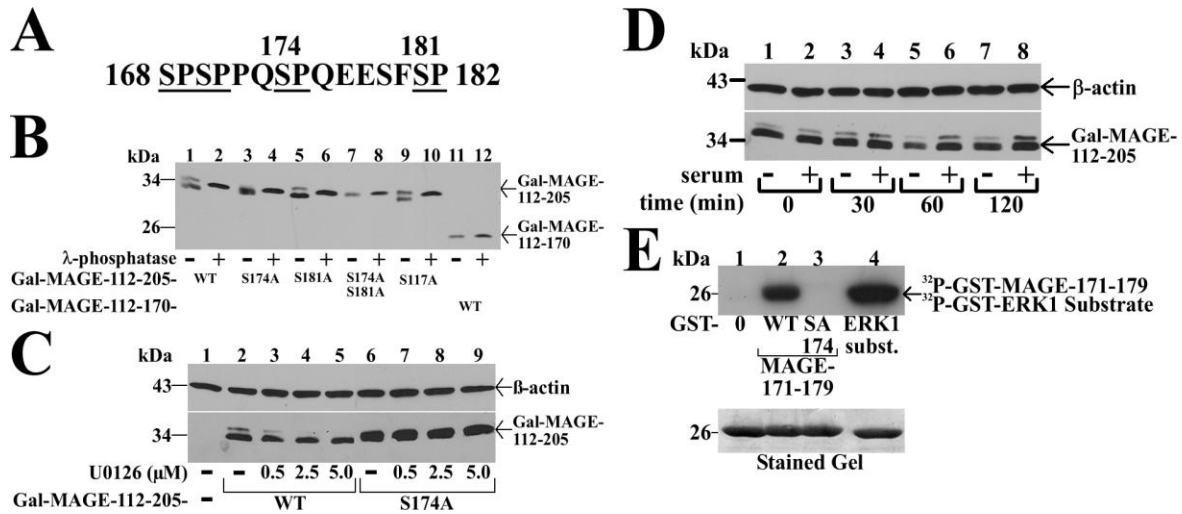


Figure 3-6. MAGE-11 and TIF2-Dependent Increase in AR AF1 Activity. (A) CV1 cells were transfected with 5 μ g of PSA-Enh-Luc and 0.05 μ g of pCMV5 empty vector (*p5*) or pCMV-AR-(1–660) in the absence and presence of 0.1 μ g of pSG5-MAGE and/or 2 μ g of pSG5-TIF2. (B) CV1 cells were transfected with 5 μ g of PSA-Enh-Luc and 0.05 μ g of *p5* or 0.05 μ g of pCMV-AR-(1–660) in the absence and presence of 2 μ g of pSG5-TIF2 and/or 1 μ g of pSG5-MAGE WT or the indicated F-box mutant.

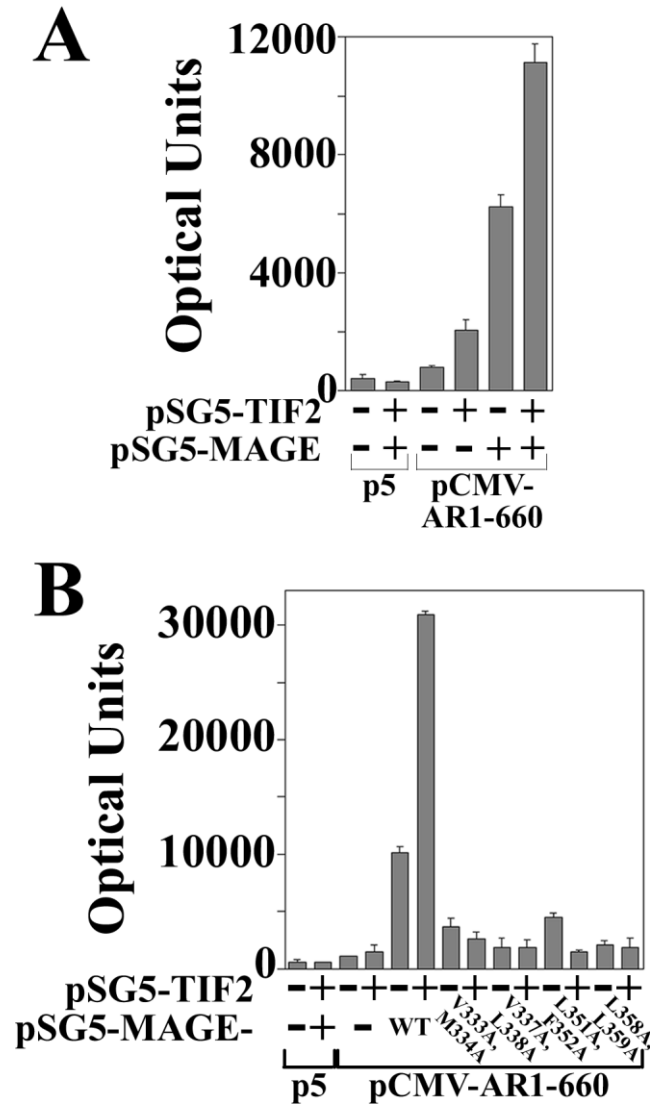


Figure 3-7. Interaction Between MAGE-11 and TIF2. (A) FLAG-b empty vector (—) (8 μ g) and 5 μ g of pSG5-HA-MAGE (*lane 1*), or 8 μ g of FLAG-TIF2 and 5 μ g of pSG5-HA-MAGE (*lane 2*) were expressed in COS cells. Cells were incubated overnight in the presence of 0.1 μ g/ml EGF and 1 μ M MG132, harvested in IP lysis buffer, and incubated with FLAG resin overnight at 4 $^{\circ}$ C. Immunoprecipitates and cell extracts (40 μ g of protein/lane) were analyzed on immunoblots probed with HA and TIF2 antibodies. (B) pSG5-TIF2 (8 μ g) was expressed with 4 μ g of FLAG-b empty vector (—) or 4 μ g of FLAG-MAGE in COS cells. Cells were incubated overnight in the presence of 0.1 μ g/ml EGF and 1 μ M MG132, harvested in IP lysis buffer, and incubated with FLAG resin overnight at 4 $^{\circ}$ C. Immunoprecipitates and cell extracts (50 μ g of protein/lane) were analyzed on immunoblots probed using FLAG and TIF2 antibodies. (C) *in vitro* GST affinity matrix assays using the indicated GST-TIF2 fusion fragments expressed in *E. coli* and 35 S-labeled MAGE-11 expressed from pSG5-MAGE-11 using the TnT T7 Quick Coupled transcription-translation system. *Input* lane contains 2% of the total 35 S-labeled MAGE-11 used in the reactions.

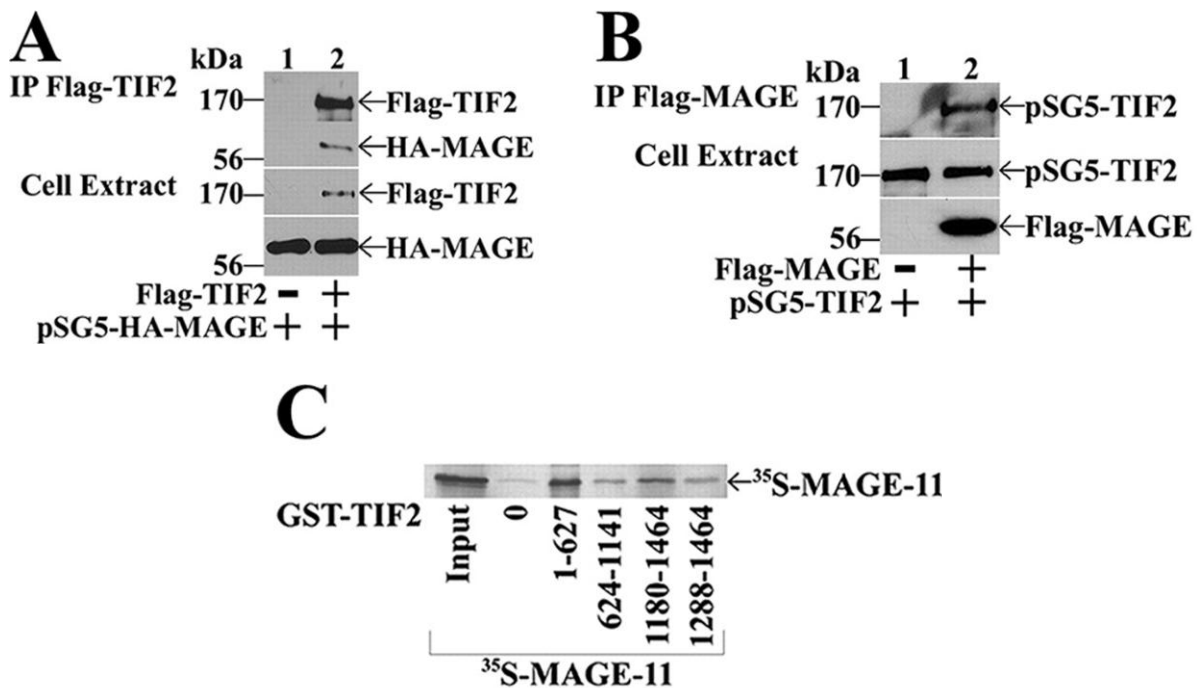


Figure 3-8. MAGE-11 and TIF2 Interaction Domains. (A) schematic diagram of full-length MAGE-11 and deletion fragments, with nuclear localization signal (*NLS*, residues 18–22), monoubiquitinylation sites Lys-240 and -245, Ser-174 and Thr-360 phosphorylation sites (19), MAGE homology domain (*MHD*), and the F-box region. (B) FLAG-b empty vector (—) (8 μ g) (*lanes 1–5*) or 8 μ g of FLAG-TIF2 (*lanes 6–10*) were expressed in COS cells with 0.5 μ g of pSG5-HA-MAGE-(112–429), 1 μ g of pSG5-HA-MAGE-(112–307), or 2 μ g of pSG5-HA-MAGE-(165–307), -(112–298), and -(112–276). Cells were incubated with 0.1 μ g/ml of EGF and 1 μ M MG132, solubilized in IP lysis buffer and immunoprecipitated using FLAG affinity resin overnight at 4 °C. IP (*upper panel*) and cell extracts (*lower panels*) (15 μ g of protein/lane for HA-MAGE, 55 μ g of protein/lane for FLAG-TIF2) were analyzed on immunoblots probed using HA and FLAG antibodies. (C) FLAG-b empty vector (*lanes 1 and 2*) (—), FLAG-TIF2 (*lanes 3 and 4*), FLAG-TIF2.0-(1–627), or FLAG-TIF2.8-(1011–1179) (8 μ g) were expressed in COS cells with 5 μ g of pSG5-HA-MAGE or 0.5 μ g of pSG5-HA-MAGE-(112–429). Cells were incubated with 0.1 μ g/ml of EGF and 1 μ M MG132, extracted in IP lysis buffer, and incubated with FLAG affinity resin overnight at 4 °C. Immunoprecipitates (*upper panel*) and cell extracts (*lower panels*) (25 μ g of protein/lane) were analyzed on immunoblots probed using FLAG and HA antibodies. (D) FLAG-b empty vector (—) (8 μ g) (*lanes 1–3*) and FLAG-TIF2.0-(1–627) (*lanes 4–6*) were expressed in COS cells with 1 μ g of pSG5-HA-MAGE-(112–429), 2 μ g of pSG5-HA-MAGE-(165–429), or 2 μ g of pSG5-HA-MAGE-(112–307). Cells were incubated with 0.1 μ g/ml of EGF and 1 μ M MG132, extracted in IP lysis buffer, and incubated with FLAG resin for 1 h at 4 °C. Immunoprecipitated proteins (*upper panel*) and cell extracts (*lower panels*) (25 μ g of protein/lane) were analyzed on immunoblots probed using HA and FLAG antibodies. (E) HeLa cells were transfected with 0.05 μ g of GAL-MAGE-(85–205) wild-type (*WT*), S174A or S174D mutant, 0.1 μ g of 5 \times GAL4Luc3, and 0.05 μ g of VP16 empty vector (—) or VP-TIF2.0-(1–627). *Bottom panel*, GAL0 empty vector (—) (2 μ g) and 2 μ g of GAL-MAGE-(85–205) *WT*, S174A, or S174D mutant were expressed in HeLa cells. Cell extracts (200 μ g of protein/lane) were analyzed on immunoblots probed using a GAL antibody.

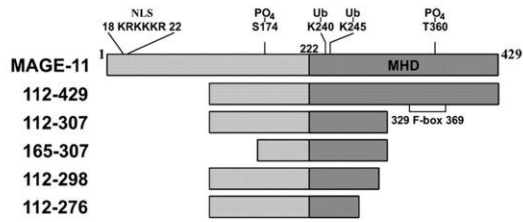
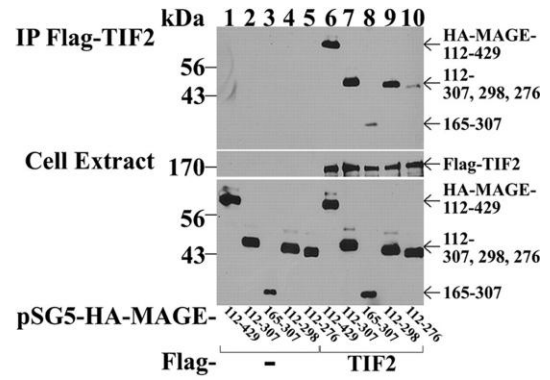
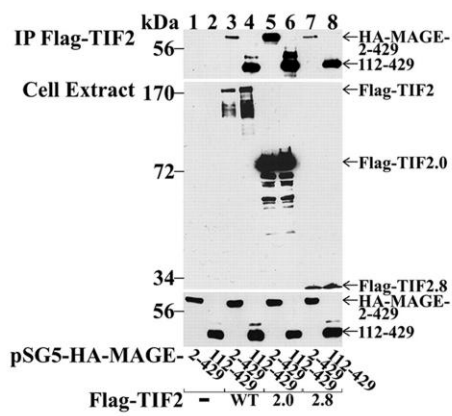
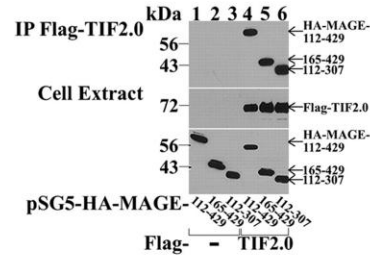
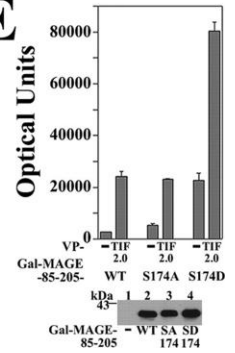
A**B****C****D****E**

Figure 3-10. FXXLF and F-box Related Sequences in AR, MAGE-11, TIF2, Skp1, and Skp2. (A) FXXLF-like motifs include AR-(15–36) FXXLF motif ²³FQNLF²⁷ that mediates the androgen-dependent AR N/C interaction with AF2 (6) and interaction with MAGE-11 (7). MAGE-11-(252–273) FXXIF motif ²⁶⁰FPEIF²⁶⁴ interacts with the AD1 region of TIF2. TIF2-(325–346) FXXIY motif ³³³FSQIY³³⁷ function is unknown. Skp1-(93–114) FXXIL motif ¹⁰¹FELIL¹⁰⁵ is in a region that interacts with the Skp2 F-box (43). Acidic and basic residues (*blue*) flank the FXXLF-like motifs (*red*). (B) F-box related sequences have predicted α -helical structure and relatively conserved spacing of two acidic residues (*blue*) and multiple hydrophobic residues (*red*). F-box-like sequences similar to the cyclin F F-box (35–73) include MAGE-11 F-box-(329–369) that interacts with the AR FXXLF motif, Skp2 F-box-(99–139) that interacts with a region that contains the Skp1 FXXIL motif (43), and TIF2 AD1 F-box-(1073–1112) that interacts with the MAGE-11 FXXIF motif.

A. FXXLF-like motifs

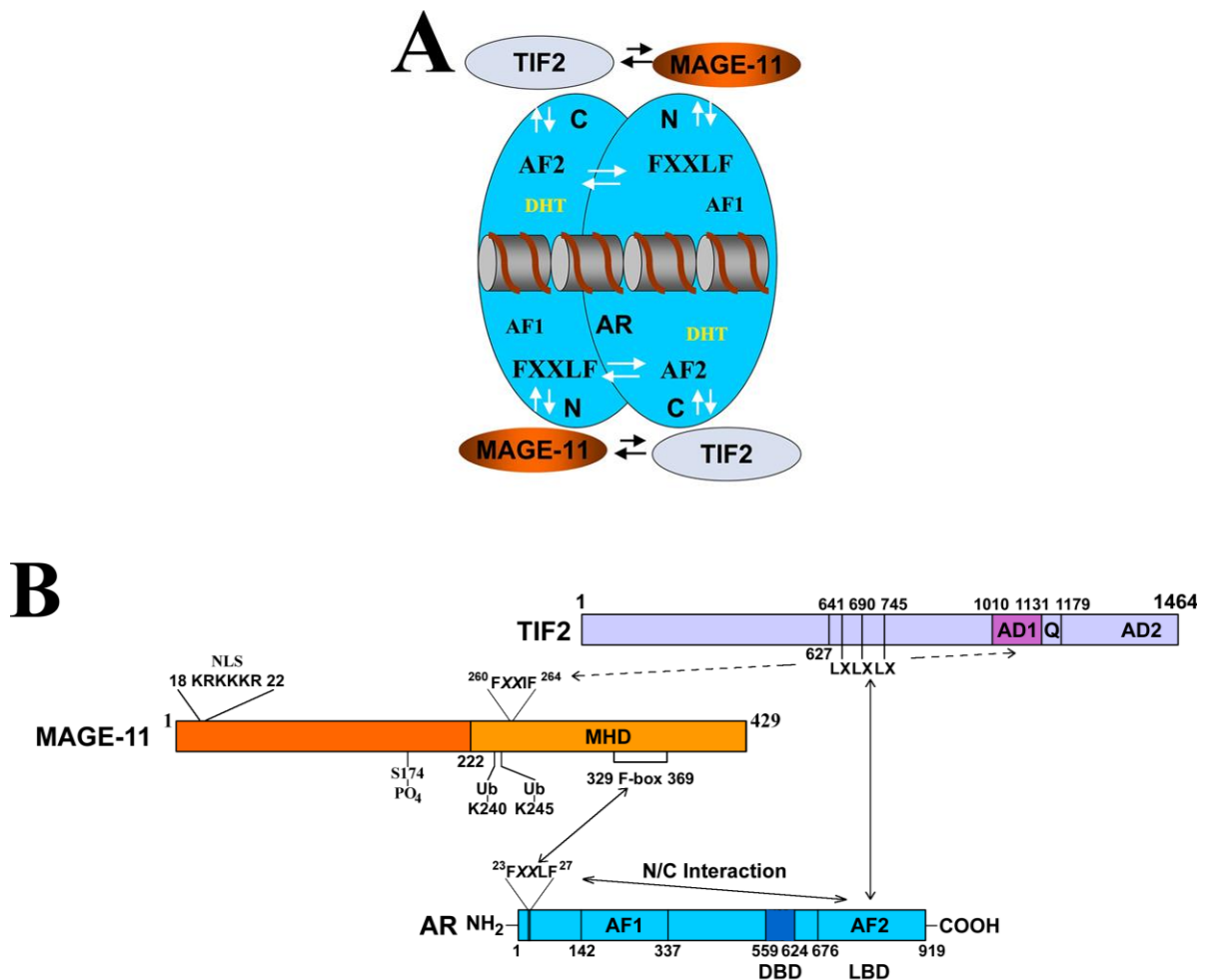
AR-15-36	PSKTYRGA ²³ FQNLF ²⁷ QSVREVIQN
MAGE-252-273	VIKNYEDY ²⁶⁰ FPEIF ²⁶⁴ REASVCMQL
TIF2-325-346	EVLROGLA ³³³ FSQIY ³³⁷ RFSLSDGTL
Skp1-93-114	LKVDQGTLELIL ¹⁰¹ LAANYLDIKG ¹⁰⁵

B. F-box related sequences

LPEDVLEFHILKWL ³⁵ SVEDILAVRAVHSQ ⁴⁰ LKDLVDN ⁴⁵ HASVW ⁵⁰	Cyclin F 35-73
IPEEVMWEVLSIMGVYAGREHFLFGE ⁶⁰ PKRLLTQ ⁶⁵ NWVQEKYL ⁷⁰	MAGE-11 329-369
LPDELLLGIFSC ⁹⁹ LCLPELLK ¹⁰⁴ VS ¹⁰⁹ GCKRWYRLASDES ¹¹⁴ LWQTL ¹¹⁹	Skp2 99-139
PSDEGALLDQLYLALRNFDGLEEIDRALGIPELVSQSAV	TIF2 AD1 1073-1112

Figure 3-11. MAGE-11 FXXIF Motif-Dependent Interaction with TIF2. (A) *top panels*, FLAG-b empty vector (*lane 1*) (—) or FLAG-TIF2.8-(1011–1179) (*lanes 2–4*) (8 µg) were expressed in COS cells with 0.5 µg of pSG5-HA-MAGE-(112–429) wild-type (WT) (*lanes 1 and 2*) or the indicated mutant (*lanes 3 and 4*). Cells were incubated with 0.1 µg/ml of EGF and 1 µM MG132 and immunoprecipitated overnight at 4 °C using FLAG resin. IP (*upper panel*) and cell extracts (25 µg of protein for HA-MAGE, 50 µg of protein for FLAG-TIF2.8, *lower panels*) were analyzed on immunoblots using HA and FLAG antibodies. *Bottom panels*, HeLa cells were transfected with 2 µg of pSG5 (—), pSG5-HA-MAGE-(2–429) WT, F260A, or F264A mutant (*left panel*), and pSG5-HA-MAGE-(112–429) WT, F260A, or F264A mutant, and pSG5 (—) (*right panel*). Cells extracts in IB lysis buffer (150 µg of protein/lane) were analyzed on immunoblots using HA antibody. (B) GAL-TIF2.1-(624–1287) or GAL-TIF2.3m123 (TIF2-(624–1179)-L644E,L645A,L693A,L694A,L748A,L749A) (0.05 µg) were transfected in HeLa cells with 0.1 µg of pSG5 (—), pSG5-HA-MAGE-(112–429) WT or mutant, and 0.1 µg of 5×GAL4Luc3. (C) CV1 cells were transfected with 0.1 µg of pCMV-AR and 5 µg of PSA-Enh-Luc with and without 2 µg of pSG5-TIF2 and 1 µg of WT or mutant pSG5-HA-MAGE. Cells were incubated in the absence and presence of 1 nM DHT. *Bottom panel*, CV1 cells were transfected with 8 µg of pSG5 (—), pSG5-HA-MAGE-(112–429) WT, F260A, or F264A mutant. Cells extracts in IB lysis buffer (200 µg of protein/lane) were analyzed on immunoblots probed with HA antibody. (D) CV1 cells were transfected with 0.1 µg of pCMV-AR Δ 120–472 with and without 2 µg of pSG5-TIF2, 2 µg of WT or mutant pSG5-HA-MAGE, and 5 µg of MMTV-Luc. Cells were incubated in the absence and presence of 1 nM DHT. *Bottom panel*, CV1 cells were transfected with 8 µg of pSG5 (—), pSG5-HA-MAGE WT, F151A, F260A, or F264A mutant. Cell extracts in IB lysis buffer (150 µg/lane) were analyzed on immunoblots using HA antibody. (E) HeLa cells were transfected with 0.1 µg of 5×GAL4Luc3, 50 ng of GAL0 empty vector (—), WT or mutant GAL-MAGE-(251–272), and 0.1 µg of VP16 empty vector (—), VP-TIF2.0-(1–627), VP-TIF2.1-(624–1287), or VP-TIF2.2-(1288–1464). *Bottom panel*, HeLa cells were transfected with 2 µg of GAL0 (*lane 1*), GAL-MAGE-(251–272) WT (*lane 2*), or F260A,F264A mutant (*lane 3*). Cell extracts (100 µg of protein/lane) were analyzed on immunoblots using GAL antibody.

Figure 3-12. Interactions Between AR, MAGE-11, and TIF2. (A) Schematic diagram of dynamic interactions between AR (blue), MAGE-11 (orange), and TIF2 (light blue) in the context of the AR antiparallel dimer bound to DNA. Indicated is the AR NH₂-terminal (N) activation function 1 (AF1), AR carboxyl-terminal (C) activation function 2 (AF2), and the AR FXXLF motif interaction site for MAGE-11 and AF2 in the N/C interaction. (B) Detailed schematic diagram of interactions between MAGE-11 (orange) F-box residues 329–369 in the carboxyl-terminal MAGE homology domain (MHD) with the AR (blue) NH₂-terminal FXXLF motif ²³FQNLF²⁷, which is modulated by phosphorylation in the MAGE-11 F-box at Thr-360, monoubiquitinylation (Ub) at Lys-240 and -245 (19), and serum stimulation of MAP kinase phosphorylation of MAGE-11 Ser-174 outside the F-box. AR transcriptional activity is increased by MAGE-11 F-box binding of the AR FXXLF motif, which competitively inhibits AR FXXLF motif binding to AF2 in the AR N/C interaction. This exposes AF2 in the AR ligand binding domain (LBD) for TIF2 (light blue) LXXLL (LX) motif binding. MAGE-11 also increases AR transcriptional activity through direct interactions with the TIF2 NH₂-terminal region and with AD1 mediated in part by MAGE-11 FXXIF motif ²⁶⁰FPEIF²⁶⁴.



CHAPTER 4

TRANSCRIPTIONAL SYNERGY BETWEEN MAGE-11 AND p300 IN ANDROGEN RECEPTOR SIGNALING

Abstract

Androgen receptor (AR) mediated gene regulation involves interactions with coregulatory proteins that include the melanoma antigen gene protein-A11 (MAGE-11). To understand the functional significance of sequence similarity between MAGE-11 and the adenovirus early protein E1A, we determined whether MAGE-11 contributes to AR transcriptional activity through an interaction with p300, a potent and ubiquitous transcriptional regulator. Here we report that MAGE-11 interacts with the NH₂-terminal region of p300 through MAGE-11 MXXIF motif sequence ¹⁸⁵MXXIF¹⁸⁹, with transcriptional activity depending on the MAGE-11 F-box and MAP kinase phosphorylation. The MAGE-11 and p300-dependent increase in AR transactivation required the NH₂-terminal regions of AR and p300, p300 acetyltransferase activity, and AR FXXLF motif sequence ²³FQNLF²⁷ interactions with MAGE-11 and p300. The p300 NH₂-terminal FXXLF motif sequence ³³FGSLF³⁷ was required for transcriptional activation by the p160 coactivator, transcriptional intermediary protein 2 (TIF2). Increased expression of p300 decreased the ubiquitinylation of MAGE-11 and transiently increased endogenous MAGE-11 levels. Autoacetylation of p300 and decreased acetylation of TIF2 was evident in the MAGE-11, p300 and TIF2 complex. The studies suggest that MAGE-11 links the AR and p300 NH₂-terminal domains to promote transcriptional synergy through a cadre of FXXLF-related interacting motifs.

Introduction

The androgen receptor (AR) regulates gene transcription required for male sex development by binding androgens with high affinity and interacting with coregulatory proteins. AR transcriptional activity derives from activation function 1 (AF1) in the NH₂-terminal region and the activation function 2 (AF2) hydrophobic surface in the ligand binding domain. AR AF2 interacts with p160 coactivator LXXLL motifs and the AR NH₂-terminal FXXLF motif ²³FQNLF²⁷ that mediates the androgen-dependent NH₂- and carboxyl-terminal (N/C) interaction (1). The competitive relationship between AR FXXLF and p160 coactivator LXXLL motif binding to AF2 exerts an inhibitory effect on p160 coactivator-induced AF2 transcriptional activity (2, 3). These findings, together with the greater AR AF2 binding affinity for the AR FXXLF than coactivator LXXLL motifs (4), suggest that AF1 in the AR NH₂-terminal region is the principal AR activation domain.

While regulation of steroid receptors through the AF2 site is relatively well described, the molecular mechanisms by which coregulatory proteins mediate AR AF1 activity are not understood. One recently described AR coregulator that interacts with the AR NH₂-terminal region, modulates the AR N/C interaction and increases AR transcriptional activity is the melanoma antigen gene protein-A11 (MAGE-11). MAGE-11 binds the AR NH₂-terminal FXXLF motif and interacts directly with p160 coactivators to increase AR transcriptional activity (5, 6). The interaction between AR and MAGE-11 is mediated by a MAGE-11 F-box and modulated by epidermal growth factor (EGF)-induced phosphorylation of Thr-360 within the F-box and monoubiquitinylation at lysine residues outside the F-box (6, 7).

The functional importance of MAGE-11 as an AR coregulator is supported by its regulated expression in both normal physiology and cancer. MAGE-11 levels increase by

~50 fold in the epithelium of the normal cycling human endometrium during the window of implantation (8), and to a similar extent in the CWR22 human prostate cancer xenograft during castration-recurrent growth. MAGE-11 levels were increased up to ~1000 fold in a subset of patients with castration-recurrent prostate cancer (9). The functional importance of AR signaling in prostate cancer initiation and progression suggests that increased expression of MAGE-11 provides a mechanism to enhance AR signaling when circulating androgen levels are low.

The ability of MAGE-11 to increase the constitutive activity of AR-(1–660), an NH₂-terminal and DNA binding fragment, when MAGE-11 itself lacks inherent transcriptional activity, provided support for the idea that MAGE-11 functions as an AR coregulator through direct interactions with coactivators. Based on sequence similarity between MAGE-11 and the adenovirus early protein E1A, an oncogenic protein that interacts strongly with p300, we investigated the possible interaction between MAGE-11 and p300, a ubiquitous transcriptional regulator and potent acetyltransferase. p300 activates gene transcription by acetylating histones and transcription factors, and as a coactivator of promoter-specific nuclear receptors (10). Studies described here address the mechanisms underlying the MAGE-11-dependent increase in AR transcriptional activity arising from AR NH₂-terminal AF1.

Materials and Methods

Expression Plasmids and Reporter Vectors—pCMV-hAR (11), pCMV-AR-(1–660) (12), VP-AR and VP-AR-(1–660) with wild-type sequence, L26A,F27A (LFAA) and Δ9–28 mutants (1, 13), pSG5-MAGE-11 (pSG5-MAGE), VP-MAGE-11-(2–429) (VP-MAGE) and pCMV-FLAG-MAGE-11-(2–429) (FLAG-MAGE) (5), pSG5-HA-MAGE-(112–429) and

FLAG-ubiquitin (FLAG-Ub) (7), wild-type and F-box mutants of pSG5-HA-MAGE fragments and pSG5-HA-MAGE-(112–429) (6), and pSG5-transcriptional intermediary factor 2 (TIF2) (14) and pCMV-FLAG-TIF2 (6) expression plasmids were described. Reporter vectors included prostate-specific-enhancer-luciferase (PSA-Enh-Luc) which contains the -3935 to -4326 upstream enhancer region of the PSA gene cloned upstream of a E4 TATA box in pGL3 basic (15), and 5XGAL4Luc3 which contains 5 copies of the GAL4 upstream enhancer element (16, 17).

pSG5-HA-p300 was prepared by blunt-end cloning a Not1/HindIII fragment of CMVb-NHAp300 (provided by Dr. David Livingston, Dana-Farber Cancer Institute) into the BamHI site of pSG5. pSG5-HA-p300-D1399Y, I97A,F98A and I188A,F189A were created by QuikChange site-directed mutagenesis (Stratagene) using pSG5-HA-p300 as template. GAL-MAGE and VP-MAGE fragments were created by PCR mutagenesis. pCMV-FLAG-p300 fragments were created by PCR amplifying pSG5-HA-p300, digesting with EcoRI/ClaI (FLAG-p300-(2–300) and 2–357) or HindIII/ClaI (FLAG-p300-(270–357), 300–670, 357–670 and 450–670) and ligating into the same sites of pCMV-FLAG. Additional FLAG-p300 fragments were created by ligating EcoRI/XbaI fragments of GAL-p300-(2–270) and 2–300 and a SalI/XbaI fragment of GAL-p300-(230–670) into the same sites of pCMV-FLAG. GST-p300-(2–357) was created by inserting the EcoRI/SalI fragment from FLAG-p300-(2–357) into the same sites of pGEX-4T-1.

GAL-p300-(2–300), 230–670, 501–999, 1000–1600, 1601–1900 and 1901–2414 were created by PCR amplifying the indicated regions of pSG5-HA-p300 and cloning SalI/ClaI digested fragments into the same sites of GAL0. GAL-p300-(2–357) was created by digesting FLAG-p300-(2–357) with EcoRI/XbaI and ligating the fragment into the same

sites of GAL0. GAL-p300-(2–300)-L36A,F37A was created using QuikChange site-directed mutagenesis and GAL-p300-(2–300) as template. GAL-p300-(230–670) was created by PCR amplifying pSG5-HA-p300, digesting with Sall/ClaI and inserting the fragment into GAL0.

Other GAL-p300 fragments were created by PCR amplifying GAL-p300-(2–300), digesting the fragments with Sall/ClaI (GAL-p300-(2–270), 2–230, 2–180, 90–300 and 90–270) or EcoRI/ClaI (GAL-p300-(48–300)) and ligating into the same sites of GAL0. All PCR amplified regions were verified by DNA sequencing.

Expression Studies—Monkey kidney CV1 cells (4×10^5 /6 cm dish) were transfected using calcium phosphate DNA precipitation (3) with 0.1 μ g pCMV-AR and the indicated amounts of wild-type and mutant pSG5-MAGE, pSG5-TIF2 and pSG5-HA-p300 and 3 or 5 μ g PSA-Enh-Luc. After transfection and 24 h later, cells were placed in serum-free, phenol-red free media in the absence and presence of 1 nM dihydrotestosterone (DHT). The next day the medium was replaced and 24 h later cells were extracted in 0.25 ml luciferase lysis buffer containing 1% Triton X-100, 2 mM EDTA and 25 mM Tris phosphate, pH 7.8. Luciferase activity was measured using an automated Lumistar Galaxy multiwell plate luminometer (BMG Labtech). Luciferase activity shown is representative of at least three independent experiments and the graphs show the mean \pm S.E.

Two hybrid transfection assays were performed in HeLa human epithelial cervical carcinoma cells using FuGENE-6 (Roche) by plating 5×10^4 cells/well in 12 well plates (4). Cells were transfected with 0.1 μ g/well 5XGAL4Luc3 and 0.05 μ g GAL-p300 fragments with 0.05 μ g pVP16 empty vector or VP-MAGE. The day after transfection, cells were transferred to serum-free medium and incubated overnight at 37°C before luciferase activity was measured.

Small interfering RNA (siRNA) was transfected into COS cells (4×10^5 /well in 6 well plates) using Lipofectamine 2000 (Invitrogen) in the absence of antibiotics with 1 μ g pSG5-MAGE, 1 μ g pSG5-TIF2 or 2 μ g pSG5-HA-p300 in the absence and presence of 5 nM MAGE-11 siRNA-2 GCACUGAUCCUGCAUGCUAUU, MAGE-11 siRNA-3 CAACUGCUCUUUGGCAUUGUU, 5 nM TIF2 siRNA-3 GAUCAGAAGUGACUAUAAA, 10 nM p300 siRNA-1 GAAAUUAGGUUACACAACA, p300 siRNA-2 GGACUACCCUAUCAAGUAA, p300 siRNA-3 GAACAUGGCUCCACAACCA, p300 siRNA-4 GGCAGUAUGUCGAUGAUAU and nonspecific siRNA-5 UGGUUUACAUGUCGACUAA (Dharmacon RNA Technologies). The day after transfection, cells were harvested or transferred to serum-free medium and harvested 24 h later for immunoblot analysis. For siRNA experiments in HeLa cells, cells were plated in antibiotic free medium and transfected using Lipofectamine 2000.

Immunoblotting—Relative expression levels of wild-type and mutant vectors were determined by transfecting COS cells (2×10^6 /10 cm dish) with 5–8 μ g DNA using DEAE dextran (4, 18). The next day cells were transferred to serum-free media with or without 1 μ M MG132 proteasome inhibitor (Sigma), and 24 h later harvested in phosphate buffered saline. Cell pellets were extracted in 0.1 to 0.2 ml of immunoblot (IB) lysis buffer containing 1% Triton X-100, 1% sodium deoxycholate, 0.1% sodium dodecyl sulfate (SDS), 0.15 M NaCl, 2 mM EDTA, 0.05 mM NaF, 2 mM sodium vanadate, 50 mM Tris-HCl, pH 7.5 with 1 mM phenylmethylsulfonyl fluoride, 1 mM dithiothreitol and complete protease inhibitor cocktail (Roche). Cell extracts were analyzed on 8, 10 or 12% acrylamide gels containing SDS. Proteins were transferred overnight to nitrocellulose membranes at 4°C and transblots were probed with the following antibodies: rabbit anti-GAL4 DNA binding domain (Santa

Cruz Biotechnology sc-577, 1:500 dilution); rabbit polyclonal FLAG-MAGE antibody-1 (0.5 µg/ml) raised against purified baculovirus-expressed FLAG-tagged human MAGE-11; affinity purified rabbit polyclonal human p300 (C-20) antibody (Santa Cruz Biotechnology sc-585, 1:75–200 dilution); mouse anti-β-actin (Abcam, 1:5000 dilution); mouse anti-TIF2 (BD Transduction Laboratories, 1:100–250 dilution); rabbit anti-MAGE-11 peptide antibodies MAGE-Ab-13–26, 59–79 and 94–108 immunoglobulin G (4–10 µg/ml) (8); mouse anti-FLAG M2 monoclonal antibody (Sigma F3165, 1:500–2000 dilution); rabbit polyclonal acetylated-lysine antibody (Cell Signaling 9441, 1:1000 dilution); and rabbit anti-HA-tag (Abcam ab9110, 1:2000 dilution). Gels were calibrated using EZ-Run prestained Rec protein ladder (Fisher Bioreagents) and immunoreactivity detected by chemiluminescence (SuperSignal West Dura Extended Duration Substrate, Pierce).

Immunoprecipitation was performed by transfecting COS cells as above with two 10 cm plates/group. For protein acetylation assays, cells were treated for 1 h prior to harvest with histone deacetylase inhibitor 5 mM nicotinamide with and without 5 mM sodium butyrate. Cell lysates were prepared in ¼ volume immunoprecipitation (IP) lysis buffer containing 1% Triton X-100, 0.5% deoxycholate, 0.15 M NaCl, 0.05 M NaF, 1 mM EDTA and 50 mM Tris, pH 7.6 with 1 mM phenylmethylsulfonyl fluoride, 1 mM dithiothreitol, complete protease inhibitor cocktail (Roche) with or without deacetylase inhibitors 5 mM nicotinamide and 5 mM sodium butyrate. Lysates were diluted 4 fold with IP buffer lacking deoxycholate and precleared for 1 h at 4°C with 0.1 ml Sepharose CL-4B (Sigma). Samples were transferred to 15 µl anti-FLAG M2 agarose (Sigma) for overnight incubation at 4°C. The next day samples were pelleted and washed with IP lysis buffer without deoxycholate, resuspended in 0.05 ml 2X SDS sample buffer containing 3.3% SDS, 10% 2-

mercaptoethanol, 10% glycerol and 0.12 M Tris-HCl, pH 6.8, incubated for 5 min at 90°C and analyzed on immunoblots as described above.

In vitro Binding Assays—Glutathione *S*-transferase (GST) interaction assays were performed using pGEX-4T-1 empty vector and pGEX-4T-1-p300-(2–357) (GST-p300-(2–357)). [³⁵S]-MAGE-11 was prepared using pSG5-MAGE and the TNT T7 Quick Coupled transcription-translation system (Promega) (1, 6, 19). GST fusion proteins were expressed in BL-21 DE3 *Echerichia coli* with 1 mM isopropyl 1-thio-β-D-galactopyranoside for 3 h at 37°C. Cell pellets were resuspended in GST binding buffer containing 0.5% Nonidet P-40, 1 mM EDTA, 0.1 M NaCl, 10% glycerol, 20 μg/ml bovine serum albumin and 20 mM Tris-HCl, pH 8.0 with 1 mM dithiothreitol and complete protease inhibitor cocktail (Roche). Glutathione-Sepharose 4B (GE Healthcare) was incubated for 1.5 h at 4°C with GST-0 and GST-p300-(2–357) cell lysates after sonication. Beads were washed with GST buffer, combined with 25 μCi [³⁵S]-MAGE-11 and incubated overnight at 4°C. The resin was washed, eluted with SDS and analyzed on an 8–16% gradient minigel containing SDS (Invitrogen). The dried gel was exposed to x-ray film for 48 h.

Results

MAGE-11 Increases p300-Dependent AR Transcriptional Activity—To determine whether MAGE-11 increases AR transcriptional activity through mechanisms that involve p300, AR was expressed in the absence and presence of MAGE-11 and p300. Androgen-dependent AR transcriptional activity increased to a greater extent with the expression of MAGE-11 than with p300, and was highest when MAGE-11 and p300 were coexpressed (Fig. 4-1A). MAGE-11 and p300 further increased AR transcriptional activity when expressed with TIF2 (Fig. 4-1B), consistent with previous findings that MAGE-11 binds the

AR FXXLF motif, exposes AF2 for p160 coactivator recruitment and interacts directly with TIF2 (5, 6).

Further investigation determined whether the effects of MAGE-11 and p300 on AR transcriptional activity are mediated through the AR NH₂-terminal AF1 region. Expression of MAGE-11 or p300 increased activity of AR-(1–660), an AR NH₂-terminal and DNA binding domain fragment, and were synergistic when expressed together (Fig. 4-1C). As seen with full-length AR, TIF2 alone did not increase AR-(1–660) activity unless expressed with p300 or MAGE-11 (Fig. 4-1D).

The MAGE-11 dependence of the TIF2-induced increase in AR transcriptional activity could be explained by previous findings that MAGE-11 interacts with TIF2 (6), and binding of MAGE-11 to the AR FXXLF motif overcomes an inhibitory effect of the AR N/C interaction on TIF2 binding to AF2 (3) (see diagram, Fig. 4-11). However, dependence on MAGE-11 for the p300-induced increase AR transcriptional activity through the AR NH₂-terminal region raised the possibility that MAGE-11 interacts with p300.

MAGE-11 Interacts with the NH₂-terminal Region of p300—An interaction between MAGE-11 and p300 was demonstrated in mammalian two hybrid assays by expressing VP-MAGE and p300–GAL4 DNA binding domain fusion proteins (Fig. 4-2A). MAGE-11 interacted with the p300-(2–300) NH₂-terminal region to a greater extent than with p300-(230–670) (Fig. 4-2B). MAGE-11 did not interact with the p300 501–999 Kix domain, 1000–1600 Bromo domain, PHD (plant homeodomain) and histone acetyltransferase domains (20–22) or the 1601–1900 ZZ and TAZ2 domains (23). Constitutive activity of carboxyl-terminal fragment p300-(1901–2414) that includes an IBID domain (24) was only slightly increased by MAGE-11.

To further localize and establish an influence of MAGE-11 on transcriptional activity from the p300 NH₂-terminal region, additional GAL-p300 fragments were expressed with the MAGE-(112–429) carboxyl-terminal fragment (Fig. 4-2C). Similar to the two hybrid interaction results (Fig. 4-2B), MAGE-(112–429) increased the activity of GAL-p300-(2–357), 2–300, 2–270 and 230–670 compared to other p300 NH₂-terminal fragments (Fig. 4-2C). Overall activity decreased with deletion of the p300 NH₂-terminal region in GAL-p300-(48–300) or with mutations in a p300 NH₂-terminal FXXLF motif sequence ³³FGSLF³⁷ in GAL-p300-(2–300)-L36A,F37A. The results suggest that MAGE-11 interacts with and increases transcriptional activity of the p300 NH₂-terminal region.

p300 Interacts with the Carboxyl-terminal Region of MAGE-11—To identify the region in MAGE-11 that interacts with p300, VP-MAGE fragments were expressed in mammalian two hybrid assays with GAL-p300-(2–300) (Figs. 4-3A and 4-3B). Full-length VP-MAGE and VP-MAGE-(112–429) interacted with GAL-p300-(2–300), but not with MAGE-(112–362) or 112–252 (Fig. 4-3B). This suggested that the entire MAGE-11 carboxyl-terminal region is required to interact with p300 as demonstrated previously for MAGE-11 binding to the AR FXXLF motif (5). In agreement with results of Fig. 4-2B, MAGE-(112–429) strongly increased GAL-p300-(2–300) activity. However, there was little to no increase with shorter fragments and less of an increase with full-length MAGE-11 (Fig. 4-3C), even though GAL-p300-(2–300) interacted with full-length MAGE-11 (Fig. 4-3B).

The carboxyl-terminal region of MAGE-11 contains a conserved F-box (Fig. 4-3A, amino acid residues 329–369) that interacts with the AR FXXLF motif (6). The requirement for the MAGE-11 F-box to increase GAL-p300-(2–300) transcriptional activity was indicated by the loss of activity with a series of single amino acid MAGE-11 F-box mutants (Fig. 4-

3D) shown previously to decrease MAGE-11 binding to the AR FXXLF motif (6). Mutation of mitogen-activated protein (MAP) kinase site Ser-174 blocked the MAGE-(112–429)-dependent increase GAL-p300-(2–300) activity, and was recovered with the MAGE-(112–429)-S174D phosphomimetic (Fig. 4-3E). A predicted MAGE-11 phosphorylation site at Ser-298 when mutated to alanine decreased the MAGE-(112–429)-dependent increase in GAL-p300-(2–300) activity, but was only partially restored with the S298D phosphomimetic. A direct interaction between MAGE-11 and the p300 NH₂-terminal region was supported by in vitro binding studies in which GST-p300-(2–357) interacted with [³⁵S]-labeled MAGE-11 (Fig. 4-3F).

The results suggest that the carboxyl-terminal region of MAGE-11 interacts with the NH₂-terminal region of p300 and increases p300 transcriptional activity through mechanisms that depend on the MAGE-11 F-box and MAP kinase phosphorylation. The inhibitory effect of the MAGE-11 NH₂-terminal region on GAL-p300 transcriptional activity suggested an auto-regulatory mechanism.

MAGE-11 MXXIF Motif Interacts with p300—To characterize further the MAGE-11 interaction with p300, full-length p300 was expressed with a series of GAL-MAGE fragments (Fig. 4-4A). p300 activated full-length GAL-MAGE and GAL-MAGE-(112–429) to only a limited extent (Fig. 4-4B), even though these regions interacted with p300 (Fig. 4-3B). However, p300 strongly activated GAL-MAGE-(112–205), 140–205, 161–205, 85–205 and 85–152, but not 100–152 (Fig. 4-4B).

Within the MAGE-(85–205) region activated by p300 are two M/IXXIF motifs, ⁹⁴ITQIF⁹⁸ and ¹⁸⁵MDAIF¹⁸⁹ (Fig. 4-4A). Functional importance of the ¹⁸⁵MXXIF¹⁸⁹ motif was suggested by decreased p300-dependent GAL-MAGE-(85–205)-I188A,F189A activity, and

loss of GAL-MAGE-(140–205)-I188A, F189A activity in a MAGE-11 fragment that lacked the ⁹⁴IXXIF⁹⁸ motif (Fig. 4-4C). Disruption of the ⁹⁴IXXIF⁹⁸ motif in GAL-MAGE-(85–205)-I97A, F98A, a fragment that contained the ¹⁸⁵MXXIF¹⁸⁹ motif, had no effect on p300-dependent activity. However, p300-dependent transcriptional activity decreased with GAL-MAGE-(85–152)-I97A,F98A, a ⁹⁴IXXIF⁹⁸ motif mutant that lacked the ¹⁸⁵MXXIF¹⁸⁹ motif.

The functional requirement for the MAGE-11 ¹⁸⁵MXXIF¹⁸⁹ motif was also evident in AR transcription assays. Mutations in either the MXXIF or IXXIF motif in full-length MAGE-11 did not significantly decrease AR transcriptional activity when p300 or TIF2 were not expressed (Fig. 4-4D). However, mutations in the ¹⁸⁵MXXIF¹⁸⁹ motif minimized or eliminated the MAGE-11-dependent increase in AR transcriptional activity with the expression of p300 and/or TIF2, whereas AR activity remained similar to wild-type with mutations in the ⁹⁴IXXIF⁹⁸ motif.

The results suggest that the MAGE-11 MXXIF motif ¹⁸⁵MDAIF¹⁸⁹ is a primary interaction site for p300, and IXXIF motif sequence ⁹⁴ITQIF⁹⁸ is a secondary interaction site. The inability of p300 to increase GAL-MAGE or GAL-MAGE-(112–429) activity when smaller fragments were strongly activated suggested that the MAGE-11 carboxyl-terminal region has an inhibitory effect.

Functional Requirement for AR and p300 NH₂-terminal FXXLF Motifs—p300 contains an FXXLF motif sequence ³³FGSLF³⁷ in a similar relative position to the AR FXXLF motif (Fig. 4-5A). Evidence that the p300 FXXLF motif was required to enhance GAL-p300-(2–300) activity (Fig. 4-2C) and the close proximity of flanking charged residues (Fig. 4-5A) suggested that the p300 NH₂-terminal FXXLF motif is functionally important. Since previous studies demonstrated AR activation of androgen responsive enhancer/promoters depends on

the AR FXXLF motif (25), we investigated the requirement for these NH₂-terminal FXXLF motifs in AR interaction with p300.

Interaction between VP-AR-(1–660) and GAL-p300-(2–300) required the AR FXXLF-motif since the interaction was eliminated with VP-AR-(1–660)-L26A,F27A when the p300 FXXLF motif was present (Fig. 4-5B). Deletions of the p300 FXXLF motif in GAL-p300-(48–300) or GAL-p300-(90–300) decreased overall activity and the requirement for the AR FXXLF motif, but did not eliminate the interaction with AR. A weak androgen-dependent interaction between full-length VP-AR and GAL-p300-(2–300) was inhibited with VP-AR-L26A,F27A and VP-AR Δ 9–28 in which the AR FXXLF motif was mutated or deleted (Fig. 4-5C). However, deletion of the p300 FXXLF motif increased the androgen-dependent interaction between GAL-p300-(48–300) and VP-AR that was eliminated with VP-AR-L26A,F27A or VP-AR Δ 9–28.

To better understand the functional requirement for the p300 NH₂-terminal FXXLF motif, GAL-p300-(2–300) was expressed with TIF2. GAL-p300-(2–300) was strongly activated by TIF2 (Fig. 4-5D) in a p300 FXXLF motif-dependent manner. TIF2-dependent GAL-p300-(2–300) activity was inhibited with GAL-p300-(48–300) where the p300 FXXLF motif was deleted, and with GAL-p300-(2–300)-L36A,F37A in which the p300 FXXLF motif was mutated.

The contribution of endogenous MAGE-11 to the TIF2-dependent increase in GAL-p300-(2–300) activity was indicated through the use of siRNAs to lower protein levels. MAGE-11 siRNA-2 reduced MAGE-11 levels (Fig. 4-6A, top panel) and inhibited inherent GAL-p300-(2–300) transcriptional activity, but did not eliminate the increase in activity with TIF2 (Fig. 4-6B). MAGE-11 siRNA-3 was less effective in decreasing MAGE-11 levels

(Fig. 4-6A), and the TIF2-induced increase in GAL-p300-(2–300) activity was similar to that seen in the absence and presence of nonspecific siRNA. TIF2 siRNA-3 decreased both TIF2 expression (Fig. 4-6A, bottom panel) and the TIF2-dependent increase in GAL-p300-(2–300) activity (Fig. 4-6B).

The results suggest that the AR interaction with p300 is influenced by NH₂-terminal FXXLF motifs present in both proteins, and that the p300 FXXLF motif facilitates transcriptional activation by TIF2.

Multiple Functions of the AR FXXLF Motif—Previous studies have demonstrated the requirement for the androgen-dependent AR N/C interaction between the AR FXXLF motif and AF2 for AR to activate androgen responsive enhancer/promoters (1, 25). These findings and the requirement for the AR FXXLF motif in interactions with MAGE-11 and p300 provided evidence that the AR N/C interaction influences AR transactivation by p300.

To investigate this further, we determined the effect of MAGE-11 and p300 using an experimental paradigm that depended on the AR N/C interaction. AR-(507–919), a DNA and ligand binding domain fragment that retains high affinity androgen binding (26), was not activated by DHT with or without the expression of MAGE-11 or p300 alone or together (Fig. 4-7A). However, expression of AR-(507–919) with AR-(1–503), an AR NH₂-terminal fragment that lacks the AR DNA and ligand binding domains, increased androgen-dependent transcriptional activity. Activity was further increased with the expression of MAGE-11 or p300, and was greatest when expressed together. Dependence on the AR N/C interaction was demonstrated by loss of activity when AR-(507–919) was expressed with MAGE-11 or p300 alone or together with AR-(1–503)-L26A,F27A in which the AR FXXLF motif was mutated.

The requirement for endogenous p300 in AR N/C interaction-dependent AR transactivation was further demonstrated using p300 siRNA. p300 siRNA-1, 3 and 4 each decreased both p300 levels (Fig. 4-7B) and the androgen-dependent activity of AR-(507–919) and AR-(1–503) expressed with MAGE-11 (Fig. 4-7C). Specificity of siRNA inhibition was suggested by wild-type activity using nonspecific siRNA, or with p300 siRNA-2 that did not reduce p300 levels.

To demonstrate further that MAGE-11 functionally links AR and p300 through the AR FXXLF motif, GAL-AR-(16–36), which contains only the AR NH₂-terminal FXXLF motif region, was expressed with wild-type or mutant MAGE-11 and p300 alone or together. Neither MAGE-11 nor p300 alone increased GAL-AR-(16–36) activity, but were strongly synergistic (Fig. 4-7D). Mutations in the MAGE-11 ¹⁸⁵MXXIF¹⁸⁹ motif that was required for MAGE-11 to interact with p300 (Fig. 4-4) reduced p300 activation of GAL-AR-(16–36), with only a slight decrease with mutations in the MAGE-11 ⁹⁴IXXIF⁹⁸ motif in agreement with the results in Fig. 4-4. Dependence of p300-induced GAL-AR-(16–36) activity on AR FXXLF motif binding to MAGE-11 was demonstrated by loss of the transcriptional response with MAGE-11 F-box mutants MAGE-L358A and T360A, and the ubiquitinylation site mutant K240A,K245A, where each mutation disrupts MAGE-11 binding to the AR FXXLF motif (6, 7). Dependence on the AR FXXLF motif was also shown by the lack of activity with the GAL-AR-(16–36)-L26A,F27A FXXLF motif mutant. GAL-AR-(16–36) activity was also reduced by p300-D1399Y, a p300 acetyltransferase mutant (27).

The results suggest that AR transcriptional activity mediated by the AR N/C interaction depends on the ability of MAGE-11 to link AR and p300 by binding the AR FXXLF motif that also mediates the AR N/C interaction. The results support the notion that

AR transcriptional activation by p300 is mediated through sequential AR FXXLF motif interactions with the AR AF2 site, MAGE-11 and p300.

Dependence on p300 Acetyltransferase Activity—The decrease in MAGE-11-dependent GAL-AR-(16–36) activity with the p300 acetyltransferase mutant led us to investigate the requirement for p300 acetyltransferase activity in MAGE-11-induced AR activity. AR transcriptional activity in the presence of MAGE-11 or TIF2 alone or together increased with p300 but not with p300-D1399Y (Fig. 4-8A). Similarly, the p300-dependent increase in GAL-MAGE-(85–205) and 140–205 activity was eliminated with the p300-D1399Y acetylation mutant (Fig. 4-8B).

Since protein stability can be influenced by acetylation or ubiquitinylation of lysine residues (28), we determined whether p300 acetyltransferase activity influences MAGE-11 ubiquitinylation. In the absence of p300, MAGE-(112–429) was strongly ubiquitinated (Fig. 4-8C) as reported previously (7). Coexpression of p300 or the p300-D1399Y acetyltransferase mutant inhibited MAGE-(112–429) ubiquitinylation. However, there was no evidence that MAGE-11 was acetylated by p300 (data not shown), although acetylated forms of TIF2 and p300 were present in the complex with MAGE-11 that were not detected with p300-D1399Y (Fig. 4-9A). Acetylation of TIF2 declined with the coexpression of MAGE-11, and was not detected with p300-D1399Y (Fig. 4-9B).

The results indicate that p300 acetyltransferase activity is required for MAGE-11 and p300 to increase AR transcriptional activity. However, MAGE-11 was not acetylated by p300 even though there was evidence for the acetylation of both p300 and TIF2. In agreement with these findings, p300 inhibited MAGE-11 ubiquitinylation independent of acetyltransferase activity, and MAGE-11 had an inhibitory effect on TIF2 acetylation.

p300 Increases Endogenous MAGE-11—Evidence that p300 inhibits the ubiquitinylation of MAGE-11 (Fig. 4-8C) raised the possibility that p300 might influence the endogenous levels of MAGE-11. To pursue this further, p300 was expressed in COS cells and assayed at the indicated times in serum-free medium. MAGE-11 was not detected when p300 was not expressed or through 5 h when p300 was expressed (Fig. 4-10). However, endogenous MAGE-11 was detected at 7 h but not at 9, 14 and 24 h when p300 levels declined. The transient increase in MAGE-11 suggests that p300 influences its cell cycle expression.

Discussion

AR Transcriptional Regulation by MAGE-11 and p300—We have demonstrated transcriptional synergy between AR, the AR coregulator MAGE-11 and p300, a ubiquitous and potent transcriptional regulator and acetyltransferase (22, 29, 30). MAGE-11 links the NH₂-terminal regions of AR and p300 to increase AR transcriptional activity dependent on p300 acetyltransferase activity through FXXLF-related motif interactions in the AR, MAGE-11, p300 and TIF2 transcription complex. The AR FXXLF motif functions not only in the androgen-dependent AR N/C interaction (1, 2) and binding of MAGE-11 (1, 5), but also is involved in AR interaction and activation by the p300 NH₂-terminal region (Fig. 4-11). The multiple AR FXXLF motif interactions were each eliminated by AR-L26A,F27A mutations that disrupt the AR FXXLF motif α -helical structure (1, 5). The ability of MAGE-11 to link AR and p300 was demonstrated further by the transcriptional activity of two AR fragments that depends on the AR N/C interaction. MAGE-11 and p300 also increased the activity of GAL-AR-(16–36), an AR FXXLF motif fusion peptide.

The findings suggest that the AR FXXLF motif mediates an increase in AR transcriptional activity not only through the AR N/C interaction, but also by recruiting MAGE-11 and interacting with the NH₂-terminal region of p300. The critical function of the AR N/C interaction is supported by AR AF2 site mutations that disrupt AR FXXLF motif binding and AR function (19). The studies support the supposition that a single interaction motif undergoes multiple transient interactions during the process of AR mediated transcription. Dependence of androgen responsive enhancer/promoters on the AR NH₂-terminal FXXLF motif (25) may be explained by the AR FXXLF motif-dependent AR N/C interaction, the functional requirement of the AR FXXLF motif to bind MAGE-11, and for MAGE-11 to link AR to p300. However, we found little evidence that p300 could increase AR transactivation in the absence of MAGE-11. In agreement with this, the previously reported ability of p300 to increase AR transcriptional activity made use of prostate cancer cell lines (31) that have relatively high levels of AR and MAGE-11.

Sites that interact with FXXLF-related motifs also serve multiple functions that differ in specificity. For example, the AF2 site in the AR ligand binding domain binds the AR NH₂-terminal FXXLF motif, p160 coactivator LXXLL motifs and FXXLF-related motifs in putative AR coactivators (25, 32), but does not bind the p300 NH₂-terminal FXXLF motif (18). In contrast, the MAGE-11 F-box binds the AR FXXLF motif but not FXXLF motifs present in AR coactivators or p300 (6). However, the MAGE-11 F-box was required for the functional interaction between MAGE-11 and p300, where MAGE-11 increased GAL-p300 activity. The MAGE-11 F-box at amino acid residues 329–369 begins with the sequence ³²⁹IPEE³³² followed by a conserved arrangement of hydrophobic amino acids similar to the F-box of cyclin F (6). p300 contains a similar ⁴³LPDE⁴⁶ sequence positioned close to the ³³FGSLF³⁷

FXXLF motif but with a different arrangement of hydrophobic residues than the MAGE-11 F-box. Deletion of this putative p300 F-box region in GAL-p300-(48–200) increased the interaction with full-length AR that was influenced by the AR FXXLF motif. This suggests that an F-box-like sequence in the NH₂-terminal region of p300 may interact with another protein that competes with AR binding to p300. The existence of multiple overlapping motifs and surfaces is consistent with MAGE-11 and p300 coordinating temporal interactions during AR transactivation.

Both MAGE-11 and p300 are downstream targets of MAP kinase (6, 33), and p300 is phosphorylated in a time-dependent manner in response to EGF (34). In response to serum stimulation, MAGE-11 is phosphorylated by MAP kinase at Ser-174, a conserved residue in the MAGE-A subfamily (6). The MAGE-S174A mutant eliminated the functional interaction between MAGE-11 and p300 that was restored with the S174D phosphomimetic. The MAGE-11 S174A mutation also diminished MAGE-11 interaction with the AR FXXLF motif (6). Inhibition of GAL-p300 activity by MAGE-S174A suggests that phosphorylation-dependent changes influence the ability of p300 to function with MAGE-11 to modulate AR transcriptional activity. The results suggest that MAP kinase phosphorylation at Ser-174 regulates several important aspects of MAGE-11 function.

Requirement for p300 Acetyltransferase Activity—p300 has a modular structure with multiple protein interaction sites. These include a cysteine and histidine rich Taz1 domain at residues 332–417, a Kix domain (566–646) that interacts with CBP binding protein CREB, a bromo domain that interacts with p53 (1053–1156), a PHD domain (1198–1278), a glutamine-rich C-terminal region that interacts with the p160 coactivator activation domain-1

(14, 35, 36), and a lysine acetyltransferase domain between amino acid residues 1284–1517 (22).

The NH₂-terminal region of p300 was implicated previously in ligand-dependent nuclear receptor signaling, although the interaction sites were not defined (10, 37). The closely related cyclic AMP response element binding protein-binding protein (CBP) (10, 29) mediated ligand-independent effects of the AR NH₂-terminal region through the CBP 271–452 amino acid region (31), and the CBP steroid receptor coactivator 1 (SRC1) interaction domain (SID) carboxyl-terminal residues 2058–2130 interact with SRC1 activation domain 1 (AD1) residues 926–960 conserved among p160 coactivators (36, 38). We found that the ability of MAGE-11 to partner with p300 and increase AR transcriptional activity depended on p300 NH₂-terminal FXXLF motif ³³FGSLF³⁷ in a location similar to the AR FXXLF motif. The p300 FXXLF motif was required for a functional interaction of the NH₂-terminal region with TIF2, and for the MAGE-11-dependent increase in GAL-p300 transcriptional activity.

p300 acetyltransferase activity has multiple targets that include the acetylation of histone tail lysine residues that opens the chromatin structure for active transcription. p300 also acetylates nonhistone proteins such as p160 coactivators, p53 and β-catenin (29, 39–42). TIF2 was reported to be acetylated by CBP, and the p160 activator for thyroid hormone and retinoid receptors (ACTR) was acetylated by p300 and modulated the interaction of ACTR with nuclear receptors (43). p300 acetyltransferase activity was also linked to AR signaling. AR was acetylated at Lys-632 and 633 by p300 and p/CAF, a p300 associated protein (44). However, these basic residues are part of the AR bipartite nuclear targeting signal (45) so that inhibitory effects on AR nuclear transport may complicate interpretation of the consequences of acetylation on AR transcriptional activity. The dependence of MAGE-11 on

p300 acetyltransferase activity to increase AR transcriptional activity was associated with the acetylation of p300 and TIF2.

Protein stability and function are influenced by the competing and complementary effects of acetylation and ubiquitinylation at lysine residues (28). For example, p300 regulates the levels of p53 by promoting p53 degradation through association with the MDM2 E3-like ubiquitin ligase (46). Although MAGE-11 was not acetylated by p300, p300 inhibited MAGE-11 ubiquitinylation through an acetylation-independent mechanism. The transient increase in endogenous MAGE-11 when p300 was expressed appeared to be cell cycle regulated, in agreement with evidence that MAGE-11 is cell cycle regulated in CWR-R1 prostate cancer cells (6).

MAGE-11 is monoubiquitinated at Lys-240 and 245 and undergoes polyubiquitinylation in association with its degradation (7). While the E3 ligase that ubiquitinates MAGE-11 has not been identified, some evidence suggests that MAGE-11 itself functions as part of a ubiquitin ligase complex. MAGE-11 contains an F-box similar to the F-box in S-phase kinase-associated protein 2 (Skp2) and MAGE-11 interacted with Skp1 (6). p300 was reported to have E4 ubiquitin ligase activity (47) that could influence the ubiquitinylation of MAGE-11. The requirement for the MAGE-11 F-box for p300 NH₂-terminal transcriptional activity suggests a role for a ubiquitin ligase.

A Primate-Specific AR Transcriptional Scaffold—The evolution of MAGE-11 among primates suggests a novel mechanism arose to increase AR signaling by facilitating interactions between AR, p300 and TIF2. One potential mechanism is that MAGE-11 functions as a transcription factor scaffold assembly protein for AR. A similar function as transcription factor nucleation site has been attributed to p300 to increase gene expression at

select enhancers and function as a bridge between DNA binding nuclear receptors and transcription factors to the basal transcriptional machinery (48, 49). Many transcription factors, nuclear receptors, and signaling molecules interact with p300, which is thought to be rate limiting and redistributes among different classes of transcription factor complexes (50). Competition may exist in recruiting p300 to nuclear receptor regulated enhancers. Interaction between MAGE-11 and p300 could enhance AR mediated gene regulation through the more efficient recruitment of a limiting set of factors that include p300, p160 coactivators and components of the general transcriptional machinery.

p300 and CBP were shown to increase androgen-dependent and ligand-independent AR transactivation in prostate cancer (44, 51, 52). However, p300 protein levels decrease in prostate cancer cells in response to androgen (53), and p300 mRNA levels were unchanged in the CWR22 human prostate cancer xenograft during tumor progression to castration-recurrent growth, when AR mRNA levels increased ~5 fold (9). In contrast, MAGE-11 mRNA levels increased ~50 fold in the castration-recurrent CWR22 tumor, and up to 1000 fold in a subset of castration-recurrent prostate cancer tissue specimens. The increase in MAGE-11 in castration-recurrent prostate cancer provides a mechanism for AR to more effectively recruit p300 and TIF2 and increase transactivation of AR target genes when circulating androgen levels are low.

MAGE-11 and the Adenovirus Early Protein, E1A–p300 was first identified based on its interaction with the adenovirus early oncoprotein E1A that targets p300 during viral infection (31, 35, 54, 55). Sequence similarity between the NH₂-terminal regions of MAGE-11 and E1A suggested that MAGE-11 may share properties of E1A and interact with p300. Binding to E1A decreased p300 transcriptional activity through the modification of histone

acetyltransferase (HAT) activity (35, 56–58). MAGE-11 did not interact with the HAT domain of p300, but inhibited p300 acetylation of TIF2. Inhibition of p300 HAT activity was also associated with p300 phosphorylation at Ser-89 (59), suggesting that allosteric effects extend from the p300 NH₂-terminal region and could be influenced by MAGE-11.

E1A also has a modular structure of interaction motifs for transcriptional regulators associated with the induction of S phase of the cell cycle, cell immortalization, cell transformation and transcriptional regulation (60–62). Based on evidence that E1A binds p300 and promotes cell growth, it was suggested that p300 functions as a tumor suppressor (29). The E1A FX(D/E)XXXL motif sequence ⁶⁶FPDSVML⁷² was reported to interact with one of several domains in p300/CBP (63). MAGE-11 contains the similar FX(D/E)XXXL motif sequence ⁶⁶FREQANL⁷² in the same relative position to the NH₂-terminus as in E1A. However, single amino acid mutations in the MAGE-11 FX(D/E)XXXL motif did not interfere with p300 binding (data not shown), suggesting that other MAGE-11 regions possibly homologous to E1A bind p300 (60). Instead, interaction between MAGE-11 and p300 depended on the MAGE-11 MXXIF motif sequence ¹⁸⁵MDAIF¹⁸⁹, and secondarily on the IXXIF sequence ⁹⁴ITQIF⁹⁸, as well as the MAGE-11 F-box and on MAP kinase phosphorylation. The MAGE-11 ¹⁸⁵MXXIF¹⁸⁹ motif and Ser-174 MAP kinase site are in close proximity and homologous to a region in E1A. The reported E1A FX(D/E)XXXL interaction site for p300 is preceded by ⁶²VSQIF⁶⁶ which, based on sequence homology and position, could be a previously unrecognized E1A interaction site for p300.

While there is no known human genomic counterpart for E1A, sequence similarity between MAGE-11 and E1A suggests that MAGE-11 may share some of the functional properties of E1A. The late evolutionary species-specific expansion of the MAGE gene

family among primates suggests that like E1A, MAGE-11 may have hijacked transcription factor binding sites required for its function as an AR selective coregulator.

REFERENCES

1. He, B., Kempainen, J. A., and Wilson, E. M. (2000) *J. Biol. Chem.* **275**, 22986–22994
2. He, B., Gampe, R. T., Kole, A. J., Hnat, A. T., Stanley, T. B., An, G., Stewart, E. L., Kalman, R. I., Minges, J. T., and Wilson, E. M. (2004) *Mol. Cell* **16**, 425–438
3. He, B., Bowen, N. T., Minges, J. T., and Wilson, E. M. (2001) *J. Biol. Chem.* **276**, 42293–42301
4. Askew, E. B., Gampe, R. T., Stanley, T. B., Faggart, J. L., and Wilson, E. M. (2007) *J. Biol. Chem.* **282**, 25801–25816
5. Bai, S., He, B., and Wilson, E. M. (2005) *Mol. Cell. Biol.* **25**, 1238–1257
6. Askew, E. B., Bai, S., Hnat, A. T., Minges, J. T., and Wilson, E. M. (2009) *J. Biol. Chem.* **284**, 34793–34808
7. Bai, S., and Wilson, E. M. (2008) *Mol. Cell. Biol.* **28**, 1947–1963
8. Bai, S., Grossman, G., Yuan, L., Lessey, B. A., French, F. S., Young, S. L., and Wilson, E. M. (2008) *Mol. Hum. Reprod.* **14**, 107–116
9. Karpf, A. R., Bai, S., James, S. R., Mohler, J. L., and Wilson, E. M. (2009) *Mol. Cancer Res.* **7**, 523–535
10. Vo, N., and Goodman, R. H. (2001) *J. Biol. Chem.* **276**, 13505–13508
11. Lubahn, D. B., Joseph, D. R., Sar, M., Tan, J., Higgs, H. N., Larson, R. E., French, F. S., and Wilson, E. M. (1988) *Mol. Endocrinol.* **2**, 1265–1275
12. Simental, J. A., Sar, M., Lane, M. V., French, F. S., and Wilson, E. M. (1991) *J. Biol. Chem.* **266**, 510–518
13. Langley, E., Kempainen, J. A., and Wilson, E. M. (1998) *J. Biol. Chem.* **273**, 92–101
14. Voegel, J. J., Heine, M. J., Tini, M., Vivat, V., Chambon, P., and Gronemeyer, H. (1998) *EMBO J.* **17**, 507–519
15. Huang, W., Shostak, Y., Tarr, P., Sawyers, C., and Carey, M. (1999) *J. Biol. Chem.* **274**, 25756–25768
16. He, B., and Wilson, E. M. (2003) *Mol. Cell. Biol.* **23**, 2135–2150

17. Wagner, B. L., Norris, J. D., Knotts, T. A., Weigel, N. L., and McDonnell, D. P. (1998) *Mol. Cell. Biol.* **18**, 1369–1378
18. He, B., Minges, J. T., Lee, L. W., and Wilson, E. M. (2002) *J. Biol. Chem.* **277**, 10226–10235
19. He, B., Kemppainen, J. A., Voegel, J. J., Gronemeyer, H., and Wilson, E. M. (1999) *J. Biol. Chem.* **274**, 37219–37225
20. Haynes, S. R., Dollard, C., Winston, F., Beck, S., Trowsdale, J., and Dawid, I. B. (1992) *Nucleic Acids Res.* **20**, 2603
21. Jeanmougin, F., Wurtz, J. M., Le Douarin, B., Chambon, P., and Losson, R. (1997) *Trends Biochem Sci.* **22**, 151–153
22. Ogryzko, V. V., Schiltz, R. L., Russanova, V., Howard, B. H., and Nakatani, Y. (1996) *Cell* **87**, 953–959
23. Ponting, C. P., Blake, D. J., Davies, K. E., Kendrick-Jones, J., and Winder, S. J. (1996) *Trends Biochem. Sci.* **21**, 11–13
24. Finlan, L., and Hupp, T. R. (2004) *J. Biol. Chem.* **279**, 49395–49405
25. He, B., Lee, L. W., Minges, J. T., and Wilson, E. M. (2002) *J. Biol. Chem.* **277**, 25631–25639
26. Zhou, Z. X., Lane, M. V., Kemppainen, J. A., French, F. S., and Wilson, E. M. (1995) *Mol. Endocrinol.* **9**, 208–218
27. Muraoka, M., Konishi, M., Kikuchi-Yanoshita, R., Tanaka, K., Shitara, N., Chong, J. M., Iwama, T., and Miyaki, M. (1996) *Oncogene* **12**, 1565–1569
28. Galbiati, L., Mendoza-Maldonado, R., Gutierrez, M. I., and Giacca, M. (2005) *Cell Cycle* **4**, 930–939
29. Giordano, A., and Avantaggiati, M. L. (1999) *J. Cell Physiol.* **181**, 218–230
30. Bannister, A. J., and Kouzarides, T. (1996) *Nature* **384**, 641–643
31. Frønsdal, K., Engedal, N., Slagsvold, T., and Saatcioglu, F. (1998) *J. Biol. Chem.* **273**, 31853–31859
32. Hsu, C. L., Chen, Y. L., Yeh, S., Ting, H. J., Hu, Y. C., Lin, H., Wang, X., and Chang, C. (2003) *J. Biol. Chem.* **278**, 23691–23698
33. Legube, G., and Trouche, D. (2003) *EMBO Rep.* **4**, 944–947

34. Chen, Y. J., Wang, Y. N., and Chang, W. C. (2007) *J. Biol. Chem.* **282**, 27215–27228
35. Goodman, R. H., and Smolik, S. (2000) *Genes Dev.* **14**, 1553–1577
36. Matsuda, S., Harries, J. C., Viskaduraki, M., Troke, P. J., Kindle, K. B., Ryan, C., and Heery, D. M. (2004) *J. Biol. Chem.* **279**, 14055–14064
37. Chakravarti, D., LaMorte, V. J., Nelson, M. C., Nakajima, T., Schulman, I. G., Juguilon, H., Montminy, M., and Evans, R. M. (1996) *Nature* **383**, 99–103
38. Sheppard, H. M., Harries, J. C., Hussain, S., Bevan, C., and Heery, D. M. (2001) *Mol. Cell. Biol.* **21**, 39–50
39. Sterner, D. E., and Berger, S. L. (2000) *Microbiol. Mol. Biol. Rev.* **64**, 435–459
40. Boyes, J., Byfield, P., Nakatani, Y., and Ogryzko, V. (1998) *Nature* **396**, 594–598
41. Gu, W., and Roeder, R. G. (1997) *Cell* **90**, 595–606
42. Lévy, L., Wei, Y., Labalette, C., Wu, Y., Renard, C. A., Buendia, M. A., and Neuveut, C. (2004) *Mol. Cell. Biol.* **24**, 3404–3414
43. Chen, H., Lin, R. J., Xie, W., Wilpitz, D., and Evans, R. M. (1999) *Cell* **98**, 675–686
44. Fu, M., Wang, C., Reutens, A. T., Wang, J., Angeletti, R. H., Siconolfi-Baez, L., Ogryzko, V., Avantiaggiati, M. L., and Pestell, R. G. (2000) *J. Biol. Chem.* **275**, 20853–20860
45. Zhou, Z. X., Sar, M., Simental, J. A., Lane, M. V., and Wilson, E. M. (1994) *J. Biol. Chem.* **269**, 13115–13123
46. Grossman, S. R., Perez, M., Kung, A. L., Joseph, M., Mansur, C., Xiao, Z. X., Kumar, S., Howley, P. M., and Livingston, D. M. (1998) *Mol. Cell* **2**, 405–415
47. Grossman, S. R., Deato, M. E., Brignone, C., Chan, H. M., Kung, A. L., Tagami, H., Nakatani, Y., and Livingston, D. M. (2003) *Science* **300**, 342–344
48. Carey, M. (1998) *Cell* **92**, 5–8
49. Iyer, N. G., Ozdag, H., and Caldas, C. (2004) *Oncogene* **23**, 4225–4231
50. Kamei, Y., Xu, L., Heinzl, T., Torchia, J., Kurokawa, R., Gloss, B., Lin, S. C., Heyman, R. A., Rose, D. W., Glass, C. K., and Rosenfeld, M. G. (1996) *Cell* **85**, 403–414

51. Aarnisalo, P., Palvimo, J. J., and Jänne, O. A. (1998) *Proc. Natl. Acad. Sci. USA* **95**, 2122–2127
52. Debes, J. D., Schmidt, L. J., Huang, H., and Tindall, D. J. (2002) *Cancer Res.* **62**, 5632–2636
53. Heemers, H. V., Sebo, T. J., Debes, J. D., Regan, K. M., Raclaw, K. A., Murphy, L. M., Hobisch, A., Culig, Z., and Tindall, D. J. (2007) *Cancer Res.* **67**, 3422–3430
54. Kim, J., Jia, L., Stallcup, M. R., and Coetzee, G. A. (2005) *J. Mol. Endocrinol.* **34**, 107–118
55. Eckner, R., Ewen, M. E., Newsome, D., Gerdes, M., DeCaprio, J. A., Lawrence, J. B., and Livingston, D. M. (1994) *Genes Dev.* **8**, 869–884
56. Chakravarti, D., Ogryzko, V., Kao, H. Y., Nash, A., Chen, H., Nakatani, Y., and Evans, R. M. (1999) *Cell* **96**, 393–403
57. Lundblad, J. R., Kwok, R. P., Lurance, M. E., Harter, M. L., and Goodman, R. H. (1995) *Nature* **374**, 85–88
58. Ait-Si-Ali, S., Ramirez, S., Barre, F. X., Dkhissi, F., Magnaghi-Jaulin, L., Girault, J. A., Robin, P., Knibiehler, M., Pritchard, L. L., Ducommun, B., Trouche, D., and Harel-Bellan, A. (1998) *Nature* **396**, 184–186
59. Yuan, L. W., Soh, J. W., and Weinstein, I. B. (2002) *Biochem. Biophys. Acta* **1592**, 205–211
60. Rasti, M., Grand, R. J., Mymryk, J. S., Gallimore, P. H., and Turnell, A. S. (2005) *J. Virol.* **79**, 5594–5605
61. Arany, Z., Newsome, D., Oldread, E., Livingston, D. M., and Eckner, R. (1995) *Nature* **374**, 81–84
62. Whyte, P., Williamson, N. M., and Harlow, E. (1989) *Cell* **56**, 67–75
63. Turnell, A. S., and Mymryk, J. S. (2006) *Br. J. Cancer* **95**, 555–560

Figure 4-1. MAGE-11 and p300 Increase AR Transcriptional Activity. CV1 cells were transfected with 5 μ g PSA-Enh-Luc and (A) 0.1 μ g pCMV-AR, 1.5 μ g pSG5-MAGE and 1.5 μ g pSG5-HA-p300 alone and together; (B) 0.1 μ g pCMV-AR in the absence and presence of 1 μ g pSG5-MAGE, 2 μ g pSG5-TIF2 and 2 μ g pSG5-HA-p300; (C) 10 ng pCMV5 empty vector (p5) or pCMV-AR-(1-660) with and without 0.5 μ g pSG5-MAGE and 2 μ g pSG5-HA-p300; and (D) 10 ng pCMV-AR-(1-660) with and without 0.5 μ g pSG5-MAGE, 2 μ g pSG5-TIF2 and 2 μ g pSG5-HA-p300. Cells were incubated in the absence and presence of 1 nM DHT.

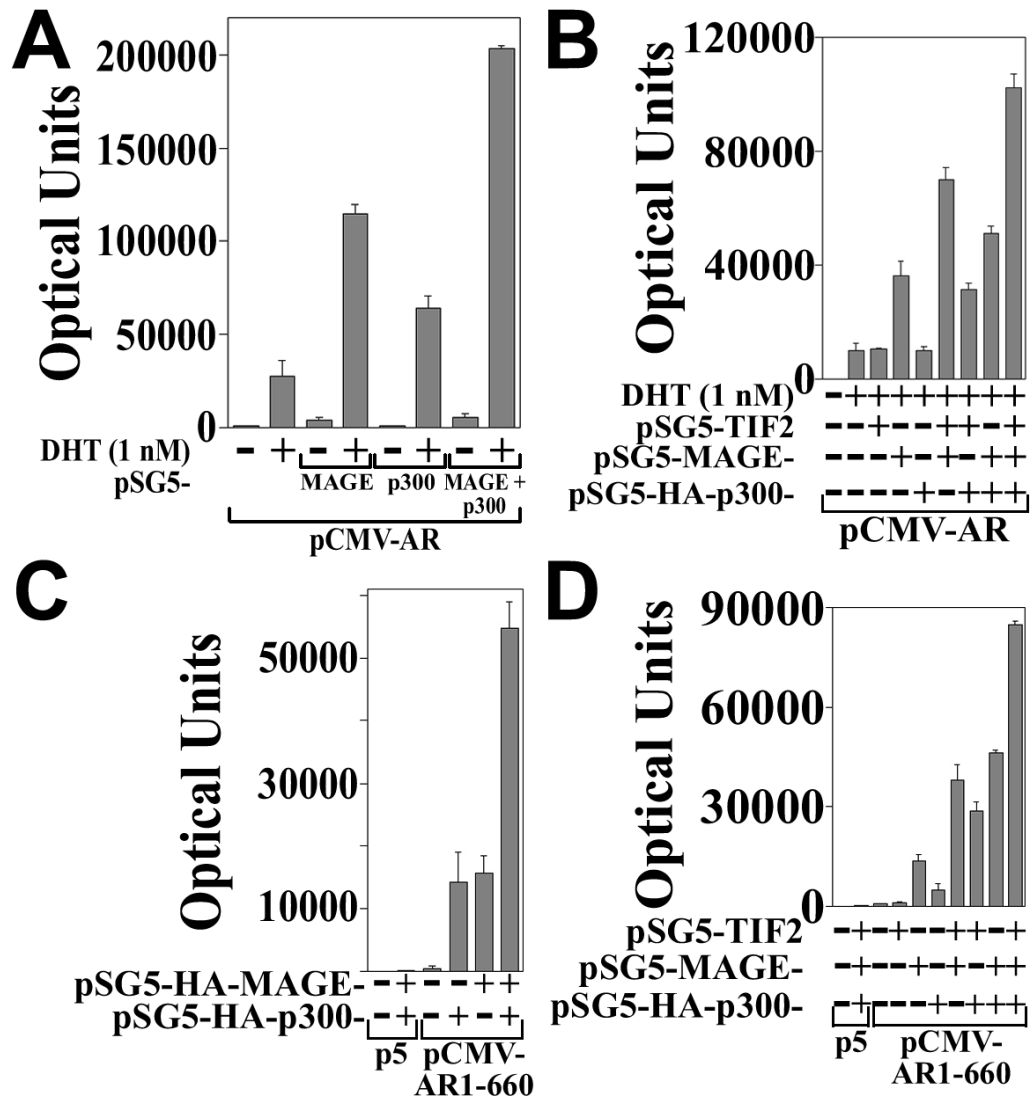


Figure 4-2. MAGE-11 Interacts with the p300 NH₂-terminal Region. (A) Schematic diagram of p300 interaction domains and fragments analyzed for interaction with MAGE-11. (B) The indicated GAL-p300 vectors (0.05 μ g) were transfected into HeLa cells with 0.1 μ g 5XGAL4Luc3 and 0.05 μ g pVP16 empty vector (-) or VP-MAGE. (Lower panel) COS cells were transfected with 8 μ g GAL-p300 vectors and incubated with 1 μ M MG132 for 24 h prior to harvest. Cell extracts (50 μ g protein/lane) were analyzed on immunoblots using anti-GAL4 DNA binding domain antibody. (C) The indicated GAL-p300 vectors (0.05 μ g) were transfected into HeLa cells with 0.1 μ g 5XGAL4Luc3 and 0.1 μ g pSG5 empty vector (-) or pSG5-HA-MAGE-(112-429). (Lower panel) COS cells were transfected with 5 μ g GAL-p300 vectors and incubated with 1 μ M MG132 for 24 h and 1 h prior to harvest. Cell extracts (60 μ g protein/lane) were analyzed on the transblot using GAL4 DNA binding domain antibody.

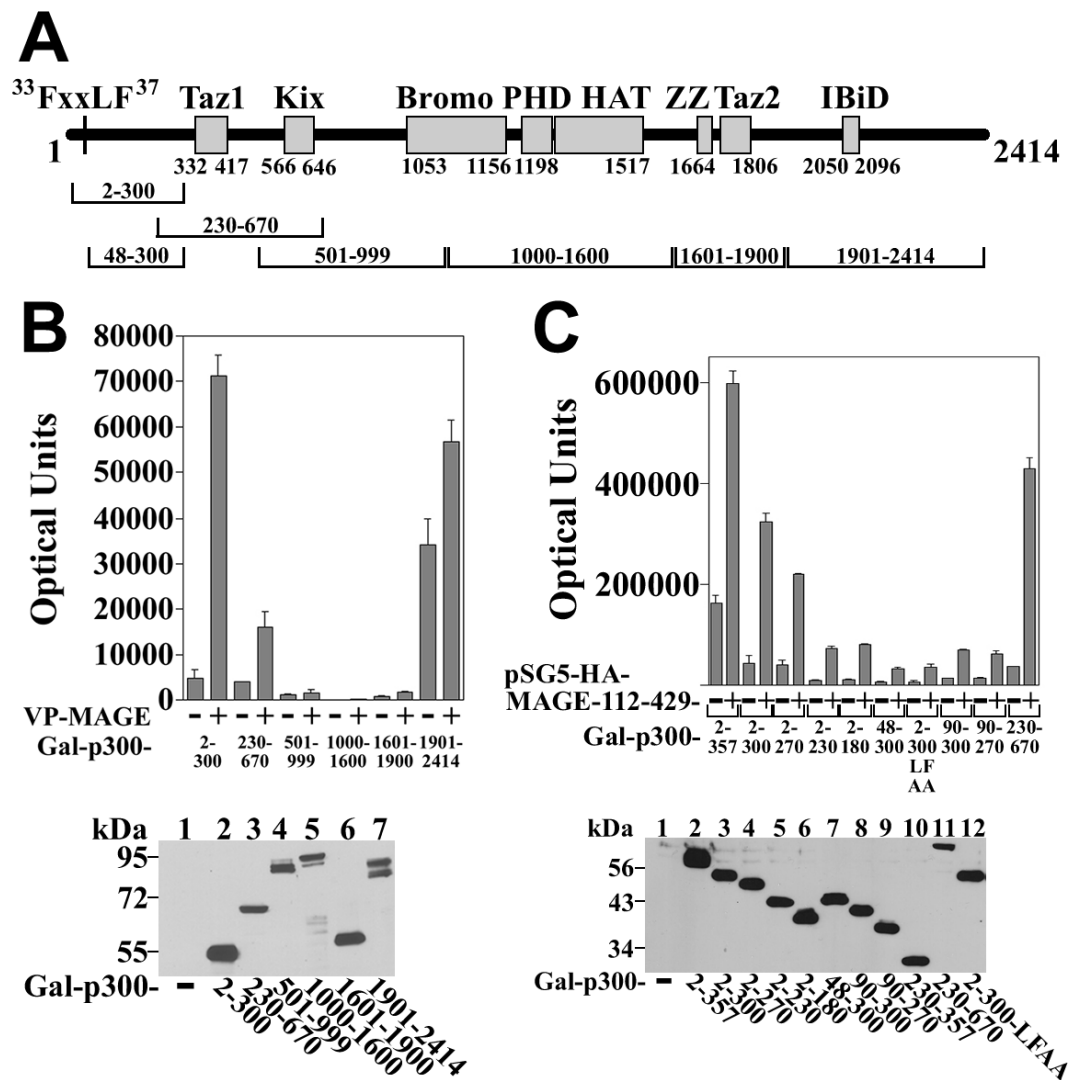


Figure 4-3. MAGE-11 Domains Interact with p300. (A) Schematic diagram of MAGE-11 showing nuclear localization signal (NLS) residues 18–22, phosphorylation sites Ser-174 (6), Ser-208 and Thr-360, ubiquitinylation sites Lys-240 and 245 (7), F-box residues 329–369 (6) and MAGE-11 fragments. HeLa cells were transfected with 0.1 μ g 5XGAL4Luc3 and (B) 0.05 μ g GAL-p300-(2–300) with 0.1 μ g VP16 empty vector (–) or VP-MAGE-(2–429), 112–429, 112–362 or 112–252; (C) 0.05 μ g GAL-p300-(2–300) and 0.1 μ g pSG5 empty vector (–) or pSG5-HA-MAGE-(2–429), 112–429, 112–362, 112–307, 112–298 or 112–276; (D) 25 ng GAL-p300-(2–300) and 0.1 μ g pSG5 (–) or wild-type (WT) pSG5-HA-(112–429) or indicated F-box mutant; (E) 0.05 μ g GAL-p300-(2–300) and 0.1 μ g pSG5 (–) or WT pSG5-HA-MAGE-(112–429) or S174A, S174D, S298A or S298D mutant. (F) In vitro interaction between MAGE-11 and p300 was tested using GST-p300-(2–357) and [³⁵S]-labeled MAGE-11. The input represents 10% of the total reaction.

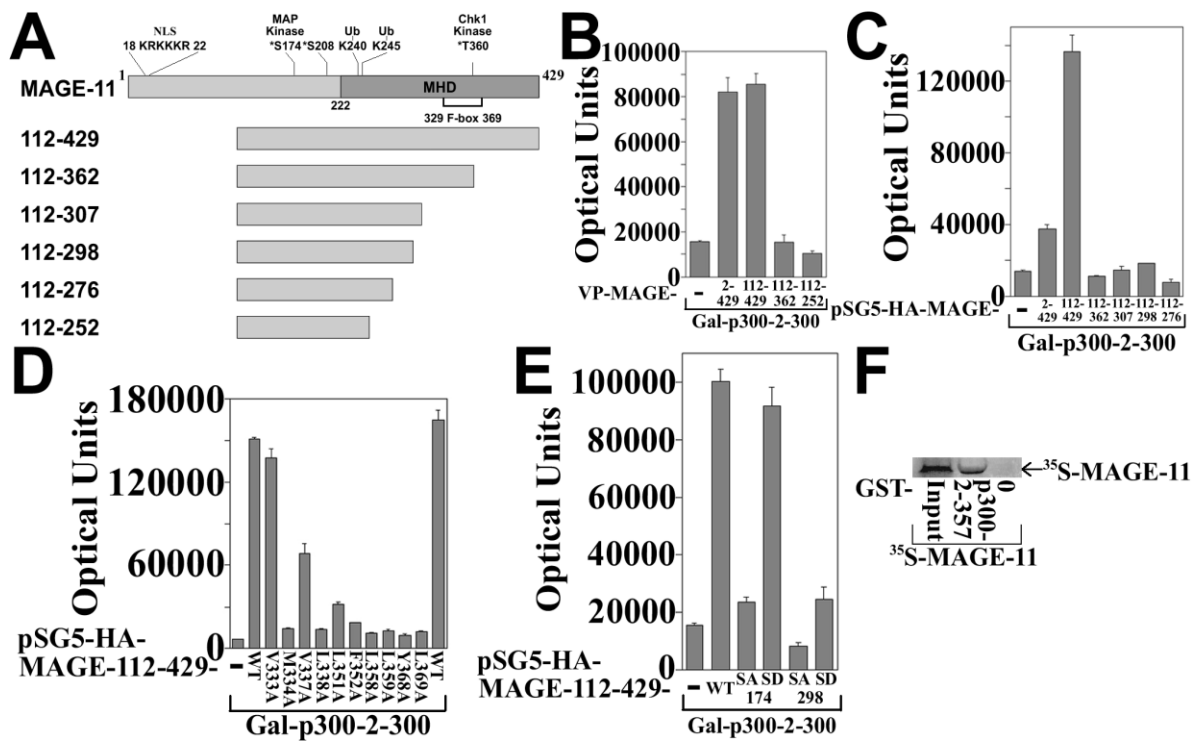


Figure 4-4. Identification of MAGE-11 ¹⁸⁵MDAIF¹⁸⁹ and ⁹⁴ITQIF⁹⁸ Interaction Sites for p300. (A) Schematic diagram of MAGE-11 showing ⁹⁴ITQIF⁹⁸ and ¹⁸⁵MDAIF¹⁸⁹ interaction motifs for p300, ²⁶⁰FPEIF²⁶⁴ interaction motif for TIF2, MAGE-11 F-box (residues 329–369) interaction site for the AR FXXLF motif (6), nuclear localization signal (NLS), Ser-174 and Thr-360 phosphorylation sites, Lys-240 and 245 ubiquitylation sites, and MAGE-11 fragments to test the interaction with p300. (Inset) GAL-MAGE fragments were expressed in COS cells transfected with 6 µg DNA and incubated with 1 µM MG132 for 24 h and 1 h prior to harvest. The transblot of cell extracts (100 µg/lane) was probed using GAL4 DNA binding domain antibody. (B) HeLa cells were transfected with 0.1 µg 5XGAL4Luc, 0.05 µg GAL-MAGE fragments and 0.15 µg pSG5 empty vector (–) or pSG5-HA-p300. (C) HeLa cells were transfected with 0.1 µg 5XGAL4Luc3, 0.05 µg GAL-MAGE fragments and 0.1 µg pSG5 (–) or pSG5-HA-p300. (Lower panel) GAL-MAGE fragments were expressed in COS cells transfected with 5 µg DNA and incubated with 1 µM MG132 for 24 h prior to harvest. The transblot of cell extracts (80 µg/lane) was probed using GAL4 DNA binding domain antibody. (D) Dependence of AR transcriptional activity on p300 and MAGE-11 ¹⁸⁵MDAIF¹⁸⁹ motif was performed by transfecting CV1 cells with 0.1 µg pCMV-AR and 3 µg PSA-Enh-Luc in the absence and presence of 1 µg pSG5-MAGE, 2 µg pSG5-TIF2 and 2 µg pSG5-HA-p300. Cells were incubated for 48 h in the absence and presence of 1 nM DHT. (Inset) Expression was verified in COS cells transfected with 3 µg pSG5 empty vector DNA (–) (lane 1), wild-type (WT) pSG5-MAGE (lane 2), and I188A,F189A and I97A,F98A mutants (lanes 3 and 4). Cell extracts (10 µg/lane) were probed using FLAG-MAGE antibody-1 (0.5 µg/ml).

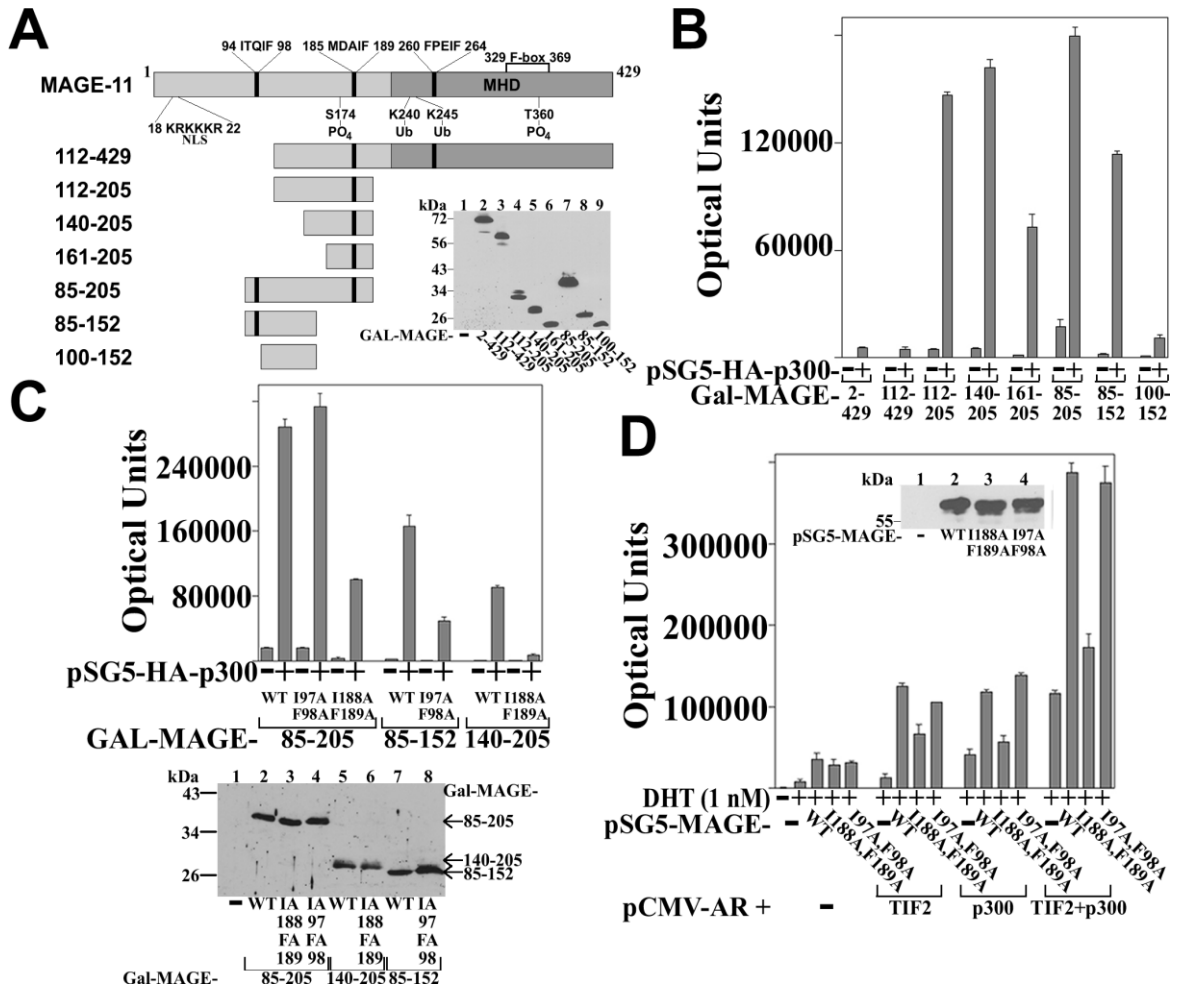


Figure 4-5. Functional Effects of AR and p300 NH₂-terminal FXXLF Motifs. (A) AR NH₂-terminal ²³FQNLF²⁷ and p300 NH₂-terminal ³³FGSLF³⁷ FXXLF motifs (red) are flanked by basic and acidic residues (cyan). (B) Two hybrid interaction between AR and p300 NH₂-terminal regions was performed in HeLa cells transfected with 0.1 μg 5XGAL4Luc3 and 0.05 μg GAL0 empty vector (-) or GAL-p300-(2-300), 48-300 or 90-300, and 0.1 μg VP16 empty vector (-) or wild-type (WT) VP-AR-(1-660) or L26A,F27A (LFAA) mutant. (C) HeLa cells were transfected with 0.1 μg/ml 5XGAL4Luc3, 0.05 μg GAL0 empty vector (-), GAL-p300-(2-300) or 48-300 with 0.1 μg VP16 empty vector (-) or full-length AR fusion vectors VP-AR WT, L26A,F27A (LFAA) or Δ9-28 mutant. Cells were incubated in the absence and presence of 10 nM DHT. (D) HeLa cells were transfected with 0.1 μg 5XGAL4Luc3 and 0.05 μg GAL-p300-(2-300), 48-300 and L26A,F27A (LFAA) with 0.1 μg pSG5 empty vector (-) or pSG5-TIF2.

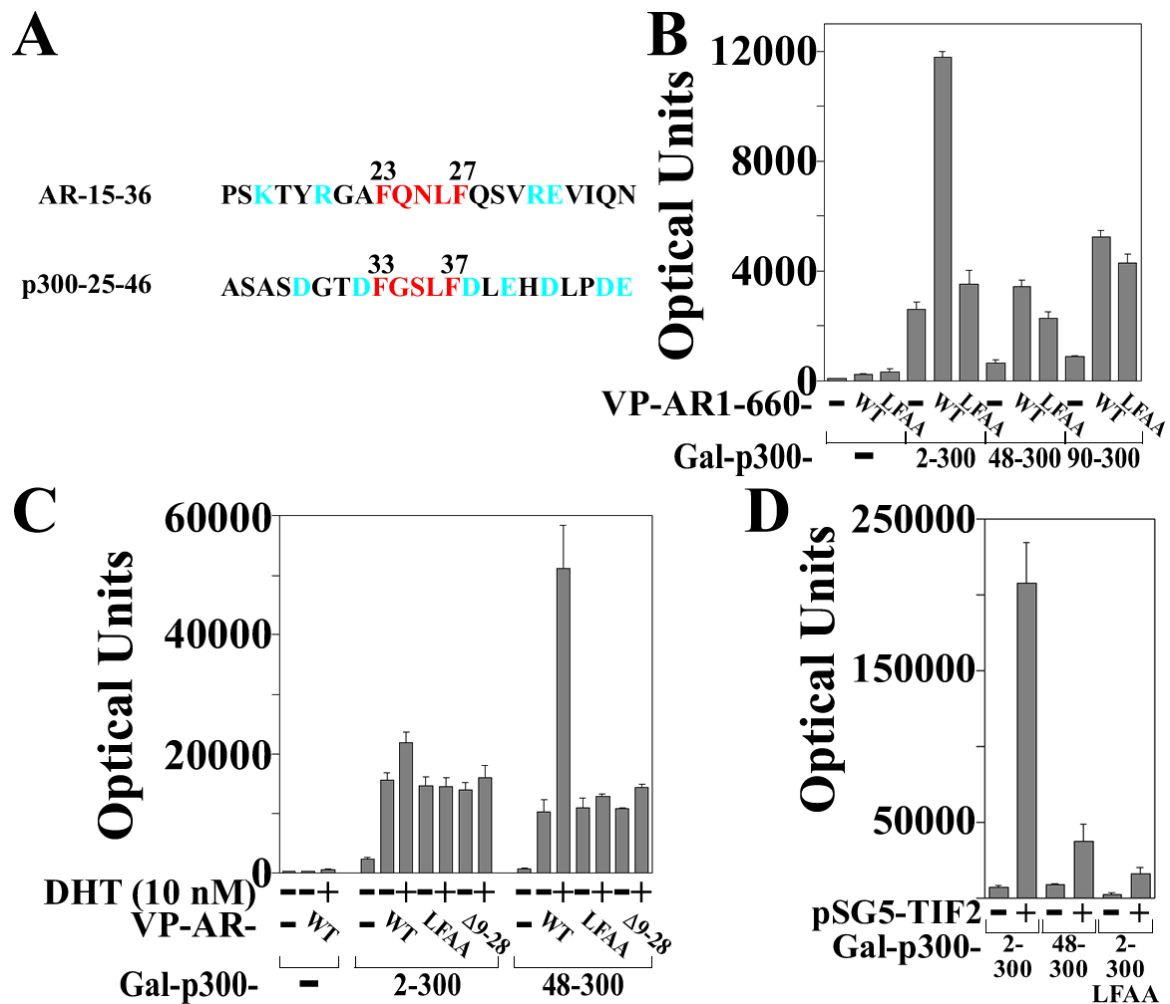


Figure 4-6. Dependence of GAL-p300-(2–300) Transcriptional Activity on MAGE-11 and TIF2. (A) Inhibition of MAGE-11 (upper panel) and TIF2 (lower panel) expression by siRNA was performed by transfecting COS cells using Lipofectamine 2000 with 1 μ g pSG5 empty vector (lane 1), 1 μ g pSG5-MAGE (top panel) or pSG5-TIF2 (bottom panel) in the absence and presence of 5 nM MAGE-11 siRNA-2 or 3, TIF2 siRNA-3 and nonspecific (NS) siRNA-5. The next day cells were harvested (TIF2) or transferred to fresh serum-free medium and harvested 24 h later (MAGE-11). Cell extracts for MAGE-11 (10 μ g protein/lane) and TIF2 (40 μ g protein/lane) were analyzed on transblots probed with MAGE-Ab-(94–108), TIF2 and β -actin antibodies. (B) HeLa cells (10^5 /well in 12 well plates) were transfected using Lipofectamine 2000 with 0.1 μ g 5XGAL4Luc3 and 0.05 μ g GAL-p300-(2–300) in the absence and presence of 0.1 μ g pSG5 empty vector (–) or pSG5-TIF2 in the absence and presence of 5 nM nonspecific siRNA-5 (NS-5), MAGE-11 siRNA-2 or 3, and TIF2 siRNA-3.

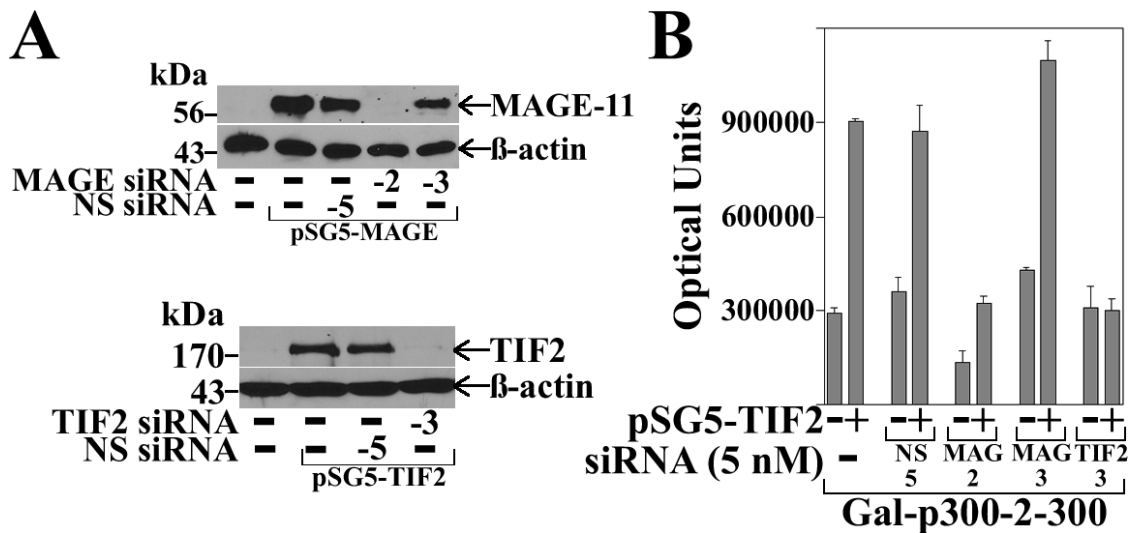


Figure 4-7. MAGE-11 Links p300 to AR N/C Interaction-Mediated Transactivation. (A) HeLa cells were transfected with 0.1 μ g PSA-Enh-Luc and 50 ng pCMV-AR-(507–919) with and without 25 ng wild-type pCMV-AR-(1–503) or the L26A,F27A (LFAA) mutant, 25 ng pSG5-MAGE and 25 ng pSG5-HA-p300. (B) COS cells were transfected using Lipofectamine 2000 with 2 μ g pSG5-HA-p300 and 10 nM nonspecific siRNA-5, 10 nM p300 siRNA 1–4 or without siRNA. Cell extracts were prepared in IB lysis buffer and probed on a transblot (15 μ g protein/lane) using p300 and β -actin antibodies. (C) HeLa cells (1.2×10^5 /well in 6 well plates) were transfected using Lipofectamine 2000 with 0.1 μ g PSA-Enh-Luc, 50 ng pCMV-AR-(507–919), 25 ng pCMV-AR-(1–503) and 25 ng pSG5-MAGE without siRNA or with 5 nM nonspecific siRNA-5 (NS5) or p300 siRNA 1–4. Cells were incubated for 24 h in serum-free media with and without 10 nM DHT. (D) HeLa cells were transfected with 0.1 μ g PSA-Enh-Luc, 50 ng pSG5 empty vector (–), wild-type (WT) pSG5-HA-p300 or D1399Y (DY) acetylation mutant, 15 ng wild-type (WT) or the indicated pSG5-MAGE mutant, and 0.1 μ g GAL-AR-(16–36) or L26A,F27A (LFAA) mutant.

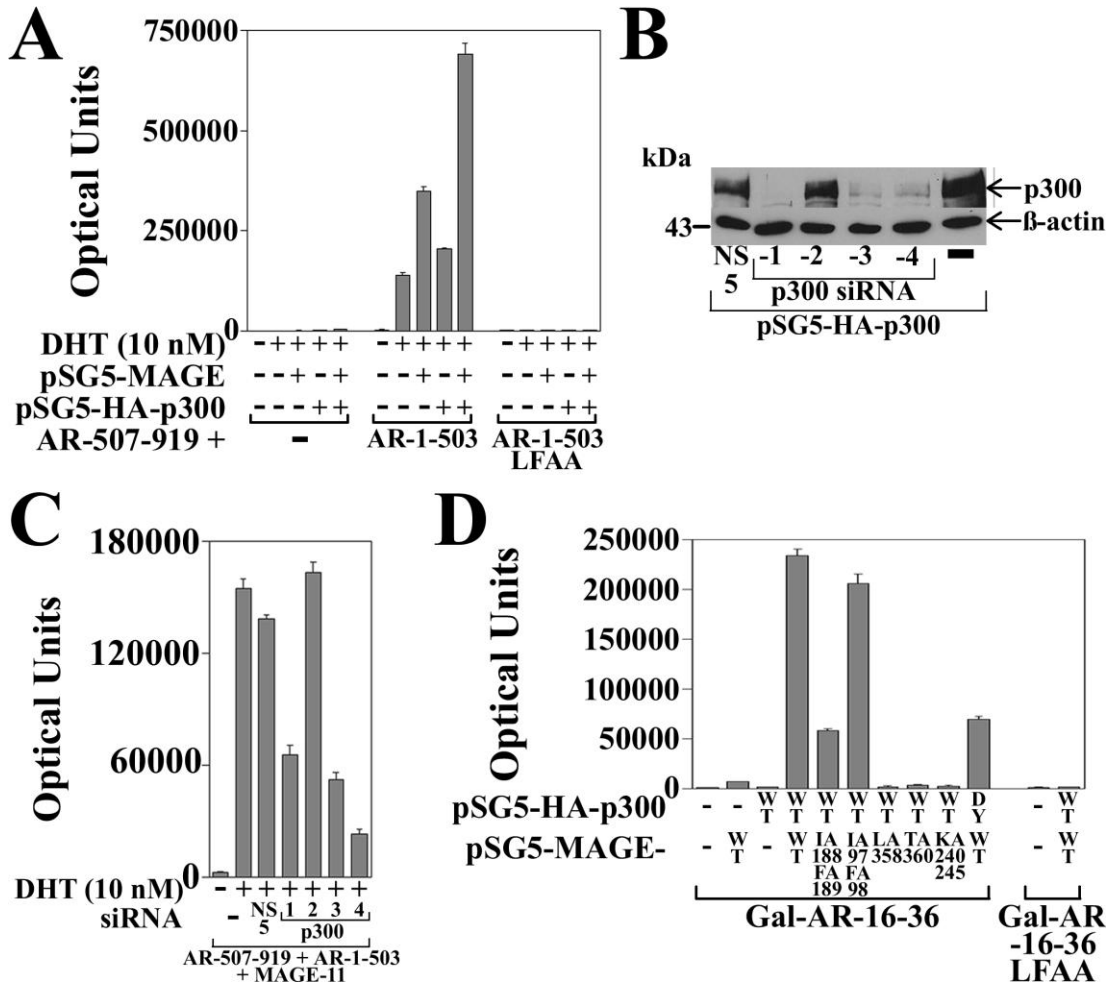


Figure 4-8. Dependence of AR Transcription Activity on p300 Acetyltransferase Activity. (A) CV1 cells were transfected with 0.1 μ g pCMV-AR and 3 μ g PSA-Enh-Luc in the absence and presence of 1 μ g pSG5-MAGE, 2 μ g pSG5-TIF2 and 2 μ g wild-type (WT) pSG5-HA-p300 or D1399Y acetyltransferase mutant (DY). Cells were incubated for 48 h in the absence and presence of 1 nM DHT. (B) HeLa cells were transfected with 0.1 μ g/ml 5XGAL4Luc3 and 0.05 μ g GAL-MAGE-(85–205) or 140–205 with 0.15 μ g pSG5 empty vector (–), wild-type (WT) pSG5-HA-p300 or D1399Y mutant (DY). (Lower panel) Expression levels were determined in COS cells transfected with 5 μ g pSG5 empty vector (–) (lane 1), wild-type (WT) pSG5-HA-p300 (lane 2) and D1399Y acetyltransferase mutant (lane 3). Cell extracts (30 μ g/lane) on the transblot were probed using p300 antibody. (C) Inhibition of MAGE-11 ubiquitinylation by p300 and p300-D1399Y was demonstrated in COS cells transfected with 6 μ g FLAG empty vector or FLAG-ubiquitin (Ub) and 3 μ g pSG5-HA-MAGE-(112–429) in the absence and presence of 5 μ g pSG5-HA-p300 or the D1399Y acetyltransferase mutant. Cells were incubated in the absence and presence of 0.1 μ g/ml EGF and immunoprecipitated using anti-FLAG M2 affinity resin. The transblot was probed with HA antibody.

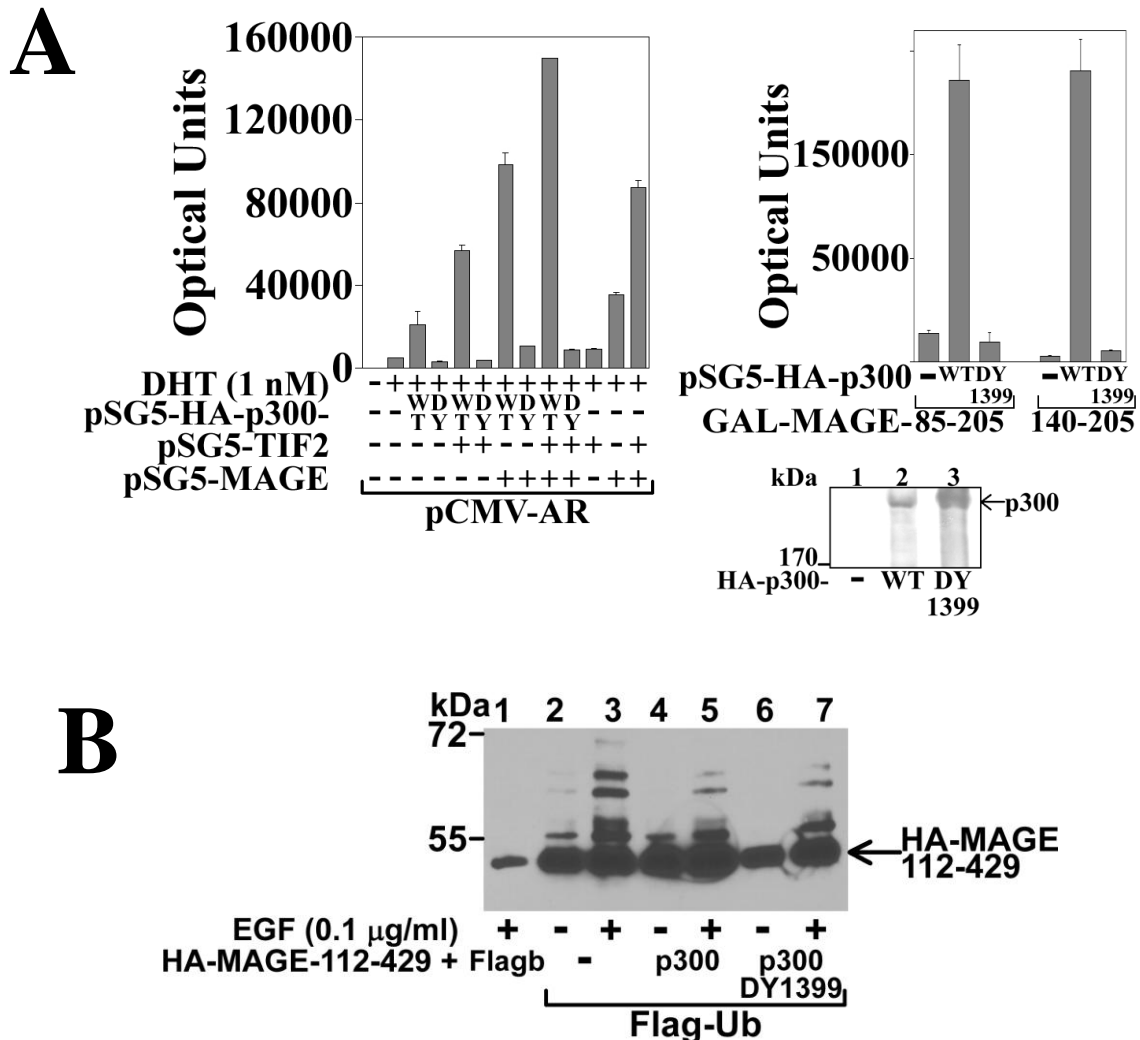
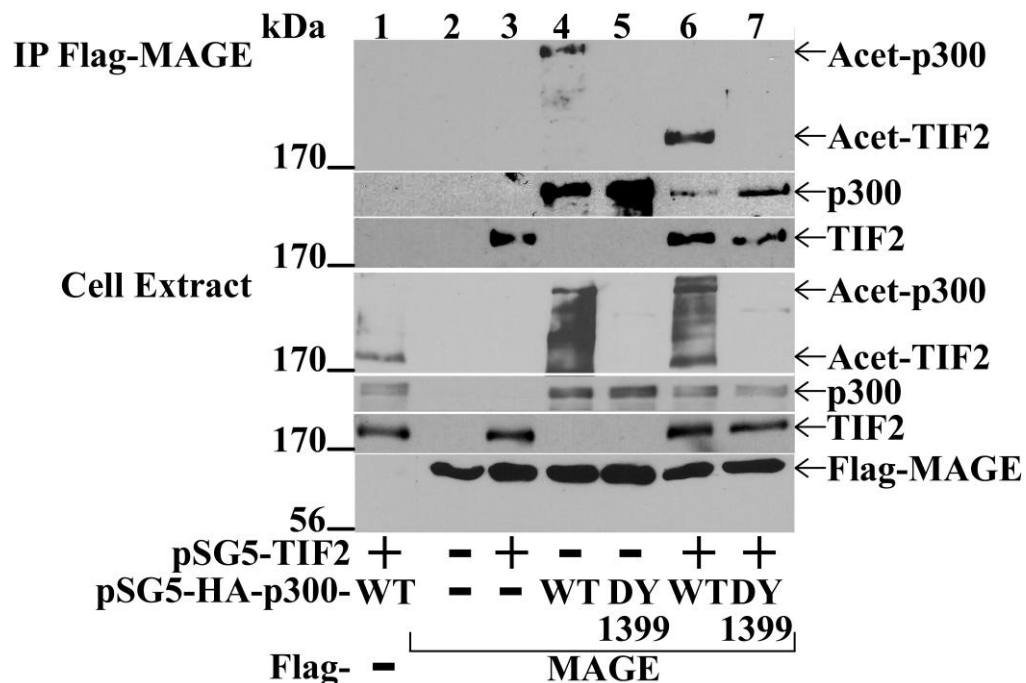


Figure 4-9. MAGE-11 Influences p300 Acetylation of TIF2. (A) Coimmunoprecipitation of acetylated TIF2 and p300 with FLAG-MAGE was performed in COS cells transfected with 4 μ g FLAG empty vector (–) or FLAG-MAGE in the absence and presence of 5 μ g pSG5 empty vector (–) or pSG5-TIF2, and 5 μ g wild-type (WT) pSG5-HA-p300 or D1399Y mutant. Cells were incubated with 0.1 μ g/ml EGF for 24 h prior to harvest and with 5 mM nicotinamide 1 hr prior to harvest. Cell extracts prepared in IP lysis buffer containing 5 mM nicotinamide were immunoprecipitated overnight at 4°C. Immunoprecipitates and cell extracts (50 μ g protein/lane) were probed using FLAG, p300, TIF2 and acetylated-lysine antibodies. (B) Inhibition of p300-mediated acetylation of TIF2 by MAGE-11 was determined by expressing 5 μ g FLAG empty vector (–) or FLAG-TIF2 with 5 μ g pSG5 empty vector (–), pSG5-HA-p300 or D1399Y mutant with and without 1 μ g pSG5-MAGE. Cells were incubated in serum-free media with 0.1 μ g/ml EGF for 24 h prior to harvest, and with 5 mM nicotinamide and 5 mM sodium butyrate for 1 h prior to harvest in IP lysis buffer containing 5 mM nicotinamide and 5 mM sodium butyrate. Immunoprecipitates and cell extracts (30 μ g protein/lane for p300, 50 μ g/lane for acetylated lysine, 70 μ g/lane for FLAG-TIF2 and MAGE-11) were probed on transblots using antibodies for FLAG-MAGE-11, FLAG and TIF2, p300 and acetylated-lysine.

A



B

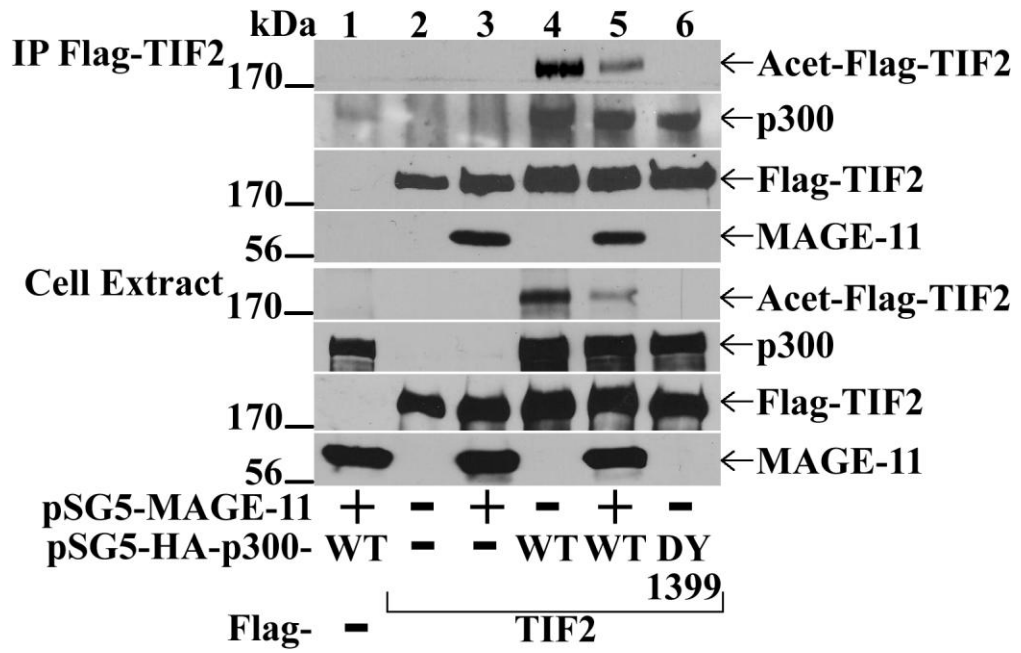


Figure 4-10. Transient Increase in Endogenous MAGE-11. COS cells were transfected with 6 μ g pSG5-HA-p300 or pSG5 empty vector. The next day cells were transferred to serum-free phenol red-free medium and 24 h later to fresh serum-free medium. Cells were harvested at the indicated times, cell extracts prepared in IB lysis buffer and 40 μ g protein/lane analyzed with the transblot probed using p300 antibody and 10 μ g/ml each of MAGE-11 antipeptide antibodies 13–26, 59–79 and 94–108.

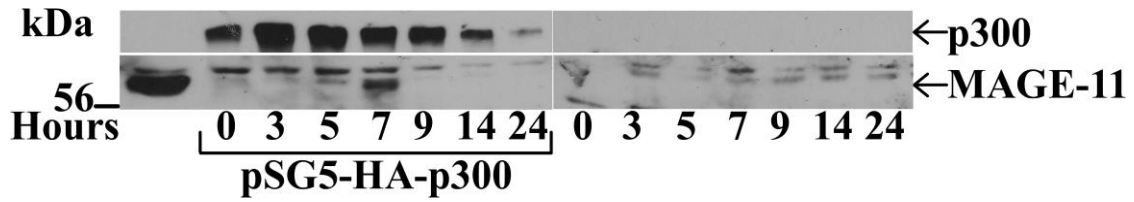
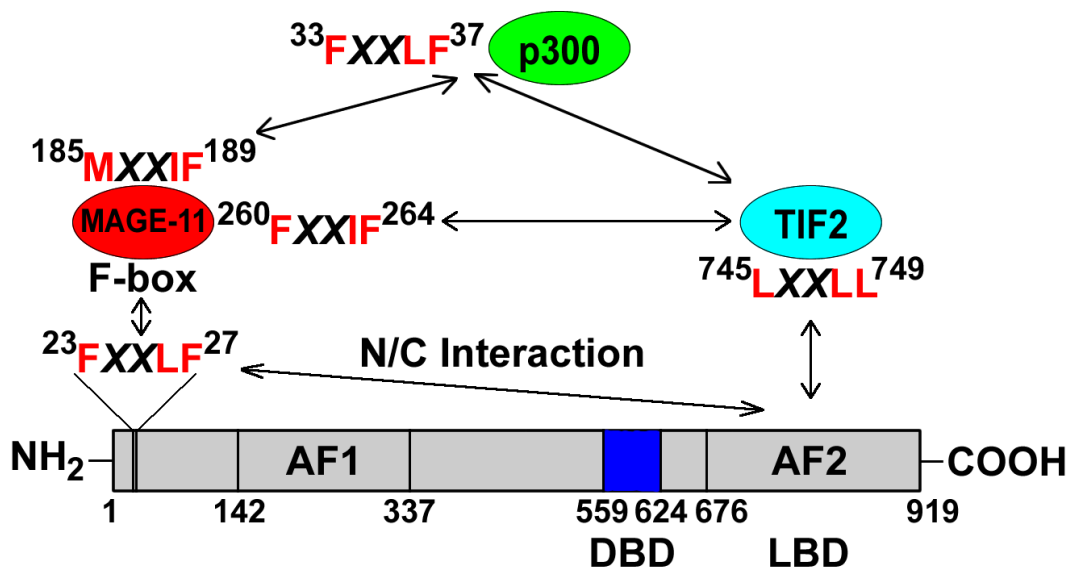


Figure 4-11. Functional Interactions Between AR, MAGE-11, p300 and TIF2. AR transcriptional activity is increased through interactions with MAGE-11, p300 and TIF2. AR contains a centrally located DNA binding domain (DBD) and activation function 1 (AF1) region in the NH₂-terminal region. AR NH₂-terminal FXXLF motif ²³FQNL²⁷ interacts with the AR activation domain 2 (AF2) region of the ligand binding domain (LBD) in the androgen-dependent AR N/C interaction, and with the MAGE-11 F-box residues 329–369 (6). MAGE-11 contains the MXXIF motif sequence ¹⁸⁵MDAIF¹⁸⁹ that interacts with the NH₂-terminal region of p300, and the FXXIF motif ²⁶⁰FPEIF²⁶⁴ that interacts with TIF2 (6). A p300 NH₂-terminal FXXLF motif ³³FGSLF³⁷ interacts with TIF2, and TIF2 LXXLL motif ⁷⁴⁵LRYL⁷⁴⁹ interacts with AF2 in the AR LBD. These motif driven interactions occur in a temporal and/or competitive manner that are influenced by the cell cycle and post-translation modification that includes phosphorylation, ubiquitinylation and acetylation. The acetylase activity of p300 is required for MAGE-11 and TIF2 to increase AR transcriptional activity.



CHAPTER 5

SUMMARY AND FUTURE PERSPECTIVES

Molecular Determinants of Testosterone (T) and Dihydrotestosterone (DHT) Binding to the Androgen Receptor (AR)

Based on our research, one can begin to associate how the different physical properties of androgens influence the molecular effects of T and DHT on AR mediated gene activation. Both T and DHT are 19 carbon steroids that only differ in the presence of a double bond in the A-ring of T that is absent in DHT. Our data suggest this subtle difference confers more hydrophilic character to T, which is reflected in the fact that T is 10 fold more water soluble than DHT, and that DHT is the more potent androgen *in vivo*. This is detrimental to AR activity and activation function 2 (AF2) FXXLF and LXXLF motif interactions.

The ligand binding pocket as well as the AR AF2 surface are hydrophobic in nature and thus, AR binding of DHT results in a more stable protein structure conducive for optimal AR transcriptional activity and AF2 motif binding. T is positioned in a more planar configuration within the AR ligand binding pocket, resulting in reduced inter-atomic distances and increased hydrogen bonding potential between a conserved water, the steroid A-ring, and AR helix 5 residue Met-745 that lies proximal to the steroid A-ring. Met-745 projects towards the AF2 surface and potentially interacts with AR residue Leu-712, which contacts the FXXLF and LXXLL motifs and is implicated in androgen insensitivity syndrome.

The prostate cancer mutant AR-H874Y binds both T and DHT with high affinity yet more effectively interacts with the AR FXXLF motif. This is reflected in the slower dissociation rate of T as well as increased T-induced AR-H874Y transactivation. While crystal structures reveal that the ligand binding pockets of DHT and T bound AR LBD are similar, AR-H874Y compensates by stabilizing the LBD and AF2 via the replacement of a water-mediated hydrogen bonding network with a direct-hydrogen bonding network. Protein flexibility is increased by structured water molecules involved in multiple H-bonds whereas direct protein-mediated H-bonds provide a more rigid foundation. Our findings suggest that altered H-bond chemistry may compensate for diminished AR activity and AF2 motif interactions, and reveals a possible mechanism for how somatic mutations in castration-recurrent prostate cancer modulate AR transactivation in the androgen-depleted patient.

Mechanisms of the Melanoma Antigen Gene Protein-11 (MAGE-11) Dependent Increase in Androgen Receptor Gene Mediated Transcription

We explored the functional characteristics underlying the MAGE-11 dependent increase in androgen receptor (AR) transcriptional activation. The site of interaction in MAGE-11 that binds the AR FXXLF motif is a highly conserved F-box within a carboxyl-terminal MAGE homology domain between residues 329 and 369. This interaction is regulated by serum-induced MAP kinase phosphorylation of MAGE-11 Ser-174, which is required for the MAGE-11 F-box interaction with the AR FXXLF motif. MAGE-11 also increases AR gene mediated activation through direct interactions with transcriptional intermediary factor 2 (TIF2) and p300, which possesses histone acetyltransferase activity.

Our studies suggest that MAGE-11 functions as a bridging factor that recruits AR coactivators through interactions involving FXX(L/I)F motifs with F-box containing proteins.

Interestingly, Skp1 contains an ¹⁰¹FELIL¹⁰⁵ FXXLF motif within its Skp2 binding region (1), further supporting the functional significance of our findings. Thus, our studies also reveal a potential regulatory mechanism in which an FXXLF motifs serve as the docking site for F-box containing proteins.

The MAGE-11 interaction with AR and associated coregulators provides a mechanism for increased AR action in castration-recurrent prostate cancer, when circulating androgen levels are low and MAGE-11 levels increase (2,3). This raises an interesting issue surrounding the potential relevance and function of F-box proteins in cancer development. Wang et al. identified an AR-Skp2 pathway in prostate-cancer cells which promotes proliferation independent of differentiation (4), and Skp2 is overexpressed in primary prostate cancer samples (5). Additionally, the F-box protein FBXW7 has been detected in human malignancies including gastric, pancreatic, and prostate cancer (6). The identification of upregulated and/or mutated F-box proteins in human malignancies suggests a universal mechanism underlying cancer progression and presents a previously unidentified therapeutic target.

MAGE-11 as a Prostate Cancer Therapeutic Target

The progression of prostate cancer to a castration-recurrent state is associated with AR-mediated signaling, which can be enhanced by overexpressed AR coactivators. Since current prostate cancer treatments are not curative, it is vital to identify new prostate cancer therapeutic targets to improve the life of the patient. In light of this, it is intriguing that the cancer-testis antigens have become the subject of antineoplastic therapy due to their restrictive expression profile in normal tissues, high expression in various tumors and their

ability to induce an immunogenic response. Recent data suggest that the expression of MAGE genes in cancer cells contributes to the malignant phenotype and response to therapy.

Data from our studies presented here suggest that a vaccine targeting MAGE-11 might be an effective therapeutic tool to combat prostate cancer progression following androgen deprivation therapy. In support of this, a portion of melanoma patients treated with an experimental MAGE-A3 peptide in a clinical trial experienced tumor regression (7), while a clinical trial evaluating the effectiveness of a MAGE-A4 cancer vaccine in advanced lung cancer is scheduled in Japan.

A detailed investigation into the immunogenicity and effectiveness of a MAGE-11 prostate cancer vaccine would be validated by human and primate preclinical investigations. In the human, an antigen capture enzyme-linked immunosorbent assay (ELISA) could be used to examine MAGE-11 antigen levels in serum obtained from prostate cancer patients. In support of this, Morrissey et al. developed an antigen capture assay to detect serum clusterin levels in prostate cancer patients (8). The immunogenicity of a tumor antigen may also be demonstrated from studies *in vitro* or in primates following challenge with MAGE-11 (9). Indeed, human MAGE-A1 overexpression has been reported to confer resistance to tumor necrosis factor-mediated cytotoxicity (10).

Role of MAGE-11 in Infertility

The Centers for Disease Control estimated that in 2009, approximately 11.8% of women in the U.S. between the ages of 15 and 44 presented with infertility. Female factor infertility is associated with ovulatory disorders including PCOS, endometriosis, tubal factors, and implantation failure (11). The role of implantation failure in infertility is not well

defined. Thus, new developments in the evaluation and identification of factors affecting endometrial receptivity may lead to the diagnosis of specific implantation defects.

MAGE-11 should be of particular interest in the search for an intrinsic cause of female factor infertility related to implantation since MAGE-11 is temporally expressed throughout the menstrual cycle. MAGE-11 regulates AR transcriptional activity through the modulation of the AR N/C interaction and direct interaction with p160 coactivators as well as p300 (1-3), which are also expressed in human endometrium (12,13). Therefore, one could speculate that low levels and/or defects in the MAGE-11 gene exist and play a role in impaired endometrial receptivity.

To study this possibility, researchers could sequence the MAGE-11 gene in genomic DNA obtained from patients presenting with infertility. It would also be interesting to determine whether MAGE-11 could be used as a screening tool to evaluate for the risk of infertility associated with implantation receptivity in the endometrium. This would require knowledge of whether or not MAGE-11 levels are altered in females unable to bear children. Comparisons of MAGE-11 mRNA and protein expression levels in tissue samples from normal and infertile patients would provide necessary preliminary evidence required to proceed with broader clinical trials investigating the potential of MAGE-11 as a biomarker and screening tool for female factor infertility.

Studies have also shown a positive correlation between gene therapy and disease outcome (14,15). Thus, if studies reveal a relationship between MAGE-11 levels and/or MAGE-11 genetic defects and fertility, MAGE-11 could be a therapeutic target for infertility. Viral vectors targeted towards MAGE-11 could be used to endogenous levels or replace a defective copy during the critical window of endometrial receptivity.

REFERENCES

1. Schulman, B. A., Carrano, A. C., Jeffrey, P. D., Bowen, Z., Kinnucan, E. R., Finnin, M. S., Elledge, S. J., Harper, J. W., Pagano, M., and Pavletich, N. P. (2000) *Nature* **408**, 381-386
2. Bai, S., He, B., and Wilson, E. M. (2005) *Mol. Cell Biol.* **25**, 1238-1257
3. Karpf, A. R., Bai, S., James, S. R., Mohler, J. L., and Wilson, E. M. (2009) *Mol. Cancer Res.* **7**, 523-535
4. Wang, H., Sun, D., Ji, P., Mohler, J., and Zhu, L. (2008) *J. Cell Sci.* **121**, 2578-2587
5. Yang, G., Ayala, G., De Marzo, A., Tian, W., Frolov, A., Wheeler, T. M., Thompson, T. C., and Harper, J. W. (2002) *Clin. Cancer Res.* **8**, 3419-3426
6. Onoyama, I., and Nakayama, K. I. (2008) *Cell Cycle* **7**, 3307-3313
7. Marchand, M., van Baren, N., Weynants, P., Brichard, V., Dreno, B., Tessier, M. H., Rankin, E., Parmiani, G., Arienti, F., Humblet, Y., Bourlond, A., Vanwijck, R., Lienard, D., Beauduin, M., Dietrich, P. Y., Russo, V., Kerger, J., Masucci, G., Jager, E., De Greve, J., Atzpodien, J., Brasseur, F., Coulie, P. G., van der Bruggen, P., and Boon, T. (1999) *Int. J. Cancer* **80**, 219-230
8. Morrissey, C., Lakins, J., Moquin, A., Hussain, M., and Tenniswood, M. (2001) *J. Biochem. Biophys. Methods* **48**, 13-21
9. Clark, C. E., and Vonderheide, R. H. (2006) *Cancer Biol. Ther.* **5**, 1226-1227
10. Park, J. H., Kong, G. H., and Lee, S. W. (2002) *Mol. Cells* **14**, 122-129
11. Healy, D. L., Trounson, A. O., and Andersen, A. N. (1994) *Lancet* **343**, 1539-1544
12. Vienonen, A., Miettinen, S., Blauer, M., Martikainen, P. M., Tomas, E., Heinonen, P. K., and Ylikomi, T. (2004) *J. Soc. Gynecol. Investig.* **11**, 104-112
13. Gregory, C. W., Wilson, E. M., Apparao, K. B., Lininger, R. A., Meyer, W. R., Kowalik, A., Fritz, M. A., and Lessey, B. A. (2002) *J. Clin. Endocrinol. Metab.* **87**, 2960-2966
14. Maguire, A. M., Simonelli, F., Pierce, E. A., Pugh, E. N., Jr., Mingozi, F., Bennicelli, J., Banfi, S., Marshall, K. A., Testa, F., Surace, E. M., Rossi, S., Lyubarsky, A., Arruda, V. R., Konkle, B., Stone, E., Sun, J., Jacobs, J., Dell'Osso, L., Hertle, R., Ma, J. X., Redmond, T. M., Zhu, X., Hauck, B., Zelenai, O., Shindler, K. S., Maguire, M. G., Wright, J. F., Volpe, N. J., McDonnell, J. W., Auricchio, A., High, K. A., and Bennett, J. (2008) *N. Engl. J. Med.* **358**, 2240-2248

15. Levine, B. L., Humeau, L. M., Boyer, J., MacGregor, R. R., Rebello, T., Lu, X., Binder, G. K., Slepushkin, V., Lemiale, F., Mascola, J. R., Bushman, F. D., Dropulic, B., and June, C. H. (2006) *Proc. Natl. Acad. Sci. USA* **103**, 17372-17377